National Library of Canada
Bibliothèque nationale du Canada

Canadian Theses Service
Service des thèses canadiennes

Ottawa, Canada
K1A 0N4

NOTICE

The quality of this microform is heavily dependent upon the quality of the original thesis submitted for microfilming. Every effort has been made to ensure the highest quality of reproduction possible.

If pages are missing, contact the university which granted the degree.

Some pages may have indistinct print especially if the original pages were typed with a poor typewriter ribbon or if the university sent us an inferior photocopy.

Previously copyrighted materials (journal articles, published tests, etc.) are not filmed.

Reproduction in full or in part of this microform is governed by the Canadian Copyright Act, R.S.C. 1970, c. C-30.

AVIS

La qualité de cette microforme dépend grandement de la qualité de la thèse soumise au microfilmage. Nous avons tout fait pour assurer une qualité supérieure de reproduction.

S'il manque des pages, veuillez communiquer avec l'université qui a conféré le grade.

La qualité d'impression de certaines pages peut laisser à désirer, surtout si les pages originales ont été dactylographiées à l'aide d'un ruban usé ou si l'université nous a fait parvenir une photocopie de qualité inférieure.

Les documents qui font déjà l'objet d'un droit d'auteur (articles de revue, tests publiés, etc.) ne sont pas microfilmés.

La reproduction, même partielle, de cette microforme est soumise à la Loi canadienne sur le droit d'auteur, SRC 1970, c. C-30.

NL-339 (r. 88/04)

Canada

THE UNIVERSITY OF ALBERTA

The Visual and Statistical Analysis of Bivariate Feature Spaces in Remote Sensing

by

Karl A. Kliparchuk

A THESIS

SUBMITTED TO THE FACULTY OF GRADUATE STUDIES AND RESEARCH

IN PARTIAL FULFILLMENT OF THE REQUIREMENTS FOR THE DEGREE

OF Master of Science

Department of Geography

EDMONTON, ALBERTA

Spring 1988

Permission has been granted to the National Library of Canada to microfilm this thesis and to lend or sell copies of the film.

The author (copyright owner) has reserved other publication rights, and neither the thesis nor extensive extracts from it may be printed or otherwise reproduced without his/her written permission.

L'autorisation a été accordée à la Bibliothèque nationale du Canada de microfilmer cette thèse et de prêter ou de vendre des exemplaires du film.

L'auteur (titulaire du droit d'auteur) se réserve les autres droits de publication; ni la thèse ni de longs extraits de celle-ci ne doivent être imprimés ou autrement reproduits sans son autorisation écrite.

ISBN 0-315-42748-5

THE UNIVERSITY OF ALBERTA

RELEASE FORM

NAME OF AUTHOR	Karl A. Kliparchuk
TITLE OF THESIS	The Visual and Statistical Analysis of Bivariate Feature Spaces in Remote Sensing
DEGREE	Master of Science
YEAR THIS DEGREE GRANTED	Spring 1988

Permission is herby granted to THE UNIVERSITY OF ALBERTA LIBRARY to reproduce single copies of this thesis and to lend or sell such copies for private, scholarly or scientific research purposes only.

The author reserves other publication rights, and neither the thesis nor extensive extracts from it may be printed or otherwise reproduced without the author's written permission.

(SIGNED) Karl Kliparchuk

PERMANENT ADDRESS:

13520-62 Street

Edmonton Alberta

T5A 0V9

DATED Oct 15 1987

THE UNIVERSITY OF ALBERTA

FACULTY OF GRADUATE STUDIES AND RESEARCH

The undersigned certify that they have read, and recommend to the Faculty of Graduate Studies and Research for acceptance, a thesis entitled The Visual and Statistical Analysis of Bivariate Feature Spaces in Remote Sensing submitted by Karl A. Kliparchuk in partial fulfillment of the requirements for the degree of Master of Science.

SUPERVISOR J. Ronald Eyton

E. Reinelt

DATED Oct. 15. 19 87

ABSTRACT

Acquisition of digital imagery by satellite and aircraft borne scanners necessitated the development of classification algorithms to handle these large quantities of data. Parametric classification algorithms, based on the assumption that each class is multivariate normally distributed, have been developed to classify digital imagery. Non-normally distributed classes can adversely affect a parametric classification. There are few published data on the results of normality tests for spectral classes, but data that have been published for individual agricultural fields indicated that a significant number of fields were non-normally distributed.

When training field data are extracted, feature space plots are usually generated and used by the analysts to visually determine the separability of spectral classes, and the effectiveness of a cleaning operation. A problem with the bivariate feature space was that the frequency of occurence of each spectral pair was not depicted. A new bivariate frequency feature space was proposed which combined the frequency information into the feature space. The frequency feature space was generated by surfacing the frequency values with a multiquadric equation and then contouring the resulting surface. A test for bivariate normality was applied to each class.

Five classes were extracted from three dates of Landsat MSS imagery during one growing season, frequency feature spaces were generated, and visually analyzed. The normality test was applied to these data and results indicated that many classes were not normally distributed. A non-parametric classifier was developed to account for non-normal classes. The decision spaces between the non-parametric classifier and three parametric classifiers were compared visually.

Spectral classes were extracted from anniversary TM and MSS images, frequency feature spaces were generated and visually compared. The test for bivariate normality was applied to the TM and MSS classes to determine if increased spatial resolution affected the classes. The MSS classes were subtracted from the TM classes and results of the

differencing indicated that the TM classes generally had a higher frequency value in the central peaks.

ACKNOWLEDGEMENT

Many people aided in the development and completion of this thesis, and the help received was deeply appreciated. I first express my gratitude to my committee: Professors J. R. Eyton, E. R. Reinelt (Emeritus), and P. H. Crown for their guidance and insights. I particularly wish to thank my advisor, Professor J. R. Eyton, for deepening my understanding of the computer programming, statistical, and numerical analysis associated with digital image processing. My thanks are also expressed to Professors J. R. Eyton and P. H. Crown for instructing me in the proper method of scientific writing.

Outside of my committee, I also express appreciation to my graduate student colleagues who provided suggestions toward this thesis as well as extended their friendship. Finally, thanks are extended to my family, relatives, and friends who supported my efforts and kept me going physically, mentally, and monetarily.

TABLE OF CONTENTS

CHAPTER	PAGE
1. INTRODUCTION	1
1.1 Multispectral Sensor Systems	1
1.2 Digital Image Processing	3
1.3 Classification	5
1.4 Objectives	9
1.5 The Study Areas	9
2. METHODOLOGY TO DERIVE FREQUENCY FEATURE SPACES	12
2.1 Generation of Frequency Feature Spaces	12
2.2 Removing Outliers From Feature Spaces and Frequency Feature Spaces	14
2.3 Cluster Analysis	15
3. ANALYZING THE FREQUENCY FEATURE SPACE GRAPHICS	16
3.1 Water	16
3.2 Forest	17
3.3 Winter Wheat and Soybeans	18
3.4 Corn	19
3.5 Bare Soil	20
4. PARAMETRIC AND NON-PARAMETRIC DECISION SPACES	21
4.1 Three Parametric Classifiers	21
4.2 The Frequency Feature Space Template Classifier	23
4.3 A Statistical Test for Bivariate Normality	24
4.4 Comparisons Between the Parametric Classifiers: Date 1	26
4.5 Comparisons Between the Frequency Feature Space Template Classifier and the Parametric Classifiers: Date 1	27
4.6 Comparisons Between the Parametric Classifiers: Date 2	28
4.7 Comparisons Between the Frequency Feature Space Template Classifier and the Parametric Classifiers: Date 2	29
4.8 Comparisons Between the Parametric Classifiers: Date 3	30
4.9 Comparisons Between the Frequency Feature Space Template Classifier and the Parametric Classifiers: Date 3	31
5. TM AND MSS FREQUENCY FEATURE SPACE ANALYSIS	32
5.1 Preprocessing and Generation of Frequency Feature Spaces	33
5.2 A Visual Comparison Between the TM and MSS Frequency Feature Spaces	35
5.2.1 Canola	35
5.2.2 Water	35
5.2.3 Aspen	36
5.2.4 Pasture	37
5.3 Results From the Test on Bivariate Normality	39
5.4 Results from Differencing the MSS Frequency Feature Spaces From the TM Frequency Feature Spaces	39
5.4.1 Pasture	40
5.4.2 Aspen	41
5.4.3 Water	41
6. CONCLUSIONS AND FUTURE RESEARCH	43

6.1 Impact of Research on Traditional Remote Sensing Classification Methods 43
6.2 Comments on the Development of the Frequency Feature Spaces 45
6.3 Observations on the Visual Interpretation of Frequency Feature Spaces 47
6.4 Results of Research on Understanding Decision Spaces 48
6.5 Ramifications of the Differences Between TM and MSS Feature Spaces 51
6.6 Summary 52

Bibliography 123

Appendix 1: Computer Programs Used in Thesis 126

LIST OF TABLES

		PAGE
1.1	Landsat MSS Configuration.	54
1.2	Landsat TM Configuration.	54
1.3	SPOT Configuration.	54
2.1	Number of Unique Pairs for Trend Surfaces.	55
2.2	Number of Pairs, Clusters, and Pairs Deleted from Cluster Analysis	55
3.1	Crop calendar for Midwest United States.	56
4.1	Kolmogorov-Smirnov Test for Date 1 Original and Cleaned Classes.	57
4.2	Kolmogorov-Smirnov Test for Date 2 Original and Cleaned Classes.	58
4.3	Kolmogorov-Smirnov Test for Date 3 Original and Cleaned Classes.	59
5.1	Number of Original and Cleaned Spectral Pairs for the Alexander Indian Reservation.	60
5.2	Kolmogorov-Smirnov Test for TM and MSS classes.	61
5.3	T-test for Skewness and Kurtosis on the Differenced Grids.	62

LIST OF FIGURES

		PAGE
1.1	A two-dimensional feature space plot.	63
1.2	The Alexander Indian Reservation.	64
2.1	A traditional feature space plot.	65
2.2	A perspective plot.	66
2.3	Two surfacing routines.	67
2.4	The feature space for forest.	69
2.5	The polynomial trend surfaces for forest.	70
2.6	The multiquadric surface for forest.	72
2.7	The multiquadric surface for the Date 3 bare soil class.	73
2.8	Smoothing filter applied to the spectral frequencies.	74
2.9	The multiquadric surface for the Date 3 bare soil class after smoothing the spectral frequencies.	75
2.10	Calculation for percent volume contours.	76
2.11	Effects of normalization on skewed data.	77
3.1	Original and cleaned frequency feature spaces for water.	78
3.2	Original and cleaned frequency feature spaces for forest.	80
3.3	Original and cleaned frequency feature spaces for winter wheat and soybeans.	82
3.4	Original and cleaned frequency feature spaces for corn.	84
3.5	Original and cleaned frequency feature spaces for bare soil.	86
3.6	Original and cleaned feature spaces for date 1.	88
3.7	Original and cleaned feature spaces for date 2.	89
3.8	Original and cleaned feature spaces for date 3.	90
4.1	Decision spaces for the parametric classifiers.	91
4.2	Increase in computing time versus number of input channels.	92
4.3	The method for defining overlap area for the Frequency Feature Space Template classifier.	93
4.4	Original and cleaned Frequency Feature Space Template classifier decision spaces.	94
4.5	Original Date 1 decision spaces for the parametric classifiers.	96
4.6	Original Date 2 decision spaces for the parametric classifiers.	97
4.7	Original Date 3 decision spaces for the parametric classifiers.	98
4.8	Cleaned Date 1 decision spaces for the parametric classifiers.	99
4.9	Cleaned Date 2 decision spaces for the parametric classifiers.	100
4.10	Cleaned Date 3 decision spaces for the parametric classifiers.	101
5.1	Precipitation in July, 1984.	102
5.2	Precipitation in July, 1986.	103
5.3	Cleaned Multispectral scanner feature space plot.	104
5.4	Cleaned Thematic Mapper feature space plot.	105
5.5	Cleaned Multispectral scanner frequency feature space plots.	106
5.6	Cleaned Thematic Mapper frequency feature space plots.	110

LIST OF PLATES

		PAGE
5.1	Multispectral Scanner image of the Alexander Indian Reservation.	114
5.2	Thematic Mapper image of the Alexander Indian Reservation.	115
5.3	Multispectral Scanner red and infrared radiation channel images.	116
5.4	Thematic Mapper red and infrared radiaiton channel images.	117
5.5	Multispectral Scanner training field locations.	118
5.6	Thematic Mapper training field locations.	119
5.7	Differenced grid for pasture.	120
5.8	Differenced grid for aspen.	121
5.9	Differenced grid for water.	122

1. Introduction

Data capture and analysis are a concern in cartography. There are many ways of collecting data, including a ground survey, aerial photography, and remote sensing from earth orbiting satellites. The latter methodology is one of the newest developments in data acquisition. Satellites scan the surface of the earth continuously and relay digital data to stations on the earth for processing. A variety of sensors available aboard satellites, and aircraft, produce digital data about the surface of the earth at different spatial and spectral resolutions. Many different image processing and classification methods are available for processing these data. A brief introduction to the different multispectral imaging sensor systems currently operating, those available in the future, digital image processing, and digital classification of imagery is presented before outlining the objectives of this thesis.

1.1 Multispectral Sensor Systems

Acquisition of earth resources satellite imagery began with the launch of Landsat 1 on July 23, 1972; subsequently Landsat 2, 3, 4, and 5 have been launched. Two types of sensor systems were placed aboard Landsat 1 and 2. The first system consisted of three return beam vidicon (RBV) cameras. Each of these television-type cameras covered a different spectral region, and imaged one frame at a time. The three RBV cameras were replaced by two panchromatic RBV cameras on Landsat 3 which produced side by side viewing. The secondary system was the multispectral scanner (MSS) which collected data in four spectral channels, from 500nm - 1100nm, in a sequential, line by line fashion and had a spatial resolution of 57m by 79m (Table 1.1). The MSS has six bit radiometric resolution. Aboard Landsat 4 and 5, the MSS was complemented by the Thematic Mapper (TM) scanner. The TM scanner imaged in seven spectral channels from 450nm - 12500nm, had a 30m x 30m spatial resolution in the first six channels and a spatial resolution of 120m x 120m in the seventh spectral channel (Table 1.2). The TM scanner has eight bit radiometric resolution. The French "Systeme Probatoire d'Observation de la

Terre" (SPOT) satellite was launched on February 21, 1986. The SPOT satellite carries two high resolution visible (HRV) sensors to produce a ground resolution cell of 20m x 20m in three spectral channels, and a 10m x 10m resolution cell in a panchromatic channel (Table 1.3) (SPOT IMAGE 1984; American Society of Photogrammetry 1983). SPOT also has the capability to "look" $\pm$ 27° off nadir allowing stereo coverage. The National Aeronautic and Space Administration (NASA) is developing a multispectral linear array scanner (Holmes 1984) with 15m x 15m ground resolution in the visual/near infrared (VNIR), and 30m x 30m ground resolution in the shortwave infrared (SWIR) employing the same seven spectral channels used by the Thematic Mapper. A shuttle imaging spectrometer is to be launched in 1988 (Holmes 1984) which will acquire data from 128 spectral channels over a 400nm - 2500nm range and have a ground resolution of 30m x 30m. Multispectral scanners are also being developed in the Federal Republic of Germany and in Japan (Holmes 1984; Jones 1985).

Aircraft imaging systems are also available for data acquisition. Spatial resolution is variable, depending on the instantaneous field of view (IFOV) of the scanner and the altitude of the aircraft. Many aircraft scanners are capable of producing a finer spectral and spatial resolution than is possible with satellite scanners. One aircraft sensor in operation is the TMS NS-001 multispectral scanner developed by NASA/Johnson Space Centre which provides the same spectral channels as the Landsat TM (Richard et al. 1978). The Bendix corporation has a 24 spectral channel MSS (Sollers et al. 1974). The Canadian Centre for Remote Sensing (CCRS) has a Multi-spectral, Electro-optical Imaging System (MEIS), an eight channel pushbroom scanner, which has a maximum spatial resolution of one metre (Alberta Environment 1986).

The trend in remote sensing scanner development appears to be toward finer spatial and spectral resolution. There has been an increase in the number of spectral bands from four to seven channels, and an increase in spatial resolution in the visible and near infrared

radiation channels from 80m to 30m from Landsat 1 to Landsat 5 to cause the amount of data in one Landsat scene to increase by a factor of 8.4. In one Landsat MSS scene there are 2256 scan lines with approximately 3240 pixels per scan line in each of four spectral channels equalling 29,237,760 pixels. One Landsat TM scene, which is slightly larger than an MSS scene, contains 5728 scan lines with approximately 6120 pixels per scan line in each of seven spectral channels equalling 245,387,520 pixels. The increase in spatial resolution and the number of spectral channels creates a large volume of data which necessitates using faster computers and classification routines. The increase in radiometric resolution from six bit MSS data to eight bit TM data may increase the amount of heterogeneity in a scene to be sensed.

1.2 Digital Image Processing

The manipulation of digital data from satellite and aircraft sensor systems by an analyst can be placed under the general heading of digital image processing. There are many different image processing techniques, excluding classification methods. These techniques can provide an end product for an analyst or can be an intermediate step for classification. Some tasks associated with digital image processing are:

1. Contrast stretching
2. Thresholding
3. Edge enhancement
4. Reducing the dimensionality of the data
5. Texture transforms
6. Band ratioing

Some of the procedures may be used to increase classification accuracy by separating the classes of interest thereby allowing more homogeneous training fields to be selected. The degree of increase in classification accuracy must be weighed against the increase in total computer processing and user analysis time.

Preprocessing is a subset of image processing which consists of correcting systematic errors and calibrating the digital data (Schowengerdt 1983). Image preprocessing at satellite image receiving stations may include corrections to remove or reduce radiometric

and geometric distortions, systematic and random noise, and other data errors (Short 1982). Geometric registration is a preprocessing technique often undertaken by the user and consists of a coordinate transformation followed by resampling. The affine transformation and polynomial least squares fit are commonly used coordinate transformation techniques (Kirby and Steiner 1978). An image can be registered to a map projection such as Universal Transverse Mercator (UTM), or can be registered to another image to give the user the ability to undertake multisensor or multitemporal analysis. Geometric registration involves determining the spatial location of a pixel from the original image in the transformed output image. The locations of output pixels seldom coincide with the locations of pixels in the original image therefore spectral values for the output image have to be determined from neighbouring input pixels.

Resampling is the process of transferring pixel values to an output image. There are three primary resampling methods: nearest neighbour, bilinear interpolation, and cubic convolution. Nearest neighbour is the simplest computationally. The pixel value from the original image that is spatially closest to the corresponding output pixel is transferred to the output pixel location. This method does not change the spectral values from the original image, but does leave the new image with a blocky appearance because pixels may be skipped over or duplicated. The output pixel value in bilinear interpolation is determined by the estimation of pixel values from the input image in two orthogonal directions. The values of the four nearest neighbours are weighted according to the linear distance between the centers of the input pixels to the center of the output pixel and the average value from the four nearest neighbours is placed into the output pixel location (Taranik 1978). Cubic convolution is an interpolation of the data using a continuous function (Shlien 1979). One interpolation method for cubic convolution is to fit cubic splines (Shlien 1979) over a span of four contiguous points in a single direction. Bilinear interpolation and cubic convolution change the spectral values of the original images and in effect smooths the

values which may detrimentally affect classification accuracy. "...Interpolation causes blurring by attenuation of high spatial frequencies, yielding effects similar to low-pass filtering..." (Verdin 1983). Verdin (1983) compared a geometrically uncorrected Landsat MSS scene with the same scene geometrically corrected using a coordinate transformation followed by cubic convolution resampling. Pixel values from a land-water interface were compared and Verdin (1983) determined that anomalous spectral values were located along the interface in the geometrically corrected image. The radiance values for water were decreased by half a radiance value and there was a decrease of a whole radiance value for land.

1.3 Classification

A classification algorithm must be "trained" to discriminate between the classes of interest. Supervised training consists of extracting training fields which are representative of each class and generating a decision space for each class with the classifier. A decision space is a region within the total measurement space defined by a classifier to be representative of a particular spectral class. Measurement space is the space defined by the entire spectral range for each sensor. Feature space graphs may be generated when training fields for each spectral class are extracted. A two-dimensional feature space plot of the spectral training field pixels for MSS band 5 against MSS band 7 would be located in a two-dimensional measurement space, with the range of axis values from 0 to 255 (Figure 1.1). When supervised training fields are extracted, some pixels in a class may be spectrally far removed from the values of neighbouring pixels. These outliers can cause the classifier to generate poor-fitting decision spaces, decreasing classification accuracy. Another cause of misclassification occurs when some of the training field pixels from one class are included with pixels from another class or classes. To eliminate this problem, the mislabelled training field pixels are deleted and the decision spaces are regenerated. Deleting outliers and mislabelled pixels constitutes cleaning the training field data.

After the classifier has been trained, the multispectral image is classified. The most common type of classifiers are the parametric classifiers. Parametric classifiers are based on the assumption that the spectral values for each class are multivariate normally distributed. Three parametric classifiers are the parallelepiped, linear classification function, and maximum likelihood classifiers. Many remote sensing textbooks briefly mention that the assumption of normality is valid for classification but do not provide any references to support this assumption. Two examples are given below;

> "...an assumption is made that the distribution of the cloud of points forming the category training data is Gaussian (normally distributed). This *assumption of normality* is generally reasonable for common spectral response distributions..." (Lillesand and Kiefer 1979)

> "We have chosen repeatedly to use the normal density function to approximate the frequency distribution associated with each of the classes. Is this a reasonable thing to do in practice? To begin with, the *multivariate normal assumption* has been observed to model rather adequately the probabilistic processes observed in a large number of remote sensing applications..." (Swain 1978)

Parametric classifiers are based on multivariate normal assumptions, yet there is a lack of published research concerning multivariate normality in spectral classification. No published tests for multivariate normality have been found in the research literature applied to SPOT, Landsat MSS, or TM data. Each of the data types from the different sensing systems should be analyzed for multivariate normality and the results published because each sensor system has differences in spatial, spectral, and radiometric resolution. One paper has been found to date which published the results for a test on the normality assumption for multispectral imagery.

Crane et al. (1972) applied a univariate chi-square (χ^2) normality test to training field data from fifty-four agricultural fields. The pixels tested were selected from the interior of the fields to avoid the inclusion of boundary pixels which increase the likelihood of non-normality. Twelve separate spectral channel values per pixel were obtained from an aircraft scan of thirty-eight fields in the summer of 1966. There was an average of 2,159

pixels per field. Sixty-eight percent of the spectral data from the twelve channels over the thirty-eight fields were univariate non-normal using the χ^2 test at the 1% significance level. Ten-channel spectral data were recorded from sixteen fields in 1969. Each field was covered by an average of 1,057 pixels. Fifty-six percent of these data were univariate non-normal as indicated by the χ^2 test. Ground resolution for each test area was not reported but the flying altitudes were provided. Ground resolution can be estimated from flight altitude. The IFOV for most aircraft scanners is 2.5 milliradians. The formula to determine the diameter of a ground resolution cell at nadir is: (Lillesand and Kiefer 1979)

$$D=H\beta$$

where;

D = diameter of the ground cell
H = flying height above terrain
ß = IFOV of the scanning system

The flight altitude for the 1966 data was 700 ft (213 m) for thirty fields and 2000 ft (610 m) for eight fields. The flight altitude was 5000 ft (1524 m) for the imagery from 1969. From the lowest to the highest flight altitude, the spatial resolution cell sizes were 1.75 ft (0.53m), 5.00 ft (1.52m), and 12.50 ft (3.81m). This high spatial resolution was far greater than the Landsat MSS spatial resolution of 80m.

Maynard and Strahler (1981) studied the effects of classifying non-normal data with a parametric classifier. The researchers simulated univariate normal, slightly skewed, and severely skewed data, and then compared the classification accuracy between a Bayes maximum likelihood classifier and a non-parametric, logit classifier. Classification accuracy was similar for the normal data. The non-parametric classifier gave better results than the maximum likelihood classifier for the slightly skewed data on all but one case where the results were equal. The largest gain in accuracy for the slightly skewed data was 15%. The non-parametric classifier outperformed the maximum likelihood classifier for all the severely skewed cases, with the largest gain in accuracy in one case of 34%. Maynard

and Strahler also tested classification accuracy between the maximum likelihood and logit classifiers on MSS imagery using a combination of bands 5 and 7. The logit classifier equalled the accuracy of the Bayes maximum likelihood classifier for half the classes; and was more accurate for the remaining classes. The largest increase in classification accuracy was 39%.

The likelihood of non-normally distributed classes may also be more pronounced at finer spatial resolutions because the variability within each class is more visible. Toll (1985) tested classification accuracy between TM and MSS imagery using a parametric classifier. Toll determined for TM imagery that increased spectral resolution increased classification accuracy, while increased spatial resolution decreased classification accuracy. To increase classification accuracy of TM imagery, Toll suggested applying a low pass filter to the pixels before classification. The problem with this approach is that the spectral data are smoothed, creating a false homogeneity. For many applications the higher spatial resolution TM imagery need not be degraded, rather new classification schemes can be developed which accounts for non-normal distributions.

Many different parametric classification and accuracy assessments have been completed on low spatial resolution MSS imagery. Classification accuracies greater than 80% were common (Wasrud and Lulla 1985; Scholz et al.1979). Higher spatial and spectral resolution satellite imagery is now more common with the advent of the TM and SPOT scanners, therefore it would be advisable to reexamine the statistical assumptions of the parametric classifiers;

> "...With the ever-increasing data received from such sensors as the Thematic Mapper and SPOT, classification efficiency will become an important consideration. Testing should be performed on data from those two new sources, in order that classification of their remotely sensed data may proceed as efficiently as possible..." (Wasrud and Lulla 1985)

The analysis of the statistical distribution and separability of the spectral values for each class could be undertaken in order to use the most appropriate type of classifier before

contextual and other ancillary data is added in a classification.

1.4 Objectives

Four problems in classification methodology were outlined in the preceding sections. The problems were associated with the limitations of feature spaces to aid in the analysis of spectral classes before classification, the assumption of spectral class normality, the limitations of parametric classifiers, and the possible change in class normality at increased spatial resolution. The objectives of this thesis were;

1. To develop a new method of displaying feature spaces and to analyze the new method by describing the changes in the feature spaces over time.
2. To determine the normality of individual spectral classes by applying a bivariate normality test.
3. To develop a simple non-parametric classifier which takes account of bivariate, non-normal classes.
4. To compare the decision spaces between the non-parametric classifier and three common parametric classifiers.
5. To analyze how different spatial resolution affects bivariate normality and feature space shape.

The objectives incorporated all aspects of the multi approach (Lillesand and Kiefer 1979). The multi approach involved multistage sensing, where data are recorded at different spatial resolutions; multispectral sensing, where data are acquired simultaneously in several spectral bands; and multitemporal sensing, where data for a study area are collected at more than one date.

1.5 The Study Areas

Two study areas were employed in this research. The first study area was located at Eudora, Kansas. The data from this study area were used to generate the frequency feature spaces and analyze the changes in the frequency feature spaces through a growing season,

to study bivariate frequency feature space normality, and to compare decision space boundaries between a non-parametric classifier and three parametric classifiers. Three dates of Landsat 1 MSS imagery were involved in these tasks. The dates of the imagery were May 11, 1976, June 16, 1976, and July 23, 1976, and are labelled dates 1, 2, and 3 for further reference. These class values came from six bit decompressed MSS data. Training fields extracted from this imagery by Eyton et al. (1979) defined five spectral classes: (Eyton 1987)

1. Forest - which consisted of hickory and oak trees located along the Kansas River.
2. Bare soil - which consisted of intersections from sandy roads and stretches of the roads. The bare soil class was chosen as an unvarying class cover over time.
3. Water - which consisted of water from the Kansas River. The river has a sandy bottom.
4. Winter wheat and soybean fields - in which winter wheat was grown in the fields for the first part of the growing season and soybeans were grown in the same fields but later on in the growing season.
5. Corn fields.

The selection of training fields was based on ground truth information obtained by field investigators during the 1976 data acquisition period (Eyton et al. 1979). The three images were deskewed and rescaled, and boundaries from a 1:60,000 colour infrared photograph were transcribed upon hardcopy images of the Landsat scenes to aid in the delineation of the training fields. The central portions of sample fields were selected to ensure that only pixels from a single crop were chosen. Very little precipitation fell in the Eudora, Kansas area during the growing season of 1976 (Ulaby et al. 1979). Between May 27th and date 2 there was only a trace of precipitation. Two centimeters of rain fell approximately five days before the date 3 scene was imaged. No meteorological records were presented by Ulaby et al. (1979) for date 1. An assumption was made for this thesis that the atmosphere for the three dates of imagery was uniform, and any differences in the atmosphere would not significantly alter the feature space shapes more than the gross changes within the classes through time.

The second study area encompassed the Alexander Indian Reservation, Alberta (Figure 1.2). This site provided data for a visual and statistical comparison of similar frequency feature spaces using imagery of different spatial resolution. Landsat 5 MSS imagery was acquired for July 20, 1986 and Landsat 5 TM imagery was acquired for July 23, 1984. The two Landsat scenes were in Canadian Centre for Remote Sensing (CCRS) computer compatible tape (CCT) format. Preprocessing procedures applied at the satellite receiving station to the tapes corrected for earth rotation and mirror velocity changes. The MSS imagery came from six bit decompressed data and the TM imagery came from eight bit data.

2. Methodology to Derive Frequency Feature Spaces

A method for generating frequency feature spaces is presented in this chapter. Different surfacing routines applied to the spectral frequencies, along with the assets and liabilities associated with each surfacing approach are described. A non-parametric method for eliminating outliers (cleaning) in a spectral class is also described. The best-fitting surfacing routine from the routines tested was applied to the original spectral classes and the cleaned spectral classes.

2.1 Generation of Frequency Feature Spaces

Feature space plots can help the analyst determine the separability between classes and to determine the effectiveness of training field cleaning operations. Standard two channel feature space plots do not allow the user to see the frequency component of each spectral pair. Figure 2.1 is a standard two channel feature space plot of the five spectral classes for date 3, over Eudora, Kansas. Figure 2.2 is a three-dimensional perspective plot of the frequency values for the same five classes. Classes that appear skewed, or multimodal, are readily identified in the perspective plot. A new two channel frequency feature space plot is presented in this thesis, which can be overlayed on the traditional feature space plot, in order to avoid the limitations of the traditional two channel feature space plot. This frequency feature space is presented as contours of equal frequency volume.

A frequency surface must be generated before contouring the spectral frequencies from each class. Two surfacing methods were tested: the polynomial least squares trend surface and the multiquadric equation. The former generated a least squares fit surface; while the latter produced an exact-fitting surface. Hardy (1971) provides an explanation of the mathematics involved with the multiquadric equation. An explanation of trend surface equations can be found in Unwin (1975). Figure 2.3 shows the form of each equation along with the solution for a simple number of observations. The output from the two procedures was a grid of frequency values, with the columns corresponding to red radiation values and the rows corresponding to infrared radiation values.

Forest training areas were extracted from a January 5, 1979, Landsat MSS scene over Georgetown, South Carolina (Eyton 1983), and surfaced to initially determine the viability of generating frequency feature spaces. MSS band 5 and band 7 grey level values were used in this test and for the subsequent Eudora, Kansas training fields. Research has shown that MSS bands 4 and 5 are highly correlated and that MSS bands 6 and 7 are highly correlated (eg. Hall et al. 1984), therefore the elimination of MSS bands 4 and 6 should not affect classification accuracy greatly. Figure 2.4 presents the feature space for forest. The spectral pairs for the forest class were changed into MSS band 5-MSS band 7-frequency triplets and then the triplets were surfaced.

Polynomial trend surfaces of different degrees were fit to the spectral frequencies. The degree of the polynomial was restricted by the number of unique band 5-band 7 pairs there were for a class (Table 2.1). The forest class had twenty-seven distinct pairs which allowed a second degree to a fifth degree polynomial trend surface to be generated. Figure 2.5 shows the frequency value contours for the polynomial trend surfaces. The fourth degree polynomial appeared to follow the traditional feature space plot, but there were two zero frequency contours in the center of the plot surrounded by contours of increasing value. One zero frequency contour should surround the larger frequency contours. The fifth degree polynomial plot was presented as a series of contours placed one on top of the other. The second degree trend surface followed the feature space the closest but there was no a priori way to determine which degree of trend surface would work satisfactorily. The lack of similarity between the plots and lack of predictability of plot shape supported the conclusion that the use of a polynomial trend surface was not feasible.

The multiquadric equation surfacing routine produced a viable approach. The frequency feature space boundary closely followed the feature space because the multiquadric equation was an exact-fitting surface (Figure 2.6). A bivariate normal class should ideally be represented as a bell-shaped surface, according to probability theory; however the opposite situation can occur. Instead of the frequency feature space

decreasing in value away from the center of the class, the surface values increase filling the entire measurement space. This situation occurred with the generation of the frequency feature space for the date 3 bare soil class (Figure 2.7). A method which allowed the multiquadric equation to generate decreasing values away from the edges of the feature space was required. The solution was to smooth the frequency values once using a low pass filter, thereby placing lower values around the higher values. A 3 x 3 filter (Figure 2.8) was applied to the frequencies and a multiquadric surface was generated from the smoothed values. Figure 2.9 shows the contours of the bare soil frequency feature space from the smoothed spectral values.

The final step in the generation and presentation of a frequency feature space was to contour the frequency surface. The contour interval was set equal to a specific surface volume, making the contours from one frequency feature space comparable to the contours from other frequency feature spaces from the same date, or over time. A contour interval of 20% surface volume was chosen for the Eudora, Kansas data. The frequency surface was changed into a percent volume surface before contouring. The total volume under any surface between the maximum frequency and zero frequency is 100%. By summing the frequency values above zero and dividing this value into each separate frequency, the percent volume at each frequency feature space location was derived. Figure 2.10 presents the method of calculating the contour levels. The percent volume at each frequency feature space location is a vertical measure, while a horizontal percent volume contour was required.

2.2 Removing Outliers from Feature Spaces and Frequency Feature Spaces

One objective in the thesis was to determine if spectral classes were bivariate normal. Training fields can be cleaned by parametric or non-parametric approaches. The problem with parametric cleaning was that the spectral values for a class were assumed to be multivariate normal, therefore the detection and removal of "outliers" was based on fitting the data to a normal distribution. Non-outliers may be deleted by the parametric method if

the spectral class was not normally distributed (Figure 2.11). A non-parametric cleaning method was preferable because no assumption was made concerning the distribution of the spectral data. The spectral data were cleaned non-parametrically using cluster analysis.

2.3 Cluster Analysis

The FASTCLUS procedure in the Statistical Analysis System (SAS) package was used to delete outliers in the training fields (SAS Institute Inc. 1985). FASTCLUS is a disjoint cluster analysis based on Euclidean distances computed from one or more quantitative variables (bands 5 and 7). FASTCLUS employed a clustering method known as nearest centroid sorting. This is a standard k-means algorithm (SAS Institute Inc. 1985) to minimize the sum of squared distances from the cluster means. FASTCLUS was documented (SAS Institute Inc. 1985) as an effective method for detecting outliers since outliers are often clusters with only one member. The number of clusters generated was user-defined. A cluster consisting of one or two pixels was considered an outlier for the purpose of the thesis. A series of runs employing different numbers of clusters was applied to these data, then an intuitive analysis of the runs determined the appropriate number of clusters to specify for a class. Care must be taken when specifying the number of clusters because FASTCLUS may break up valid data clusters. In theory, the number of clusters can be set equal to the number of unique pixel locations in the feature space. Table 2.2 lists the total number of original pairs for each class, the final number of clusters specified, and the number of pairs eliminated.

3. Analyzing the Frequency Feature Space Graphics

The utility of the frequency feature space is addressed by determining if changes through the growing season in each class from the Eudora data set can be detected. The change in frequency feature space shape after applying the cleaning operation is also described. A crop calendar (Table 3.1) was used to aid in the analysis of the frequency feature spaces. Figures 3.1 - 5 present the individual, original and cleaned frequency feature space plots from the three dates of imagery. Figures 3.6 - 8 present the original and cleaned, combined feature space plots.

3.1 Water

The frequency feature space for water was expected to change very little through the three dates of imagery, but the plots for water indicated otherwise. The date 1 frequency feature space for water (figure 3.1a) appeared as a single, normally distributed peak. The single, uniform peak probably represents clear water. At date 2 there was still one major peak which probably represented clear water (figure 3.1b). Some areas of water may have increased in suspended sediments or decreased in river depth because there was a slight skew in the frequency feature space toward larger band 5 and band 7 grey level values. Three main spectral peaks were located in the date 3 frequency feature space (figure 3.1c). The largest peak, which contained the lowest grey level values, may represent clear water. Little spectral variance was present in the main peak. The second peak, directly above the first peak, may represent vegetation near the edge of the water, while the third peak may indicate a decrease in river depth plus the presence of vegetation.

The water class from all three dates benefitted from the cleaning operation. Pixels with high band 5 and band 7 grey level values were deleted (figures 3.6 - 8). These pixels may represent water that had abnormally large amounts of suspended sediments, the land-water interface, or shallow portions of the river. The cleaning operation separated the water class from the corn class at date 3 (figure 3.1f). The deleted water pixel may have been from the area of the land-water interface.

3.2 Forest

The forested area around Eudora, Kansas is mainly deciduous. In date 1 the leaves of the deciduous trees had recently emerged and the pigments in the leaves had not fully developed. The frequency feature space appeared as a normally distributed peak, which may indicate that the light green leaves appeared homogeneous to the MSS. The frequency feature space at date 2 (figure 3.2b) was more disperse; the large variation in MSS band 7 grey level values may be accounted for by the Fresnel effect. The Fresnel effect requires leaves to have a well-defined cell structure and is caused by near infrared light entering the spongy mesophyl of leaves and then being randomly scattered (Barrett and Curtis 1982). Only one main spectral peak was present going from date 1 to date 2, but the peak had shifted toward higher MSS band 7 values and lower MSS band 5 values which suggested that the leaves were becoming more mature. Two minor peaks were located in the frequency feature space. The larger of the two peaks may represent a different tree type which has become spectrally separable or trees suffering from moisture stress. A decrease in the MSS band 7 range was present at date 3 (figure 3.2c). The decrease of the MSS band 7 range in the main peak may be attributable to a lessening of the Fresnel effect in the leaves caused by droughty weather.

The cleaning operation provided the greatest benefit for the forest class. An outlier with a low band 7 grey level value and a high band 5 grey level value was deleted from the date 2 training field values (figures 3.2e, 3.7). The forest class had two peaks, with one dominant peak in the frequency feature space. The cleaning operation did not delete the minor peak, which could be a spectrally distinct tree type. In date 3, the major and minor peaks had more similar band 7 values. An outlier with small band 7 grey level values, below the main peak was deleted (figure 3.8). A hole of zero frequency was located between the major and minor peaks in the original frequency feature space. The cleaning operation enlarged the hole between the major and minor peaks and created two separate forest frequency feature spaces.

3.3 Winter Wheat and Soybeans

Winter wheat and soybeans, grown in the American midwest, are often cultivated in the same fields but at different times of the year. After the winter wheat is harvested, soybeans are planted. Winter wheat was growing and should have total coverage above the soil for the first date of the imagery. The frequency feature space (figure 3.3a) portrayed winter wheat as one large, homogeneous peak surrounded by three small peaks. The main winter wheat peak had lower band 7 and higher band 5 grey level values compared to the main forest frequency feature space peak which possibly indicated that the Fresnel effect for winter wheat was not as strong as it was for forest. The winter wheat was harvested and the soybeans planted during the second date of the imagery. Bare soil was visible in the fields because there was a large overlap between the bare soil and winter wheat-soybean frequency feature spaces (figures 3.3b, 3.5b). A straight line placed along the bottom of the winter wheat-soybean frequency feature space (figure 3.3b) in the direction of maximum spectral variation could represent a soil line. Pixels located perpendicular to the soil line may represent soybean plants at various degrees of growth in the fields, or different amounts of winter wheat in the fields. Soil type and moisture content also probably contributed to the shape of the frequency feature space. Soybean crops were at the middle to end of the growing season by the third date of imagery. The frequency feature space (figure 3.3c) was one, very large, dispersed peak which showed that there was large spectral variability among the soybean plants. The frequency feature space may display different levels of maturity, different amounts of moisture availability, and different varieties of soybean plants and other management differences.

The cleaning operation was responsible for a major change in the date 1 class and a smaller change in the date 2 class. There were three definite outliers in the date 1 class eliminated by the cleaning operation, which left winter wheat as one cluster (figure 3.3d). There was a transition from winter wheat to soybean crops at the second date of imaging which meant that the soil in the fields was detected by the MSS. The pixels deleted, which

contained large band 5 and band 7 values, along the main diagonal probably represented dry, unvegetated soil and/or crop residue. The deleted pixels located away from the main diagonal of the data cluster may represent green vegetation on the fields.

3.4 Corn

Corn was planted before the first date of imagery and may have up to 20% ground cover, therefore a soil signature should have been present in the frequency feature space. There was a large overlap between the corn-soil and the soil frequency feature spaces (figures 3.4a, 3.5a) which indicated that soil was visible in the cornfields. The corn frequency feature space (figure 3.4a) had twice the range in the band 5 grey level values compared to the band 7 grey level values. Band 5 grey level values are generally larger than band 7 grey level values for bare soil. The high spectral frequency peaks were evenly distributed through the frequency feature space which indicated that there was no central class type as was present in other classes. At the second date of imagery there was a large change in the frequency feature space shape. The corn frequency feature space (figure 3.4b) had moved away from the bare soil frequency feature space because the corn plants were more mature and covered more of the soil. Two "arms" radiated outward from the main peak in the corn frequency feature space. The upper arm may represent corn suffering from moisture stress, or immature, late planted corn which had more surrounding soil visible to the MSS, while the lower arm may represent immature, late planted corn located in moister soil. The main spectral frequency peak had shifted toward lower band 7 and higher band 5 grey level values at date 3 (figure 3.4c). The decrease in band 7 grey level values and increase in band 5 values may be caused by tasseling or by a decrease in that the Fresnel effect. Corn was harvested at this time therefore the plants should be dried out. There were two small peaks with larger band 7 and smaller band 5 grey level values compared to the main peak. Corn represented by these grey level values may have been planted late.

The cleaning operation did not drastically change the shape of the corn frequency

feature spaces. A single outlier, separate from the main cluster, was deleted for date 1 (figure 3.6). The cleaning operation began to separate a minor peak away from two much larger peaks in the date 3 frequency feature space (figure 3.4f). The minor peak may have been separated from the main cluster, or totally deleted from the frequency feature space, if more clusters had been defined in FASTCLUS.

3.5 Bare Soil

The bare soil frequency feature spaces for all three dates, which consisted of stretches of sandy roads and road intersections, were very similar. All three frequency feature spaces were positively correlated and had numerous, evenly spaced peaks of similar value. The bare soil frequency feature spaces were likely affected by three factors: the moisture content of the soil, the physical variability of the soil, and the amount of green vegetation growth on and along the soil-road. The peak with the smallest band 5 and 7 grey level values in the date 1 frequency feature space (figure 3.5a) may represent a moist, unvegetated, dark soil-sand. The peak with the largest band 5 and 7 grey level values may represent a dry, light coloured soil (sand) with some vegetation growth. A soil line can be drawn along the bottom of the date 3 frequency feature space (figure 3.5c) in the direction of maximum spectral variation. Values located perpendicular to the soil line may suggest a vegetation line.

The bare soil class was influenced by many factors and created a highly dispersed, multi-peaked frequency feature space. Three pixels with low band 5 and band 7 values were deleted from the date 2 frequency feature space (figure 3.5e). The cleaning procedure deleted one quite separate soil pixel which had a high band 7 and a low band 5 grey level value from the date 3 class (figure 3.5f). The deleted pixel possibly covered an area that contained an excess of vegetation growth. Another pixel from the date 3 soil class was deleted at the end with the highest band 5 and band 7 values (figure 3.8). Determining outliers for a bare soil class is a difficult task, regardless of the cleaning operation employed.

4. Parametric and Non-Parametric Decision Spaces

Wasrud and Lulla (1985) pointed out the need to understand how classifiers create decision space boundaries. "Further comparison of classification algorithms may also focus on the different ways in which the algorithms partition feature space. This may explain the differences in classifier accuracy, and additionally, may aid in determining the most effective parameters to use with the classifiers." Many analysts use the confusion matrix to determine the accuracy of a classification. Other analysts use measures such as transformed divergence to calculate class separability. Abstract measures are employed to determine what is happening between the feature spaces, decision spaces, and the resulting classification, while the complementary, concrete, graphic displays are ignored. A graphic display of the decision spaces could enhance the ability of the analyst to interpret the results presented in a confusion matrix. A non-parametric classifier is described in this chapter and the decision spaces from this classifier are compared against the decision spaces from three parametric classifiers. A simple non-parametric test is also presented which determines bivariate class normality.

4.1 Three Parametric Classifiers

Three common parametric classifiers are the parallelepiped, linear classification function, and maximum likelihood classifiers. The parallelepiped classifier has the simplest decision space geometry and is the fastest computationally. The algorithm is sensitive to class variance in each spectral channel by taking into account the range of spectral values in a class. The decision space for a class is defined by the minimum and maximum spectral values in each spectral channel used in the classification (Lillesand and Kiefer 1979). A two channel parallelepiped classification has rectangular decision spaces (figure 4.1a). The decision space boundaries of the parallelepiped classifier must be parallel to the feature space coordinate axes which creates a poor-fitting decision space when the spectral values for a class are highly correlated. The decision space geometry is also prone to considerable overlap in adjacent classes, especially when the spectral values

in one class are highly correlated. An image processing technique to decorrelate the spectral channels, such as principal component analysis, could be used prior to a parallelepiped classification.

Linear classification function classifications are more accurate than a parallelepiped classification although computing costs are increased. A linear classification function decision space is characterized by straight boundaries which need not be parallel to the feature space axes (figure 4.1b). Although the decision space fit to correlated data is better than the parallelepiped decision spaces, the linear boundaries cannot closely follow a non-linear feature space. The decision space boundary between two classes is based on the crossover point where the probability of belonging to either class is equal, assuming equal prior probabilities. Many different distance functions can be used to define decision space boundaries (see Batchelor 1974) resulting in many different decision space boundaries for the same classes. Curvilinear classification functions have been developed to create closer fitting decision spaces, although this entails more computing costs and still is based on the assumption that the classes are multivariate normal. For a fuller discussion of linear classification functions refer to Klecka (1980) or Davis (1973).

The maximum likelihood classifier is the most accurate and most computationally complex of the three parametric classifiers. The maximum likelihood classifier is very accurate because both the variance and correlation of each class is taken into account when classifying an unknown pixel (Lillesand and Kiefer 1979). The decision space is defined by an equiprobability ellipse (figure 4.1c). A highly correlated class is represented by an ellipse with a very long major axis and a very short minor axis, while an uncorrelated class is represented by an ellipse where the major and minor axes lengths are equal. A drawback of the maximum likelihood classifier is the large number of computations required for a classification. Classification time increases with the square of the number of spectral bands added, therefore the increase in computing time cost must be weighed against the increase in accuracy with the additional time needed to analyze a large number of spectral

channels (figure 4.3).

There is a need in classification not only to separate the specified classes from each other, but also from unknown or unwanted classes (Schowengerdt 1983). Parametric classifiers will force all pixels from an image into one of the defined classes unless probability threshold boundaries are introduced for each class. A user may define five different forest classes and no water class, for example. When the satellite image is classified, all water pixels will be placed into one of the five forest classes, unless probability thresholds are defined for each forest class.

Three problems were associated with the parametric classifiers. The first problem was concerned with the fact that parametric classifiers were based on the assumption that the spectral classes were multivariate normal. The second problem was that the rigid decision space geometry of the parametric classifiers did not always accurately follow the geometry of the feature space. The third problem arose from the large number of calculations needed to classify each pixel in a multispectral image. This last problem is more relevant for the linear classification function and the maximum likelihood classifiers.

4.2 The Frequency Feature Space Template Classifier

A non-parametric classifier was developed with a decision space geometry that conformed closely to feature space. Percent volume contours were generated for the frequency feature spaces. These contours can also be used as a non-parametric decision space boundary for a class. The decision space fits closely to the feature space but does not have a predetermined geometric shape. A more natural decision space was generated because the data were not forced to behave as if they were multivariate normal. The decision space conformed to the feature space rather than having the feature space conform to the decision space.

The non-parametrically derived decision spaces (frequency feature space boundaries) were stored in a template for classification. A template for the Frequency Feature Space Template (FFST) classifier was a grid which used two spectral channels in a classification.

The number of rows and columns in a template for a two channel classification equalled the range of possible grey level values in each channel. The brightness range of many spectral channels is 0 - 255 therefore 256 rows and 256 columns will be present in a two channel template. Each grid cell in the template was assigned a unique class number, (eg. 0 = unclassified, 1 = soil), which corresponded to the location of each decision space. The overlap area between classes was given a separate number and relabelled as CLASS A + CLASS B (Figure 4.3). The classification scheme using the template entailed storing the template in computer memory, reading in the spectral values for each pixel from the satellite image, checking the class number in the template defined by the spectral values for each pixel, and placing the class number into an output file to contain the classified image. The certainty of correct classification could be increased by choosing a smaller percent volume contour as the threshold for each class. Figure 4.4 presents the FFST classifier decision spaces for the original and cleaned classes. Figures 4.5 - 10 present the decision spaces derived by the three parametric classifiers from the original and cleaned class values. Each class was cleaned using cluster analysis to keep the comparisons between the classifiers equal. The decision spaces from the non-parametric and parametric classifiers are discussed in detail later in the chapter. The spectral classes were first tested for bivariate normality to help determine the similarities and differences between the decision spaces derived by each classifier.

4.3 A Statistical Test for Bivariate Normality

Crane et al. (1972) determined that the spectral values of many agricultural crops were non-normal by applying a univariate chi-square (χ^2) normality test to the spectral values. Two or more spectral channels are commonly used in a classification therefore classes should be tested for multivariate normality. Two non-parametric statistical tests were required for a check on bivariate normality: the χ^2 test, and the Kolmogorov-Smirnov

test. The χ^2 and Kolmogorov-Smirnov tests are "goodness-of-fit" tests which determine how closely a sample distribution fits a theoretical distribution. The procedure applied was duplicated from work done by Eyton (1984). Spectral pairs from each class were first fit into a χ^2 distribution, then χ^2 deciles were generated and the number of spectral pairs falling within each decile were counted. The Kolmogorov-Smirnov test was applied to determine whether the frequency feature spaces, presented as χ^2 deciles, were bivariate normal. The Kolmogorov-Smirnov test is based on the maximum value of the absolute difference between the sample cumulative frequency distribution (CFD) and the theoretical CFD for each class. The formula for the Kolmogorov-Smirnov test is: (Harnett 1982)

$$D = \text{Max} \mid T_i - S_i \mid$$

where;

D = the test statistic
T = the theoretical CFD
S = the sample CFD

The decision to reject the null hypothesis (H_o: there is no difference between the sample and theoretical distributions) depended on the value of D. A large value of D increased the probability that H_o was false (Ebdon 1985; Harnett 1982). The theoretical frequency in each decile should be the same, based on the normality assumption. Surfaced values from the multiquadric equation were used in the test rather than the original training field values because of the small sample size of many classes. A minimum of 100 spectral pairs are recommended to be used in the Kolmogorov-Smirnov test. The smoothing and surfacing operations did not create normally distributed classes when the data were non-normal, or create non-normally distributed classes when the data were normal.

Tables 4.1 - 3 provide the value of D for the classes and the critical value for each class at α=0.05. Four out of five original spectral classes for each date were bivariate non-normal. The cleaning operation had little effect on bivariate normality except when an

isolated outlier was removed from an otherwise tightly clustered spectral class. Some observations based on the statistical test are given for the cleaned classes. The corn class was bivariate normal only at date 3 which was when corn was at maximum maturity. More bare soil than corn plants should be visible at date 1 therefore a soil signature would mainly be recorded. Bare soil was non-normal for all three dates; the multimodality of the frequency feature space was probably due to differences in soil type, moisture content, and amount of vegetation growth. The forest frequency feature space at date 3 was probably bimodal. The bivariate non-normality of the date 2 water class may be due to a lack of precipitation causing the water bodies to decrease in size and become more shallow. The growth of winter wheat crops in the fall of the previous year probably helped form a normally distributed date 1 class. There was a transition from winter wheat to soybean crops in date 2, leaving a large amount of soil visible, thereby making the class bivariate non-normal. The soybean class at date 3 remained non-normal through the cleaning operation, yet appeared to be bivariate normal. The difference between the critical value (α) and D was only 0.008 which indicated that the distribution was very nearly normal. The distribution of the soybean class may be platykurtic.

4.4 Comparisons Between the Parametric Classifiers: Date 1

The parallelepiped decision space boundary for the winter wheat class exhibited a considerable decrease in size after the cleaning operation. The original parallelepiped decision space for winter wheat enclosed the original decision space for forest (figure 4.5a); after cleaning, the forest and winter wheat classes did not overlap (figure 4.8a). Another dramatic reduction in parallelepiped decision space size came from cleaning the soil class. The high positive correlation between the band 5 and 7 values for the corn-soil class created large areas of potential misclassification within the parallelepiped decision space.

One difference between the parallelepiped and linear classification function decision

spaces was the absence of overlap areas between the decision spaces for the linear classification function. The linear classification function created non-overlapping decision spaces (figure 4.5b). Some decision spaces from the parallelepiped classifier fit closer than the linear classification function decision spaces to the feature spaces. Decision spaces of forest, winter wheat, and water, defined by the parallelepiped classifier were more compact than the same linear classification function decision spaces. The linear classification function decision space for forest included nearly half of the measurement space. Other decision spaces defined by the parallelepiped classifier did not fit as closely as the linear classification function decision spaces to the feature spaces. The parallelepiped decision space for the corn class overlapped the forest, winter wheat, water, and soil decision spaces defined by linear classification function classifier.

The decision spaces for the forest, winter wheat, and water classes from the parallelepiped and maximum likelihood classifiers (figure 4.5a,c) covered near identical areas, although the parallelepiped classifier required a smaller amount of computation time to generate the decision spaces. As a spectral class became more correlated, the maximum likelihood classifier geometry allowed the decision space to more closely follow the feature space. The maximum likelihood classifier decision space for corn was smaller than the parallelepiped classifier decision space for corn because the maximum likelihood classifier took the correlation between spectral bands into account in the generation of the decision space. The maximum likelihood classifier decision spaces followed the trend of the feature spaces for all but two classes: corn-soil and bare soil. These two classes were bivariate non-normal. The ends of the major axes from the maximum likelihood decision spaces fell outside the feature spaces to create a statistically optimal fit based on the normality assumption.

4.5 Comparisons Between the Frequency Feature Space Template Classifier and the Parametric Classifiers: Date 1

Cleaned FFST decision spaces (figure 4.4d) for the forest, winter wheat, and water

classes corresponded closely to the cleaned maximum likelihood decision spaces (figure 4.8c). The FFST decision spaces were slightly larger and encompassed the maximum likelihood decision spaces. The decision spaces from the FFST classifier fit much better to the highly correlated, bivariate non-normal corn-soil and soil feature spaces. Interband correlation was accounted for parametrically by the maximum likelihood classifier, while the FFST classifier accounted for interband correlation non-parametrically. The FFST classifier decision spaces were similar to the maximum likelihood classifier decision spaces except that the FFST classifier followed the trend of each class closer and displayed more of the variability along the boundary of the feature spaces.

The deletion of outliers created only small, local changes in the FFST decision spaces and left the remainder of the decision spaces unaffected. The overlap area between the winter wheat class with the forest, corn-soil, and bare soil classes was minimized after the classes were cleaned (figure 4.4a,d). Overlap between the corn-soil and water classes was also minimized. Part of the overlap between classes was due to the spread of the multiquadric surface caused by smoothing the original data.

4.6 Comparisons Between the Parametric Classifiers: Date 2

The cleaning operation greatly decreased the size of the parallelepiped classifier decision spaces and the overlap between decision spaces (figures 4.6a, 4.9a). The correlated winter wheat-soybean class had the largest potential for misclassification because of the decision space overlap with the corn and soil decision spaces, and the poor fit of the parallelepiped decision space to the feature space. A much smaller area in measurement space was occupied by the decision space for soil after the cleaning operation.

Three observations in regard to the decision spaces for the linear classification function classifier (figure 4.6b) can be made. The first observation concerns the difference between the large decision space area for the forest class compared to the small feature space. A pixel with band 5 and band 7 grey level values of 70 and 60 respectively has a low

probability of belonging in the forest class for example, yet falls within the linear classification function decision space for forest. The second observation regards the poor fit of the decision space to the corn feature space. Band 5 and 7 grey level values were negatively correlated in the corn feature space, while a positive correlation was displayed in the corn decision space. The third observation concerns the poor decision space fit to the winter wheat-soybean feature space. The winter wheat-soybean decision space was defined by a triangular area with greater band 7 variation toward the larger band 5 grey level values, while the feature space indicated larger band 7 variation occurred towards smaller band 5 grey level values. The triangular decision space for winter wheat should be rotated 180 degrees for an optimal visual fit.

The maximum likelihood decision spaces (figure 4.6c) generally followed the trend of the feature spaces. Two, long, highly correlated, bivariate non-normal classes (soil and winter wheat-soybeans) had a visually suboptimal fit between the maximum likelihood decision spaces and the feature spaces. The less correlated, cleaned water and forest classes had very similar maximum likelihood and parallelepiped decision spaces. A more economic approach to classification may be the use of the parallelepiped classifier for slightly correlated classes and the use of the maximum likelihood classifier for highly correlated classes.

4.7 Comparisons Between the Frequency Feature Space Template Classifier and the Parametric Classifiers: Date 2

The FFST and parallelepiped decision spaces (figures 4.4b, 4.6a) were similar for all but the soil and winter wheat-soybean classes. The parallelepiped classifier had a poor-fitting decision space for these two classes because the spectral channel values in each class were highly correlated. Overlap between the winter wheat-soybean and soil decision spaces for the FFST classifier was tremendously decreased after applying the cleaning operation (figure 4.4b,e). The FFST classifier decision spaces for the winter wheat-soybean and soil classes fit closer to the feature spaces than the corresponding

maximum likelihood decision spaces. Decision spaces from the FFST classifier (figure 4.4b) were larger than the maximum likelihood decision spaces (figure 4.6c) which allowed more variability to be captured in the delineation of each class. The smoothing operation enlarged the FFST decision spaces, therefore if a closer fitting decision space was required, a smaller percent volume contour could be used.

4.8 Comparisons Between the Parametric Classifiers: Date 3

Class values were less correlated between bands 5 and 7 at this date compared to dates 1 and 2 which lessened the overlap between the parallelepiped decision spaces. One outlier from the water class was deleted by the cleaning operation which made the cleaned parallelepiped decision space much smaller and eliminated the overlap with the corn decision space (figures 4.7a, 4.10a). There was an area of overlap between the parallelepiped decision spaces for soybean, forest, and corn. The linear classification function classifier placed this triple overlap area into the forest class (figure 4.7b). The linear classification function decision space for water did not fit well to the feature space. Most of the water feature space was located on the left side of the decision space. The soybean and soil decision spaces covered most of measurement space yet the feature spaces (figure 3.8) occupied small areas in measurement space.

The decision spaces defined by the maximum likelihood classifier (figure 4.7c) fit closer to the feature spaces than the decision spaces defined by the parallelepiped and linear classification function classifiers (figure 4.7a,b). The triple overlap area between soybeans, forest, and corn was mostly unclassified by the maximum likelihood classifier. A 95% confidence threshold was set for the maximum likelihood classifier, therefore if a different confidence threshold had been set, a different amount of class overlap would be displayed. The geometry of the maximum likelihood decision space allowed the negative correlation in the soybean feature space and the positive correlation in the water feature space to be displayed in the decision space plots, while the linear classification function classifier fit did not allow the correlation to be viewed in the decision space plots.

4.9 Comparisons Between the Frequency Feature Space Template Classifier and the Parametric Classifiers: Date 3

Two separate FFST decision spaces for forest were created after applying the cleaning operation (figure 4.4c,f). A hole of zero frequency was located in the original forest decision space which corresponded to the area between the two frequency feature space peaks. The main forest peak after cleaning was separated from both the minor forest peak and the overlap area between the soybean and corn classes. Both forest peaks were encompassed by the parallelepiped and linear classification function decision spaces, while the maximum likelihood classifier centered the decision space on the main peak. The two separate peaks may represent two different tree types, or healthy trees in the main peak and stressed trees in the minor peak. There was not enough ground truth information available to qualify the analysis. The FFST classifier decision spaces (figure 4.4c) covered a larger portion of each feature space than the corresponding maximum likelihood classifier decision spaces (figure 4.7c). The FFST classifier and the maximum likelihood classifier had different forest and soybean decision spaces. There were two separate peaks in the forest frequency feature space. The main peak had a major axis parallel to the band 7 axis which indicated a large variation in band 7 grey level values, while the maximum likelihood classifier ellipse had a major axis oriented at approximately 170° which indicate larger band 5 variation. The maximum likelihood classifier must align the major axis of the decision space between the major and minor peaks and will therefore not show the large band 7 variability in the major peak. The FFST classifier did not present this problem and the shape of both peaks was retained. Forest was a bivariate non-normal class and the inadequacy of the parametric maximum likelihood classifier decision space to fit to the forest class was evident. There was some overlap between the cleaned FFST decision spaces for corn and water, but this overlap was due to the spread of the multiquadric surface caused by smoothing the original data.

5. TM and MSS Frequency Feature Space Analysis

Greater intraclass variability is detected as the spatial resolution increases for satellite scanners, therefore a change in feature space shape and decrease in the probability of bivariate normality is expected with this increase in spatial resolution. Two anniversary Landsat images, one TM and the other MSS, over the Alexander Indian Reservation (A.I.R.) in Alberta (Plates 5.1, 2) were used to test these two assumptions. These colour plates and the remainder of the colour plates of the study area were linearly stretched interactively on a Decision Images image processing system, therefore grey level values/colours in one image are not directly comparable to other images.

July meteorological summaries for both years were obtained for the Edmonton area and used to account for possible class differences due to weather variations (Atmospheric Environment Service 1984; Atmospheric Environment Service 1986). Figures 5.1, 2 present histograms showing the amount of precipitation received during the month of July for both years. The total amount of precipitation for July 1984, before the date of imaging by the TM, was 45.1 mm. The total amount of precipitation for July 1986, before the date of imaging by the MSS, was 107.0 mm. Approximately 2.4 times more rain fell in July 1986 than in July 1984. July 1986 exceeded the monthly record for the amount of precipitation that fell in the Edmonton area. The monthly average for precipitation in July is 88.7 mm. Three days before the MSS imaged A.I.R., approximately 43.0 mm of rain fell and the following day another 8.0 mm of rain fell. In the second and third days before the TM imaged the study area, less than 3.0 mm of rain fell in total. Wind speed for both dates was minimal - 10.3 km/hr for July 20, 1986 and 10.9 km/hr for July 23, 1984 - therefore class differences caused by wind should be negligible.

The frequency feature spaces were compared visually to determine differences between general cover classes at different spatial resolutions. The χ^2 and Kolmogorov-Smirnov tests were applied to the TM and MSS imagery to determine whether the probability of

bivariate normality decreased at a finer spatial resolution. The MSS frequency feature spaces were subtracted from the TM frequency feature spaces to determine which portions of the frequency feature space showed a change in frequency value at the increased spatial resolution. Effects related to differences in radiometric resolution between TM and MSS data were not addressed.

5.1 Preprocessing and Generation of Frequency Feature Spaces

Preprocessing consisted of geometrically registering the two Landsat scenes to a UTM grid. Pixels in the TM scene were resampled to a ground cell size of 20m x 20m and the pixels in the MSS scene were resampled to a ground cell size of 50m x 50m using the nearest neighbour method. The size of the TM scene was 550 scan lines by 550 pixels per scan line and the size of the MSS scene was 220 scan lines by 220 pixels per scan line. Nearest neighbour resampling was chosen because this method did not change the grey level values of the original data. A first degree polynomial transformation was used to place the Landsat scenes into UTM coordinates. The images were preprocessed at the Province of Alberta Remote Sensing Center on a Dipix Aries II image analysis system. There were two reasons for preprocessing the imagery; the first reason was that most mapping procedures require satellite images to be placed into a map projection coordinate system, and the second reason was that geometric registration and resampling facilitated the accurate extraction of training fields.

Four general cover classes were picked for classification. Three of the classes (water, aspen, and pasture) had training field locations similarily located in both scenes. The fourth class was canola crop and since crop type in each field changes from year to year, different canola fields were chosen from the two images. Ground truth for the study area consisted of:

1. Terrestrial 35mm colour slides taken of the study area on July 21, 1986.
2. Oblique 35mm black and white aerial photographs taken over the study area on

December 3, 1986 and were used to discriminate between deciduous and coniferous trees.

3. 1:12,000 Land use/cover maps provided by the Government of Canada, Department of Indian Affairs.
4. 1:60,000 black and white stereopairs of May 9, 1985 produced by the Province of Alberta, Resource Evaluation and Planning Branch.
5. An interpretation key produced by the Province of Alberta Remote Sensing Center for the TM scene (Sutherland 1986).
6. A hardcopy image of the TM scene corresponding to the above key using channels 3, 4, and 5.
7. Outlines on aerial photographs of the canola fields for the summer of 1986 provided by the Alexander Indian Reservation agricultural officer.

MSS bands 5 and 7 were chosen for this thesis because research (eg. Hall et al. 1984) has shown that bands 4 and 6 were highly correlated to bands 5 and 7 respectively. MSS band 4 is also noisier than the other bands because Rayleigh scattering is more pronounced at these wavelengths. TM channels 3 and 4 were compared with MSS channels 5 and 7. There is some difference between the spectral range for MSS band 7 (800nm - 1100nm) and TM channel 4 (760nm - 900nm), but research (Crist and Cicone 1984) has indicated that the significance of this difference may be minimal. Crist and Cicone (1984) using simulated TM and MSS imagery determined that the correlations of MSS bands 4, 5, and 7, with TM channels 2, 3, and 4 respectively were approximately 0.99. Plates 5.3, 4 show the images for the red and infrared channels from the TM and MSS scanners.

Two or more training fields were chosen for each class to try to capture intraclass variability. An assumption was made that the training fields chosen were truly representative of the cover types in the study area. Plates 5.5, 6 show the locations of the training fields. The choice of training field size was limited by the resolution cell size of

the MSS. Table 5.1 lists the total number of original and cleaned spectral pairs for each class from the two images. Cluster analysis was used to clean the classes. Frequency feature spaces were generated only for the cleaned training fields.

5.2 A Visual Comparison Between the TM and MSS Frequency Feature Spaces

The assumption that increased spatial resolution increased intraclass variability was studied by a visual comparison of four TM and MSS frequency feature space plots. Figures 5.3,4 present the cleaned spectral classes for the TM and the MSS images in a traditional feature space plot. Figure 5.5 presents the individual frequency feature space plots for the cleaned MSS classes. Figure 5.6 presents the individual frequency feature space plots for the cleaned TM classes. The frequency feature spaces are presented as 10% volume contours.

5.2.1 Canola

The varieties of canola and contrast in planting dates causes flowering to occur at slightly different times in July therefore different frequency feature spaces can be expected yearly. The TM and MSS frequency feature spaces for canola were different (figures 5.5a, 5.6a). The MSS frequency feature space was more disperse than the TM frequency feature space. The highest peaks in the MSS frequency feature space were located toward high band 5 and high band 7 grey level values, while lesser peaks were located toward lower band 5 and lower band 7 values. This dispersion may represent canola crops at various stages of flowering. Three, large, tightly clustered peaks were located in the TM frequency feature space which indicated that the canola plants from the training fields selected were near to the same stage of flowering. Both frequency feature spaces were positively correlated which was expected when canola plants flowered.

5.2.2 Water

The TM frequency feature space for water was more tightly clustered than the MSS

frequency feature space for water (figures 5.5b, 5.6b). The TM frequency feature space had one main peak located at the low channel 3 and 4 grey level values which was suggestive of water with little sediment load or algal scum. The MSS frequency feature space had a large range of band 7 grey level values which may represent a large sediment load in the water bodies. Heavy rainfalls preceded the date of MSS imaging and possibly caused runoff to carry soil into the water bodies. Training fields were extracted from three differently sized water bodies. The training field from the interior of Sandy Lake probably had the clearest water therefore the grey level values would be expected to be low. The two other water bodies were smaller and shallower than Sandy Lake and the grey level values from the two water bodies may represent the larger band 7 grey level values in the frequency feature space. There was little precipitation before the TM imaged the study area therefore the grey level values from the training fields would be expected to be more similar. There was only one main peak in the TM frequency feature space which supports this assertion.

5.2.3 Aspen

The TM and MSS frequency feature spaces had a very similar shape (figures 5.5c, 5.6c). Both frequency feature spaces showed a large variation in the infrared radiation values and a small variation in the red radiation values. The frequency feature spaces were neither strongly positively or negatively correlated. A negative correlation for aspen was expected because trees have leaves in July. The lack of correlation may be caused by radiometric striping in the image. Both frequency feature spaces showed two large peaks. Within the two peaks in the TM frequency feature space there was little internal variation. There was much more spectral variability in the peak with the lower band 7 grey level values from the MSS frequency feature space. The top peak from both frequency feature spaces may represent healthy, green leaved aspen, while the lower peak may represent stressed aspen. An inspection of the study area (July 21, 1986) revealed that the aspen on

the south side of the highway and west of Low Water Lake had fewer leaves than the aspen to the north of the highway. The aspen on the south side of the highway were attacked by tent caterpillars in previous years (secretary from the Alexander Indian Reservation 1986) and the leaves were just now returning to the same vigour as the untouched aspen on the north side of the highway.

The symmetry of the peaks along the band 5 and 7 axes for the MSS aspen frequency feature space may be caused by radiometric striping. Within the two main peaks for aspen there were subpeaks, and the subpeaks appeared to be paired. The paired peaks may represent aspen with a certain band 5 and band 7 value on the left, and to the right, aspen with the same band 7 value, but larger band 5 values caused by radiometric striping. The MSS band 5 image (Plate 5.3a) showed much more radiometric striping than the band 7 image (Plate 5.3b) therefore the band 7 values for aspen between the calibrated and miscalibrated scan lines were more similar. Subpeaks within the two central peaks in the TM frequency feature space were expected if the radiometric striping in the image was severe. The increased spatial resolution of the TM scanner may have minimized the spectral differences between the calibrated and miscalibrated scan lines.

5.2.4 Pasture

Two sections can be defined in the frequency feature space for pasture. The first section covered the area parallel to the infrared axis, while the second section had lower infrared values and displayed a positive correlation between the infrared and red radiation channels for the TM frequency feature space (figure 5.6d) and a negative correlation for the MSS frequency feature space (figure 5.5d). Pasture at A.I.R. was unirrigated grassland, which contained scattered aspen and willows. Grey level values from pasture should be mainly from the grasses. The grass in the pasture was kept short by cattle grazing. The pasture at A.I.R. can be divided into two sections; the northern half is hilly and has scattered trees while the southern half is flatter and the trees are more clustered together.

Training fields were extracted from both parts of the pasture.

High intraclass variability was present in the MSS frequency feature space for pasture. The two sections in the TM frequency feature space were presented as two smooth peaks while the MSS frequency feature space for pasture showed many subpeaks within the two peaks. This observation is contrary to the assumption that greater internal variability is visible with higher spatial resolution TM imagery. The finer TM spatial resolution may have allowed large areas with trees and grasses to be broken up into smaller resolution cells which contained purer areas of grasses and purer areas of trees and shrubs. The spectrally purer pixels from the TM would form two homogeneous peaks in the frequency feature space, while the MSS, with the coarser spatial resolution, would create more heterogeneous class cover pixels and have a more diverse frequency feature space. There was a higher degree of radiometric striping in the MSS imagery therefore the heterogeneity in the pasture class may also be caused by the differences between the calibrated and miscalibrated scan lines. The top section of the frequency feature space with large infrared and small red radiation values was probably lesser grazed grasses while the bottom section was probably intensely grazed grasses. The soil signature was more prominent in the lower portion of the frequency feature space because of intensive grazing by cattle. The fresnel effect would not be strong for the entire area of shorter grasses, therefore the infrared values in the lower peak would not be as large as the infrared values in the upper peak. The degree of grazing and the amount of soil moisture may be two factors that helped define the shape of the lower peak. An area of intense grazing and little soil moisture would have a soil-type signature while an area with little grazing and a moist soil would have a healthy, green grass signature. Differences in the amount of soil moisture may help determine why the lower section of the TM frequency feature space was negatively correlated and the MSS frequency feature space was positively correlated. A tremendous amount of precipitation fell a few days previous to the date the MSS imaged

the study area, therefore the grasses would be expected to be very green and vigorous. The grass that had been grazed less should be longer and cover more of the soil than the grass which had been intensively grazed. Only a trace of precipitation fell a few days previous to the date the TM scanned the study area. The lack of precipitation combined with the cattle grazing could cause a large amount of soil to be visible to the TM and make the lower portion of the frequency feature space positively correlated.

5.3 Results From the Test on Bivariate Normality

The χ^2 and Kolmogorov-Smirnov tests were applied to the TM and MSS frequency feature spaces to determine whether the classes were bivariate normal. The surfaced values, rather than the original grey level values were used in the test. Table 5.2 lists the "D" value from the Kolmogorov-Smirnov test along with the critical value at α=0.05. Results from the test indicated that all cleaned classes from the MSS scene were bivariate non-normal. All the cleaned TM classes but canola were bivariate non-normal. These results were expected considering the visual description of the frequency feature spaces. The frequency feature spaces for aspen and pasture were described as two peaks and therefore were probably bimodal. An increased sediment load in the water from the MSS image could create a dispersed, multimodal frequency feature space. The TM frequency feature space for canola was the only bivariate normal class. The training fields may have covered those areas where the canola was at the same stage of flowering. The greater frequency feature space dispersion in the MSS canola class denoted that different stages in flowering were probably captured in the selection of training fields.

5.4 Results From Differencing the MSS Frequency Feature Spaces from the TM Frequency Feature Spaces

The frequency feature spaces for aspen, pasture, and water were differenced to compare how the locations of the maximum spectral frequencies varied at increased spatial

resolution. The canola class was not analyzed because the training fields from the TM image and the MSS image were not identically located. To produce the differenced grids the mean center for each frequency feature space was determined first, then the TM and corresponding MSS frequency feature spaces were registered using the mean centers, and lastly the MSS frequency feature spaces were subtracted from the corresponding TM frequency feature spaces. Only those pixel locations with a non-negative value in both the TM and MSS frequency feature spaces were differenced. Plates 5.7 - 9 show the differenced grids. A T-test for skewness and kurtosis was applied to the differenced values and the results of the T-test (Table 5.3) indicated that the differenced grids had a significant skew and kurtosis. All three differenced grids were extremely leptokurtic. The leptokurtic peak occurred near the zero difference which indicated that the TM and MSS frequency feature space volumes were very similar at many points.

5.4.1 Pasture

The mean value of the differenced grid for pasture was 0.067. The mean value was greater than zero possibly because the TM frequency feature space for pasture was less disperse than the MSS pasture frequency feature space and would therefore have had a greater percent volume at each point. Pasture showed the closest mean difference to the theoretical mean difference of zero. Areas of zero difference were located away from the peaks. Large positive value differences were located in the peaks which indicated that the TM frequency feature space peaks for pasture had a higher percentage of the total frequency feature space volume compared to the MSS frequency feature space peaks. The finer spatial resolution of the TM may have resolved purer and therefore less variable spectral class values to create higher percent frequency volume peaks for pasture. Peaks in the MSS frequency feature space were more disperse and contained less percent frequency volume than the TM peaks. This result may have been caused by the coarse MSS spatial resolution which would result in more heterogeneous pixels. Two peaks were present in

the differenced grid. The largest positive difference was located in the upper peak and probably represented lesser grazed grasses. The lower peak may represent highly grazed grasses which would therefore show more of the soil and create more heterogeneity.

5.4.2 Aspen

The mean value of the differenced grid was 0.137. Differences with a value near zero covered a large portion of the grid. These values were located away from the two main peaks located in the TM and MSS frequency feature spaces. The small amount of differenced values below zero indicated that the MSS pixels generally did not have a higher percent value than the TM pixels at each grid point. The largest positive departures from the mean were located at the centers of the two major peaks which could indicate that the higher spatial resolution TM scanner created a more homogeneous, spectrally purer frequency feature space peak than from the MSS scanner. Away from the peaks of purer aspen pixels, the TM and MSS pixels were more similar.

5.4.3 Water

Water from one date should be very similar to water from another date. The mean difference value for water was 0.519. This was a very large mean difference value, but most of the differenced grid area had values below the mean. The water frequency feature space from the TM scene was presented as a main peak in the low red and infrared values. The MSS frequency feature space for water had three peaks with the largest peak located at the lowest red and infrared values and the remaining two peaks located at the larger infrared values. More percent frequency volume was contained in the main peak of the TM frequency feature space compared to the main peak in the MSS frequency feature space. The main peak in both frequency feature spaces should have represented clear water. Differences between the main peaks may be caused by the excessive rainfall prior to the date of the MSS scan which transported soil into the water bodies to create more heterogeneous pixel values. The two minor peaks in the MSS frequency feature space for

water may represent varying degrees of suspended sediments. These two peaks did not have large difference values when subtracted from the TM frequency feature space for water.

6. Conclusions and Future Research

6.1 Impact of Research on Traditional Remote Sensing Classification Methods

Background information on imaging systems, digital image processing, and classification was presented in Chapter 1. The type of multispectral image in addition to the type of image processing applied to the image before classification will affect classification accuracy. Many multispectral scanning systems are currently in use with different spatial resolutions and spectral channels, therefore a classification method for one group of imagery, eg. Landsat MSS, may not be appropriate for another group of imagery, eg. MEIS imagery. There appears to be a trend in the remote sensing community toward higher spatial and spectral resolution data. Acquisition of satellite multispectral imagery began with the coarse 80m spatial resolution Landsat MSS. Knowledge gained in the analysis of MSS imagery can provide researchers with a basis with which to develop better classification and analysis schemes for the higher spatial and spectral resolution TM and SPOT satellite images and the data provided by high resolution aircraft scanners.

Researchers model satellite imagery from aircraft imagery to determine what can be expected when a new satellite scanner system is launched. No research has beem found which reported on the possible change in class normality at increased spatial resolutions and could have been tested using simulated satellite imagery. An inadequate amount of reported research describing the statistical distribution of satellite image classes was also apparent. Crane et al. (1972) presented the results of a test for univariate class normality; in this thesis the results of a test for bivariate class normality was presented. Subsequent research should incorporate three or more spectral channels.

One problem associated with preprocessing is the effect of resampling pixels for the output image. Verdin (1983) determined that geometrically corrected imagery contained anomalous values which could affect classification accuracy:

"...changes in radiometric fidelity could also create problems if qualitative

> information is to be derived by digital means, as in using a maximum likelihood classifier to map land cover, or in identifying surface water area by spectral signature..."

The cosmetic appearance of a satellite image is a concern to many users. Processed satellite images are expected to be of high cartographic quality. Cubic convolution and bilinear interpolation are two resampling methods which creates a smoothed image that appears more like a photographic image. The values in the output image from cubic convolution and bilinear interpolation are not the same values as in the original image; the output image is transformed. Cubic convolution and bilinear interpolation may not drastically change the spectral values of large, relatively homogeneous areas (eg. agricultural areas) but in a spectrally heterogeneous area, such as a city, many different spectral classes can be located within a span of four pixels. The output pixel value will therefore be a compromise between the many spectrally different classes. The nearest neighbour resampling algorithm transfers the spectral value of the pixel from the input image spatially closest to the output pixel location into the output pixel location. Nearest neighbour resampling does not smooth the input spectral values but does leave the output image with a blocky appearance, especially in areas where there are many man-made geometric features. This blockiness is not as apparent in very fine spatial resolution imagery. The classes from the output images using various resampling routines could be tested for multivariate class normality. A slightly skewed class in an original image may become normally distributed after the application of the cubic convolution procedure. Geometric registration may be applied to multispectral images after classification to avoid affecting the statistical distribution of the spectral classes.

Radiometric striping is a common feature in multispectral imagery which can be minimized by a preprocessing algorithm. The striping is a result of the miscalibration of a detector in the imaging system relative to the other detectors causing one scan line to be either brighter or darker than the surrounding scan lines. These abnormally bright or dark scan lines may cause a class to be skewed toward the miscalibrated values or form a

separate peak creating a bimodal class. Some users do not destripe multispectral imagery before classification. A useful study might be to determine if radiometric striping does affect class normality.

Results from the test for bivariate normality indicated that spectral classes had a high probability of being non-normal. Maynard and Strahler (1981) ascertained how even a slight skew in a spectral class adversely affected the accuracy of a parametric classification. Non-parametric classifiers categorize non-normal classes better than parametric classifiers but are rarely used by analysts. There are three possible reasons why many analysts do not use non-parametric classifiers. The first reason is that parametric classifiers were amongst the first to be implemented and analysts became more accustomed to this approach. The second reason is that parametric classification programs were more readily available than non-parametric classification programs. The third reason is that it is easier to work with normally distributed data. Users may not want to acknowledge that data can be skewed or multimodal because this prevents an uncomplicated approach to classification.

Parametric classification schemes are employed on images of varied spatial resolution. Research could be undertaken to compare the accuracy of a parametric classification over one area at various spatial resolutions using multistage aircraft scanner data. The statistical distribution of each class can also be determined at the different spatial resolutions. The type of imagery being used and the kind of image processing which has been applied to the imagery before classification could be two factors that help the analyst determine which classification scheme is the most appropriate to use.

6.2 Comments on the Development of the Frequency Feature Spaces

Interclass and intraclass relationships were easily recognized when the spectral classes were presented graphically as frequency feature spaces because the frequency feature space exploited man's spatial processing ability. A cursory understanding of a bivariate spectral class can be gained by analyzing a traditional feature space plot and the associated histogram for each spectral band. The frequency feature space saved the user from having

to correlate peaks in the histograms with a location in the feature space. The frequency component was added into the feature space plot so that only one image need be examined.

The frequency feature space was described mathematically by an exact-fitting multiquadric equation with the result that some unsmoothed classes caused the surface to increase in frequency value rather than decrease in frequency value away from the edges of the feature space. This showed intuitively that some classes were not normally distributed; no smoothing operation would have been necessary if all the classes were normally distributed. Two surfacing methods were initially applied to the class frequencies: a polynomial trend surface and a multiquadric equation. Polynomial trend surfaces were rejected because of the lack of similarity between plots of different degrees and the lack of predictability of plot shape. The distortion of the trend surfaces was likely the result of multiple causes. "Edge effects" were quite pronounced in areas which lacked data point control, therefore a buffer region of control points outside the area of interest to control for edge effects has been suggested by Unwin (1975). The shape of a data point cluster may distort the trend surface. A cluster which is more rectangular than square has a tendency for the contours to be elongated parallel to the longer side of the data (Unwin 1975). Peculiar distributions of data points also affects the shape of a trend surface. Points distributed along lines or points that are tightly clustered cause severely distorted surfaces to be generated (Unwin 1975). Outliers associated with a tightly clustered class are given undue influence in the trend surface equation and creates a severely distorted surface (Unwin 1975). Spectral classes that were elongated, tightly clustered, contained outliers, or were not square were common; for these reasons, exact-fitting surfaces only should be applied to spectral frequencies. Computationally faster exact-fitting surface equations, other than the multiquadric equation, could be implemented on the small micro-based image processing systems. One possible exact-fitting surface equation that might be considered is the inverse-weighted distance function.

Training fields were cleaned non-parametrically to avoid invalidating the test for

bivariate normality; the cleaning operation used was cluster analysis. A parametric cleaning method may delete valid data points if a class is skewed or multimodal. Output describing the overlap between spectral classes is obtained when a classifier is trained. The misclassified spectral values are deleted from the training field data to clean the classes. This approach to cleaning was not available because the method of creating the frequency feature space, from which the decision space is derived, used a surfacing routine, not a classification routine. The number of clusters to divide a class into and the number of spectral pairs in a cluster to specify as an outlier was subjective. A highly dispersed feature space with low frequency values may require fewer spectral pairs per cluster to be declared an outlier than a tightly clustered feature space with large frequency values. One direction of future research would be to set up a method to determine when the optimum number of clusters has been reached to detect outliers. A second area of research would be to develop other non-parametric cleaning operators.

6.3 Observations on the Visual Interpretation of Frequency Feature Spaces

A crop calendar and personal knowledge about rural environments allowed inferences to be drawn for each class extracted from the three dates of imagery. The location and distribution of spectral peaks in the frequency feature space greatly aided the analysis of each spectral class. The frequency feature space may be the tool an analyst needs to obtain an overview of the intraclass variability for a particular area. A forester, for example, may require an initial analysis of a coniferous stand before inspecting the site. A representative sample of conifer pixels could be extracted from a multispectral image of the area and the frequency feature space generated. The forester may then partition the separate peaks in the frequency feature space and classify the multispectral scene by assigning each peak a different class number. The spectral location of each peak in the frequency feature space and the spatial location of each peak in the study area may give the forester unique and valuable information. This aspect of frequency feature space analysis has yet to be developed.

Plotting clusters derived by cluster analysis could be a more effective graphic alternative than generating a multiquadric surface to display the distribution of a class. One problem with this method is that the analyst would be left with two separate entities - a generalized feature space plot and the corresponding histograms. Another problem is that the analyst would not know whether significant peaks would be separable from the surrounding minor peaks within a class. Another route of research may be to use cluster analysis (unsupervised training) to derive classes then apply a surfacing routine to the classes to gain a better understanding of the variability within each class.

An excessive amount of computing time was required to go from training field data to frequency feature space plot but, the surfacing routine remained the major factor in determining processing time. A traditional feature space plot plus histograms may be a reasonable alternative but the frequency feature space is advantageous because one single image is produced which combines the information of the traditional feature space plot and histograms into one integrated whole. Faster surfacing routines could be implemented to reduce the computing time required to generate the frequency feature spaces.

The frequency feature space need not be limited to untransformed spectral values. Modified spectral values derived from principal component analysis, ratios, vegetation indices, or any other image processing procedure can be used to generate frequency feature spaces. The analyst can then compare the untransformed frequency feature spaces to the corresponding transformed frequency feature spaces.

6.4 Results of Research on Understanding Decision Spaces

A statistical test for bivariate class normality was described and implemented. The results indicated that original spectral classes using MSS bands 5 and 7 had a high likelihood of being non-normal. Cluster analysis, as a cleaning operation, did not affect the distribution of the original classes except when outliers were deleted from an otherwise tightly clustered class. Cleaning the training fields non-parametrically created some normally distributed classes, but did not make any original, normally distributed classes

non-normal. The surfaced frequencies were used in the χ^2 and Kolmogorov-Smirnov tests due to the small number of training field values for some classes. The smoothing operation plus surfacing routine do not change the normality of each class (Eyton 1987).

Users of large multispectral images are advised to run the χ^2 and Kolmogorov-Smirnov tests directly on the training field values. These tests may also be used to determine how parametric cleaning operations affect class normality compared to non-parametric cleaning operations. Normal, slightly skewed, and severely skewed data could be mathematically generated, both types of cleaning operations applied to these data, and the results from the normality test compared.

The decision spaces for the parametric parallelepiped, linear classification function, and maximum likelihood classifiers were compared to the decision spaces derived by the non-parametric Frequency Feature Space Template (FFST) classifier. The decision spaces from the parametric classifiers were presented graphically to give the first time user, as well as the experienced user, a glimpse into the different ways classifiers divide up measurement space. Trying to understand the problems associated with a classification by analyzing the omission and commission errors in a contingency table is difficult. A plot of the decision spaces can complement the contingency table. The greatest surprise concerned the decision space boundaries for the linear classification function classifier because the shape of the decision spaces did not resemble the shapes of the feature spaces. The classes with the largest grey level values occupied the largest decision space area in measurement space which may cause an undefined class with higher grey level values to be misclassified. Calculations for posterior probabilities can be set as thresholds for the linear classification function to minimize this problem. The parallelepiped and maximum likelihood decision space boundaries fit closer to the feature spaces. These boundaries are effective only if posterior probability thresholds have been set for each class or measurement space will be partitioned into one of the defined classes. The decision space

plots of the parametric classifiers showed the amount of class overlap there can be between classes.

The FFST classifier decision spaces were very similar to the maximum likelihood decision spaces. The maximum likelihood classifier achieved a close decision space fit to the feature space through a parametric analysis of the spectral values, while the FFST classifier attained a close decision space fit non-parametrically. FFST classifier decision spaces displayed more variability at the extremes of correlated classes compared to the maximum likelihood classifier. The maximum likelihood classifier decision spaces, which were ellipses, indicated that the center of each correlated feature space had more variability than the extremes of the feature space. The frequency feature space for the date 3 bare soil class showed that the two largest soil peaks were located at opposite ends of the feature space while the maximum likelihood decision space showed that the greatest amount of data was located in the center of the feature space. The FFST classifier did show the variability at the ends of the date 3 soil decision space. Spectral classes were depicted more realistically by the FFST classifier, not as the classes should be statistically, making the decision spaces very flexible.

The deletion of an outlier only affected a local area in the frequency feature spaces and the FFST decision spaces. Each spectral value in a class was assumed to be independent of the surrounding spectral values, therefore the deletion of one outlier should not affect the shape and orientation of an entire decision space. The deletion of one outlier did change the shape and orientation of the decision spaces from the three parametric classifiers, therefore these classifiers do not follow this assumption.

Some general observations may be drawn from the graphic display of the decision spaces. The FFST decision space plots and the frequency feature space plots had very irregularly-shaped geometries which indicates the limitations of parametric classifier decision spaces with regular shaped geometries. When the parallelepiped classifier placed decision space boundaries around the feature spaces, considerable overlap was evident in

the original and the cleaned cover classes. The position of one class with respect to all other classes had a large influence on the shape of the linear classification function decision spaces and the amount of area occupied by the decision spaces in measurement space. The linear classification function decision spaces did not resemble the feature space shapes. Decision spaces from the maximum likelihood classifier fit closer to the feature spaces than did the other two parametric classifiers, but the ellipses did not indicate the spectral variability that may be present at the ends of a correlated class. The FFST classifier decision space plots showed the variability there can be in a correlated class. An area for future research is the depiction of parametric and non-parametric decision spaces in three dimensions. The decision spaces would then be shown as volumes. A parallelepiped decision space would be displayed as a box in three dimensions.

6.5 Ramifications of the Differences Between TM and MSS Feature Spaces

The differences in frequency feature space shape associated with a difference in spatial resolution between MSS to TM imagery was analyzed visually and statistically. An assumption was made that the slightly different spectral ranges for the TM and MSS infrared channels and different radiometric resolutions did not significantly modify the feature spaces. All the spectral classes from the MSS imagery using bands 5 and 7 were bivariate non-normal. All the TM image classes, but canola crop, were bivariate non-normal using data from channels 3 and 4. No radiometric destriping algorithm was applied at the satellite data receiving center to the TM and MSS images. Radiometric striping was evident in the red radiation channels, therefore one area of future research would be to destripe the imagery, extract the training fields, and apply the test for bivariate normality. The results of the normality check on the original and destriped classes could then be compared. Radiometric striping may make bivariate normal classes non-normal, adversely affecting a parametric classification.

The visual comparison between the TM and MSS frequency feature spaces provided

several interesting results. The TM frequency feature spaces were less dispersed than the MSS frequency feature spaces which may be because the finer spatial resolution of the TM allowed purer, more spectrally homogenous areas to be extracted. These purer pixels would then form tightly clustered peaks. More spectrally heterogeneous pixels were expected from the coarse spatial resolution MSS imagery. Peaks in the MSS frequency feature space would have lower frequency values compared to the corresponding TM frequency feature spaces, and the peaks would be more disperse. The TM frequency feature spaces were also less heterogeneous internally. The differences may have also been caused by the difference in number of pixels between the TM and MSS training areas.

Some of the visual observations were supported by the results obtained from subtracting the MSS frequency feature spaces from the TM frequency feature spaces. One result was that the central peaks in the TM frequency feature spaces were more tightly clustered and contained more percent frequency volume than the central peaks in the MSS frequency feature spaces. The visual analysis determined that the TM frequency feature space peaks were tightly clustered and did not display as much internal variability as the MSS frequency feature space peaks. The mean value for all the differenced frequency feature space grids was above zero which indicated that the TM frequency feature space generally contained more percent frequency volume than the MSS frequency feature space at each pixel location. Away from the central peaks, the percent frequency volume at each pixel location for the TM and MSS classes was nearly equal.

6.6 Summary

Several observations and recommendations for future research based on this thesis work have been described, and are now listed formally:

1. The frequency feature space is a viable alternative to the feature space and associated histograms for visually analyzing class cover types. The frequency feature space plot can be overlayed on the feature space plot to obtain extra information about pixel locations within peaks. Frequency feature spaces provided the user with a single,

easily understood graphic to discern what is happening in a spectral class.

2. Spectral classes derived from the red and infrared radiation channels had a high probability of being bivariate non-normal. Further research is required to understand how various image processing techniques affect class normality. Research can also be undertaken to determine the degree of class normality which can be expected with each new satellite and aircraft sensor system.
3. The regular decision space geometry of the three parametric classifiers did not conform to the irregular feature space geometry as well as the non-parametric FFST classifier. A non-parametric decision space should fit better in cases where classes are skewed or multimodal.
4. Thematic Mapper scanner imagery appeared more spectrally heterogeneous at increased spatial resolution, while the frequency feature spaces indicated that the spectral values in each class were more uniform and tightly clustered than the spectral values from Multispectral Scanner imagery. This result may truly be due to spatial resolution alone, or may be influenced by the differences in precipitation between the two dates, therefore future research using TM and MSS images of the same date is required.

TABLE 1.1 Landsat MSS Configuration.

SPECTRAL CHANNEL	SPECTRAL RANGE	NOMINAL SPATIAL RESOLUTION
4	400nm - 500nm	80m
5	500nm - 600nm	80m
6	600nm - 700nm	80m
7	800nm - 1100nm	240m

TABLE 1.2 Landsat TM Configuration.

SPECTRAL CHANNEL	SPECTRAL RANGE	NOMINAL SPATIAL RESOLUTION
1	450nm - 520nm	30m
2	520nm - 600nm	30m
3	630nm - 690nm	30m
4	760nm - 900nm	30m
5	1500nm - 1750nm	30m
6	2080nm - 2350nm	30m
7	10400nm - 12500nm	120m

TABLE 1.3 SPOT Configuration.

SPECTRAL CHANNEL	SPECTRAL RANGE	NOMINAL SPATIAL RESOLUTION
1	500nm - 590nm	20m
2	610nm - 680nm	20m
3	790nm - 890nm	20m
4	510nm - 730nm	10m

TABLE 2.1 Number of unique pairs required for a polynomial trend surface.

DEGREE OF POLYNOMIAL	NUMBER OF DISTINCT PAIRS
1	4
2	7
3	11
4	16
5	22
6	29
7	37

TABLE 2.2 Cleaning the Eudora, Kansas spectral classes with cluster analysis.

	NUMBER OF PAIRS	NUMBER OF CLUSTERS	NUMBER OF PAIRS DROPPED
DATE 1 CLASSES			
Winter Wheat	131	20	12
Water	84	10	5
Forest	93	15	5
Bare Soil	43	9	1
Corn	142	20	3
DATE 2 CLASSES			
Winter Wheat/Soybeans	131	20	10
Water	84	10	4
Forest	93	15	11
Bare Soil	43	9	4
Corn	142	20	4
DATE 3 CLASSES			
Soybeans	131	20	2
Water	84	9	1
Forest	93	15	11
Bare Soil	43	7	3
Corn	142	7	3

TABLE 3.1 Crop calendar for Midwest United States.
(adapted from Seevers and Peterson 1978; Brooner and Simonett 1971)

MONTH	CROP		
	CORN	WINTER WHEAT	SOYBEANS
MAY	May 3 - May 22 planting. Mainly bare soil visible.	Total green vegetation.	Not planted yet.
JUNE	Partial coverage over soil.	Total vegetation coverage. Crop drying out and turning a golden colour. Harvesting at end of June.	Planting at end of June. Bare soil mainly visible.
JULY	Total vegetation coverage. End of growing season at end of month. Tassels on ears of corn. Corn approximately eight ft. high.	Harvesting during beginning of July. Bare soil and stubble visible after harvesting.	Planting in beginning of July. Approximately 15% ground coverage in beginning of month. Soybeans approximately 3 - 4 inches high.

TABLE 4.1 Kolmogorov-Smirnov test on Date 1 classes. (a) original classes, (b) cleaned classes.

CLASS	D	$\alpha = 0.05$	NORMAL	NON NORMAL
WINTER WHEAT	0.114	0.064		X
WATER	0.110	0.081		X
FOREST	0.061	0.081	X	
CORN	0.054	0.052		X
BARE SOIL	0.107	0.053		X

(a)

CLASS	D	$\alpha = 0.05$	NORMAL	NON NORMAL
WINTER WHEAT	0.082	0.084	X	
WATER	0.031	0.087	X	
FOREST	0.034	0.081	X	
CORN	0.079	0.053		X
BARE SOIL	0.116	0.055		X

(b)

TABLE 4.2 Kolmogorov-Smirnov test on Date 2 classes. (a) original classes, (b) cleaned classes.

CLASS	D	$\alpha = 0.05$	NORMAL	NON NORMAL
WINTER WHEAT SOYBEANS	0.092	0.052		X
WATER	0.116	0.069		X
FOREST	0.044	0.072	X	
CORN	0.074	0.063		X
BARE SOIL	0.097	0.051		X

(a)

CLASS	D	$\alpha = 0.05$	NORMAL	NON NORMAL
WINTER WHEAT SOYBEANS	0.076	0.058		X
WATER	0.084	0.075		X
FOREST	0.034	0.081	X	
CORN	0.067	0.064		X
BARE SOIL	0.111	0.058		X

(b)

TABLE 4.3 Kolmogorov-Smirnov test on Date 3 classes. (a) original classes, (b) cleaned classes.

CLASS	D	$\alpha = 0.05$	NORMAL	NON NORMAL
SOYBEANS	0.064	0.058		X
WATER	0.073	0.069		X
FOREST	0.118	0.108		X
CORN	0.026	0.055	X	
BARE SOIL	0.100	0.053		X

(a)

CLASS	D	$\alpha = 0.05$	NORMAL	NON NORMAL
SOYBEANS	0.068	0.060		X
WATER	0.065	0.072	X	
FOREST	0.095	0.044		X
CORN	0.041	0.056	X	
BARE SOIL	0.119	0.060		X

(b)

TABLE 5.1 Number of Original and Cleaned Spectral Pairs for the Alexander Indian Reservation.

	NUMBER OF ORIGINAL PAIRS	NUMBER OF CLEANED PAIRS
MSS CLASSES		
Aspen	78	75
Pasture	86	83
Water	137	134
Canola	95	92
TM CLASSES		
Aspen	379	375
Pasture	460	455
Water	744	738
Canola	442	435

TABLE 5.2 Kolmogorov-Smirnov test for MSS and TM classes.
(a) MSS classes, (b) TM classes.

CLASS	D	$\alpha = 0.05$	NORMAL	NON NORMAL
CANOLA	0.114	0.044		X
WATER	0.111	0.055		X
PASTURE	0.123	0.047		X
ASPEN	0.113	0.052		X

(a)

CLASS	D	$\alpha = 0.05$	NORMAL	NON NORMAL
CANOLA	0.032	0.051	X	
WATER	0.094	0.028		X
PASTURE	0.052	0.040		X
ASPEN	0.088	0.044		X

(b)

TABLE 5.3 T-test for Skewness and Kurtosis on the Differenced Grids.

	NUMBER OF STANDARD DEVIATIONS FROM A ZERO MEAN	
CLASS	**SKEWNESS**	**KURTOSIS**
Aspen	8.1351	9.3673
Pasture	1.4430	5.2892
Water	12.4263	21.9776

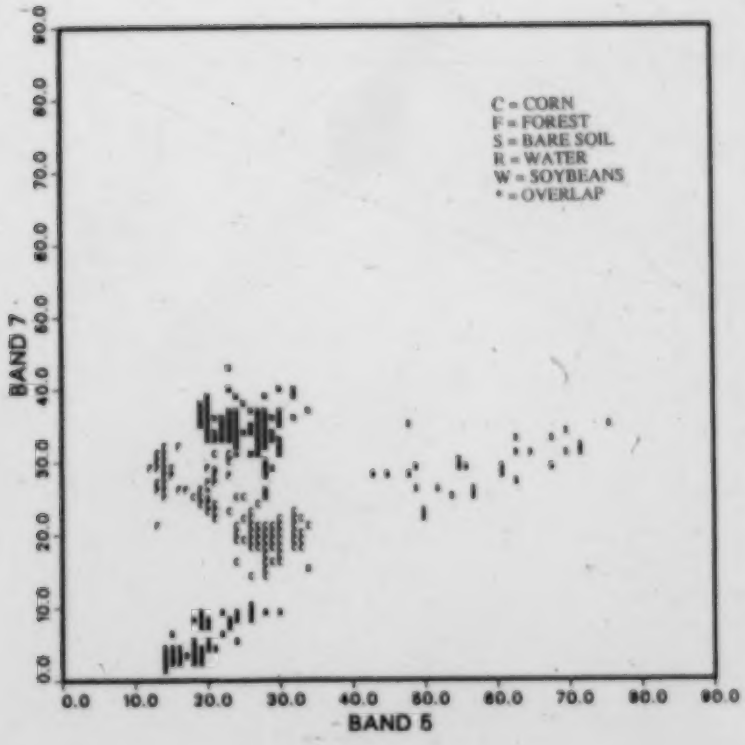

FIGURE 1.1 A two-dimensional feature space plot. (Plot truncated from 255 to 90.) (Data from Eyton et. al. 1979.)

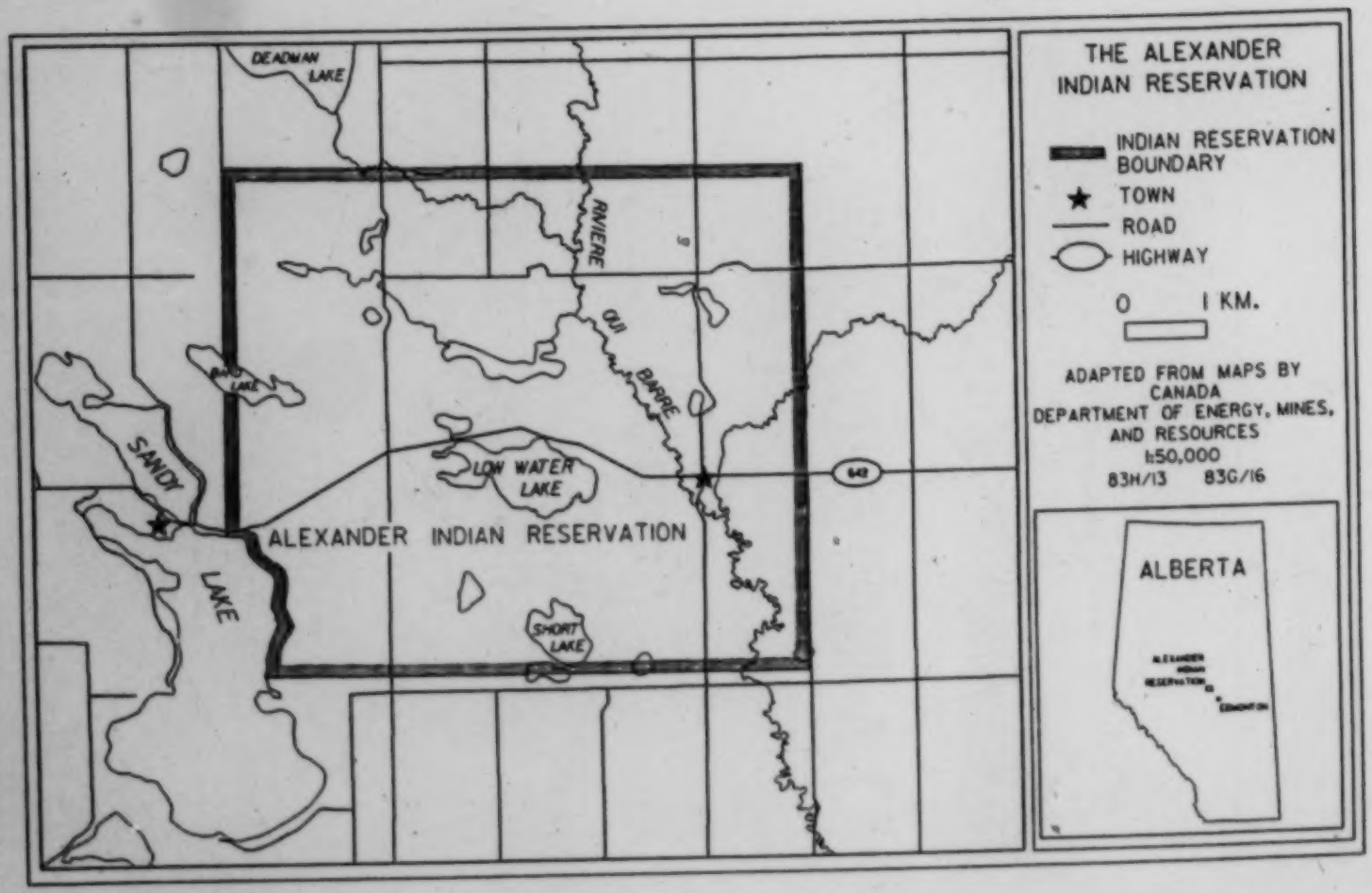

FIGURE 1.2 The Alexander Indian Reservation.

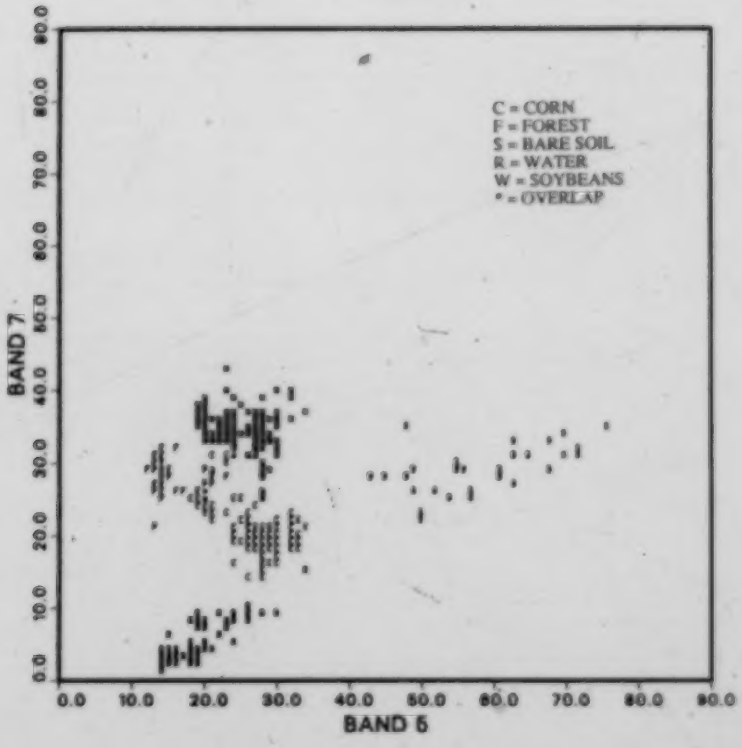

FIGURE 2.1 A traditional feature space plot. (Data from Eyton et. al . 1979.)

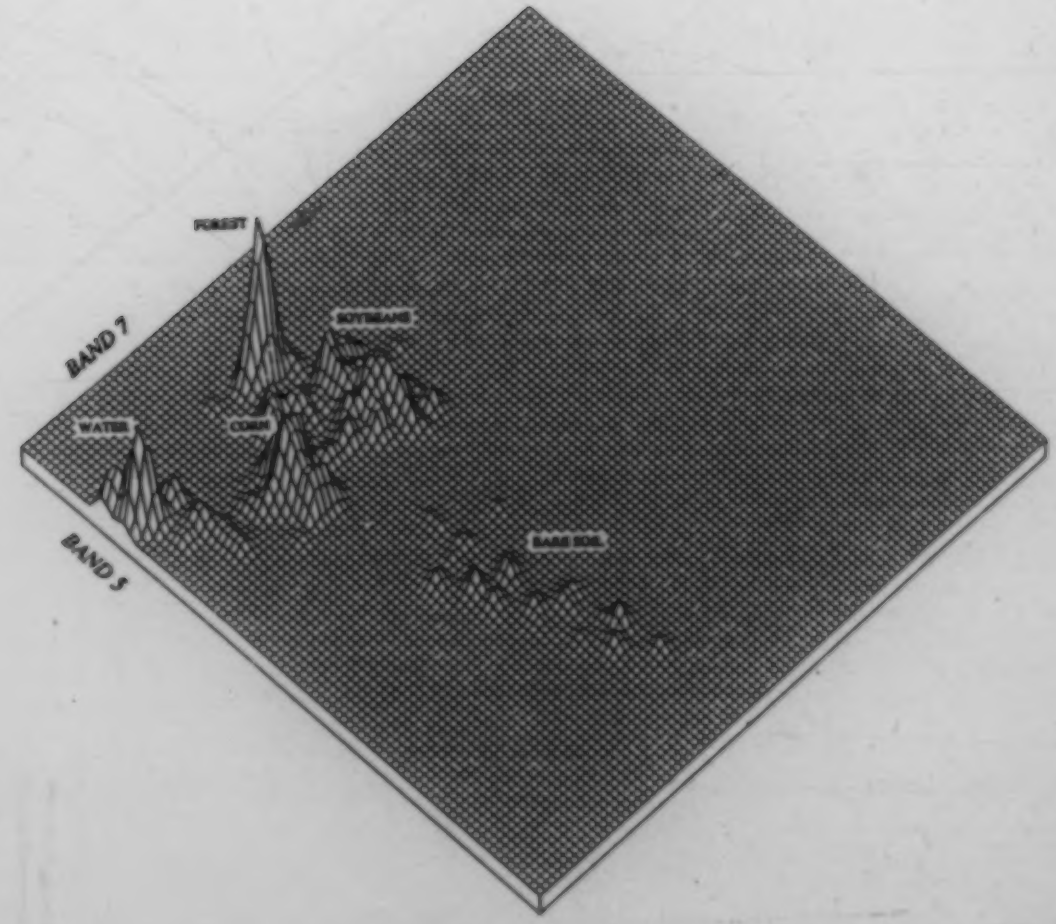

FIGURE 2.2 A perspective plot.

1. DATA:

SOURCE MAP

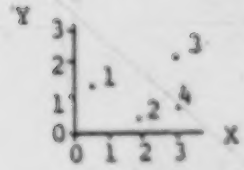

OBS (n)	SAMPLE DATA COORDINATES	Z VALUES
1.	X_1, Y_1	Z_1
2.	X_2, Y_2	Z_2
3.	X_3, Y_3	Z_3
4.	X_4, Y_4	Z_4

2. TREND SURFACE EQUATION FOR SAMPLE DATA:

First degree: $Ze_i = a_0 + a_1X_i + a_2Y_i$

where Ze_i = estimated Z value at X_i, Y_i coordinates

3. SOLUTION:

General form: $[a] = [X]^{-1}[b]$

where;

a = matrix of unknowns
b = matrix of constants
X = matrix of sums of squares and cross-products

Solution for sample data:

$$\begin{bmatrix} a_0 \\ a_1 \\ a_2 \end{bmatrix} = \begin{bmatrix} n & \Sigma X_i & \Sigma Y_i \\ \Sigma X_i & \Sigma X_i^2 & \Sigma X_i Y_i \\ \Sigma Y_i & \Sigma X_i Y_i & \Sigma Y_i^2 \end{bmatrix}^{-1} \begin{bmatrix} \Sigma Z_i \\ \Sigma Z_i X_i \\ \Sigma Z_i Y_i \end{bmatrix}$$

(a)

FIGURE 2.3 Two surfacing routines. (a) the polynomial trend surface, (b) the multiquadric equation.

1. DATA:

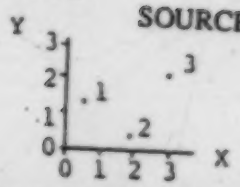

OBS (n)	SAMPLE DATA COORDINATES	Z VALUES
1.	X_1, Y_1	Z_1
2.	X_2, Y_2	Z_2
3.	X_3, Y_3	Z_3

2. MULTIQUADRIC HEIGHT SURFACE EQUATION:

General form: $$Z_e = \sum_{j=1}^{n} C_j [(X_j - X_e)^2 + (Y_j - Y_e)^2]^{.5}$$

Where X_e and Y_e = coordinates of estimated z-value (Z_e)

3. SOLUTION:

General form: $$[C_j] = [a_{ij}]^{-1} [Z_j]$$

Expanding $[a_{ij}]$ for sample data:

$$a_{11} = [(X_1 - X_1)^2 + (Y_1 - Y_1)^2]^{.5}$$
$$a_{12} = [(X_1 - X_2)^2 + (Y_1 - Y_2)^2]^{.5}$$
$$a_{13} = [(X_1 - X_3)^2 + (Y_1 - Y_3)^2]^{.5}$$
$$\vdots \qquad\qquad \vdots$$
$$a_{33} = [(X_3 - X_3)^2 + (Y_3 - Y_3)^2]^{.5}$$

Solution for sample data:

$$\begin{bmatrix} C_1 \\ C_2 \\ C_3 \end{bmatrix} = \begin{bmatrix} a_{11} & a_{12} & a_{13} \\ a_{21} & a_{22} & a_{23} \\ a_{31} & a_{32} & a_{33} \end{bmatrix}^{-1} \begin{bmatrix} Z_1 \\ Z_2 \\ Z_3 \end{bmatrix}$$

4. MULTIQUADRIC HEIGHT SURFACE EQUATION FOR SAMPLE DATA:

$$Z_e = C_1 [(X_1 - X_e)^2 + (Y_1 - Y_e)^2]^{.5} +$$
$$C_2 [(X_2 - X_e)^2 + (Y_2 - Y_e)^2]^{.5} +$$
$$C_3 [(X_3 - X_e)^2 + (Y_3 - Y_e)^2]^{.5}$$

(b)

FIGURE 2.3 continued.

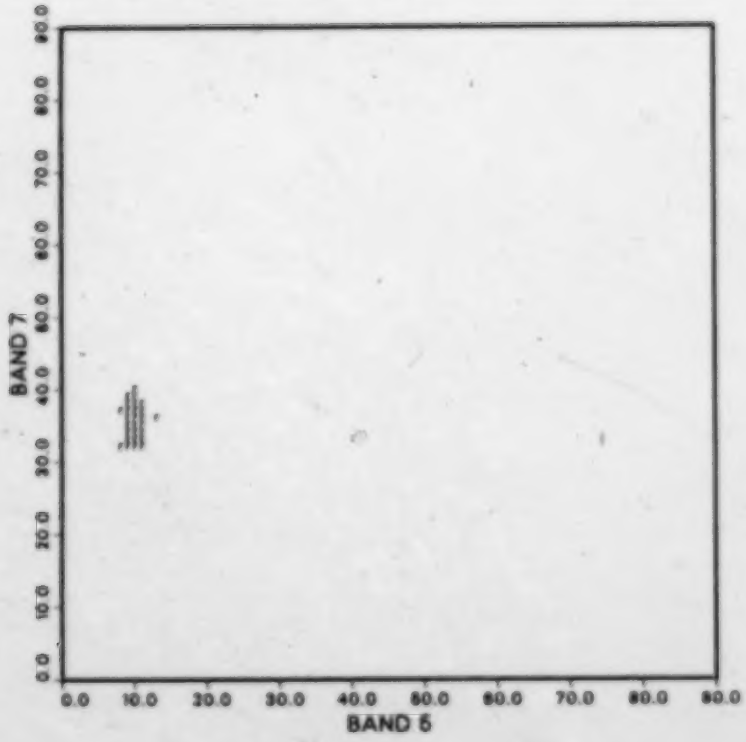

FIGURE 2.4 The feature space for forest.

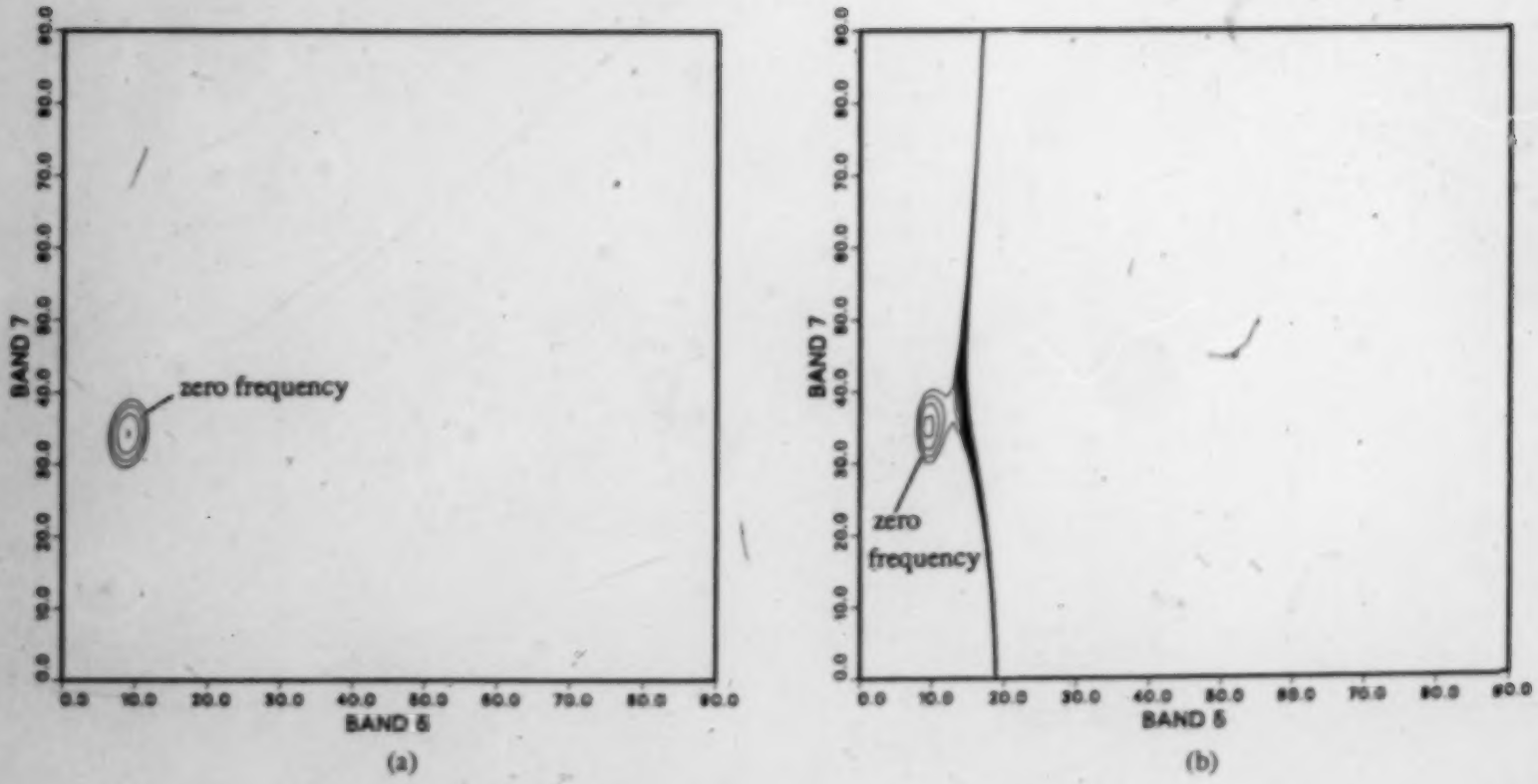

FIGURE 2.5 The polynomial trend surfaces for forest. (a) second degree, (b) third degree, (c) fourth degree, (d) fifth degree.

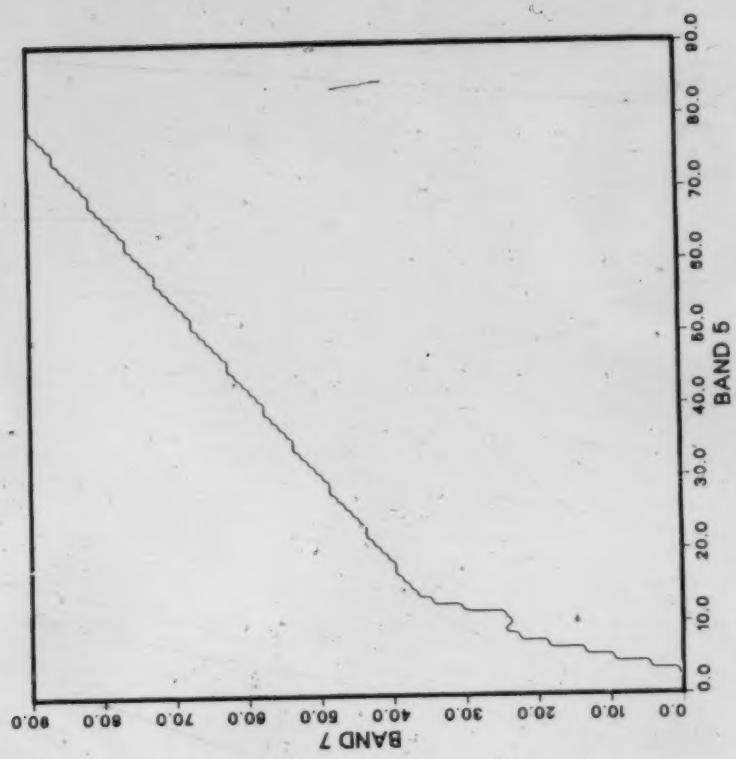

(d)

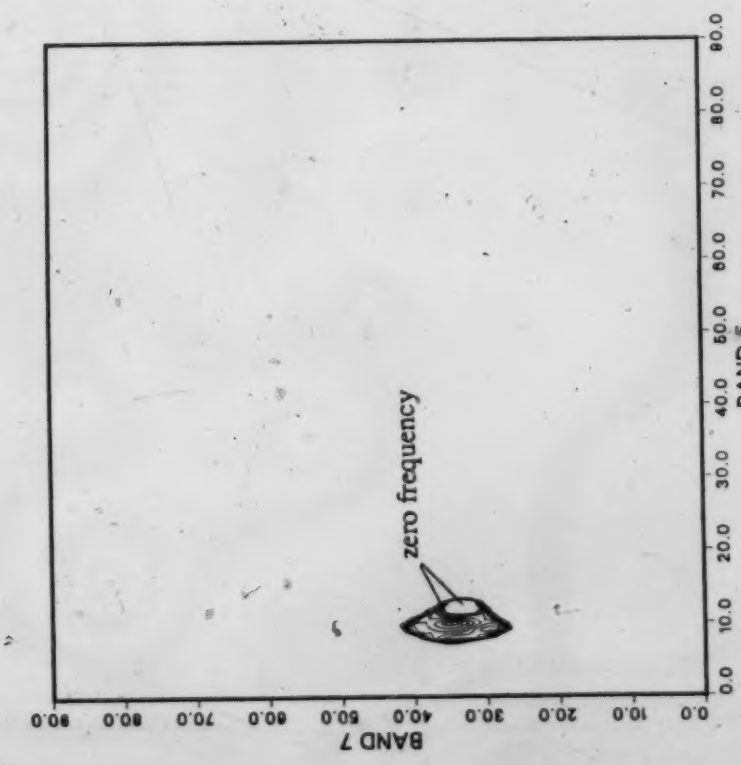

(c)

FIGURE 2.5 continued.

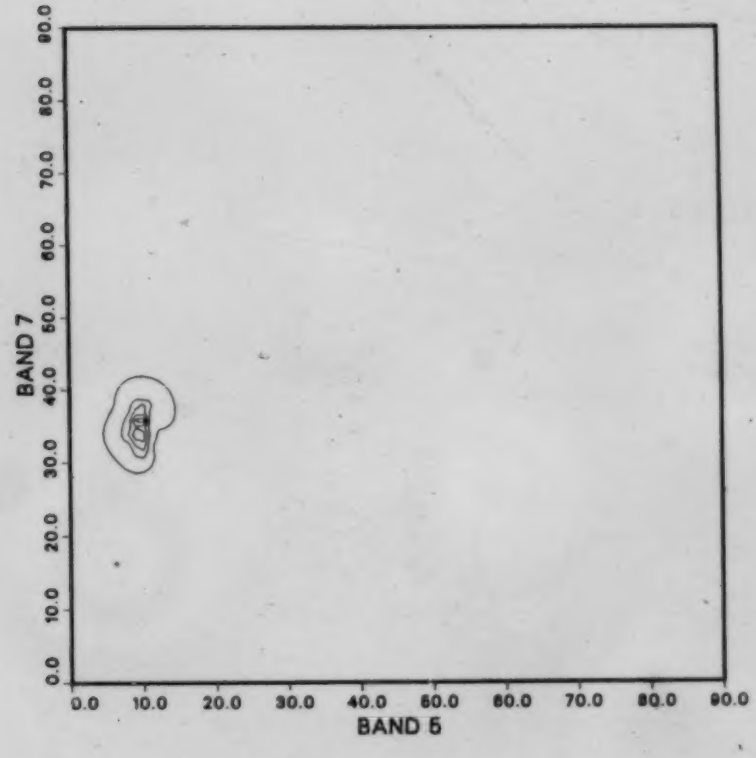

FIGURE 2.6 The multiquadric surface for forest.

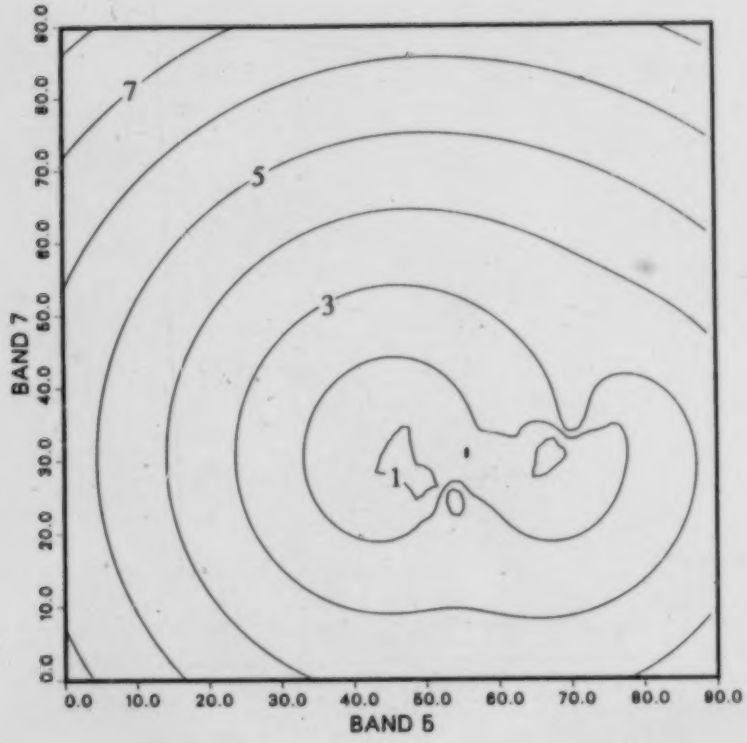

FIGURE 2.7 The multiquadric surface for the Date 3 bare soil class.

.0625	.1125	.0625
.1125	.3000	.1125
.0625	.1125	.0625

FIGURE 2.8 Smoothing filter applied to the spectral frequencies.

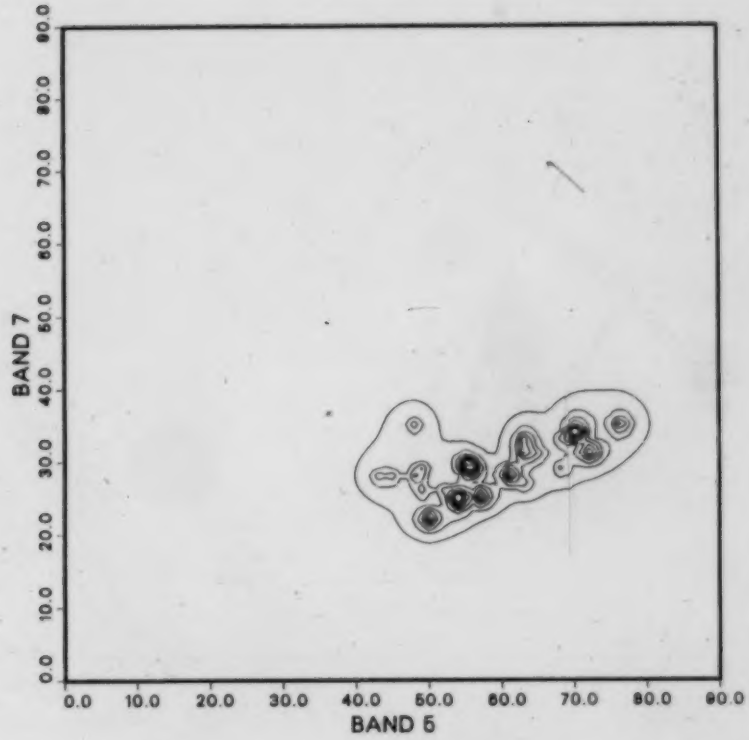

FIGURE 2.9 The multiquadric surface for Date 3 bare soil after smoothing the spectral frequencies. (contour interval = 0.1)

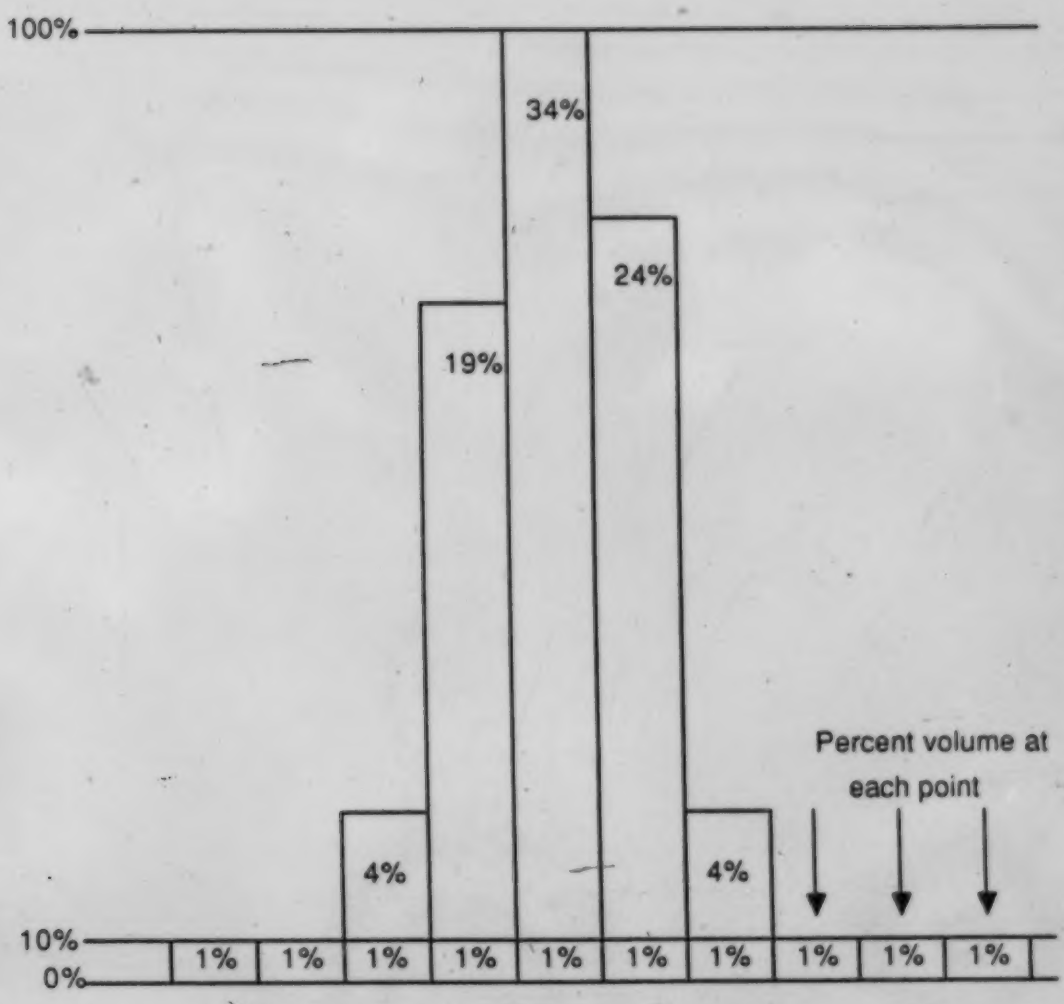

FIGURE 2.10 Calculation for percent volume contours.

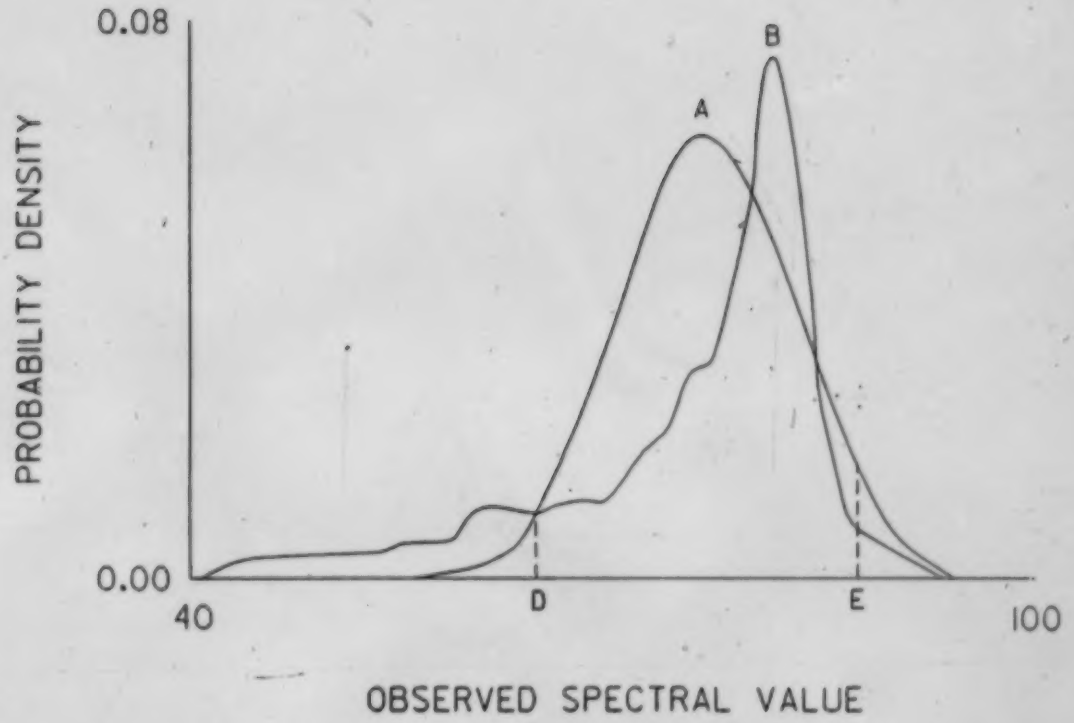

FIGURE 2.11 Effects of normalization on skewed data. A = normalized data, B = original data, D and E = thresholds (Adapted from Maynard and Strahler 1981)

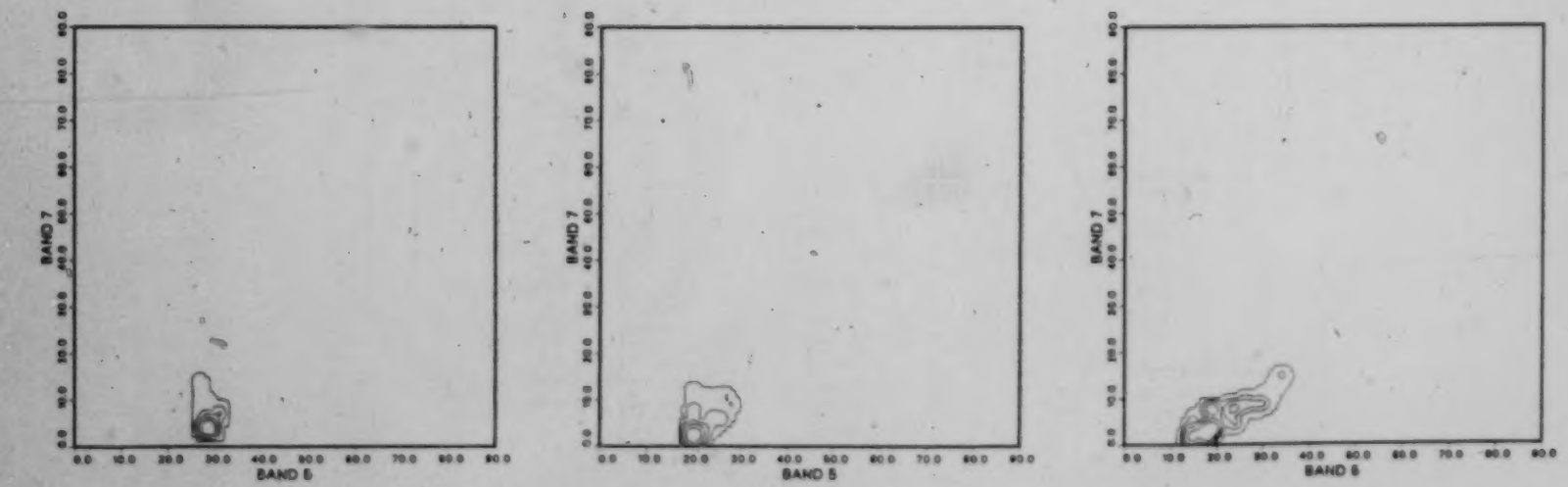

FIGURE 3.1 Original and cleaned frequency feature spaces for water. (a) date 1 original, (b) date 2 original, (c) date 3 original, (d) date 1 clean, (e) date 2 clean, (f) date 3 clean.

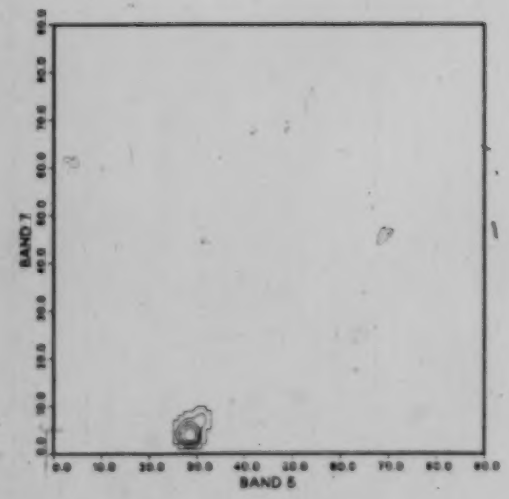

(d)

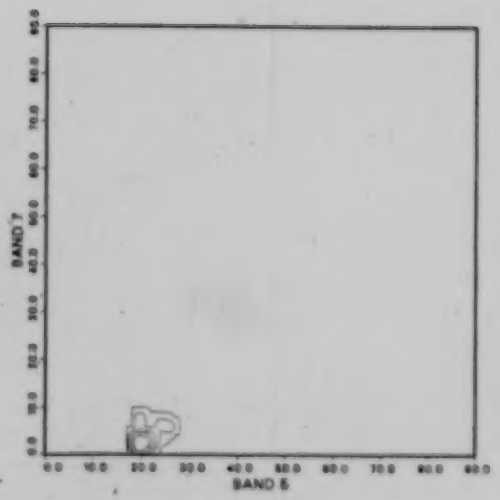

(e)

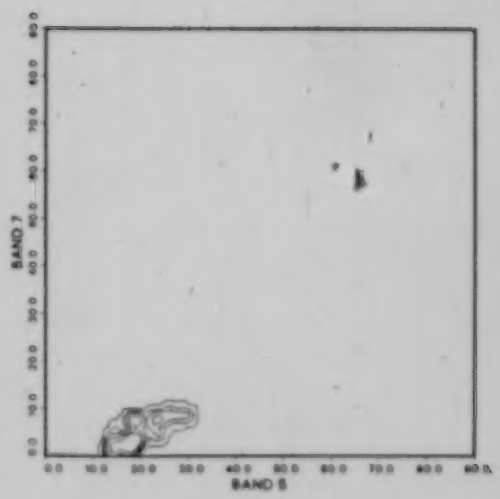

(f)

FIGURE 3.1 continued.

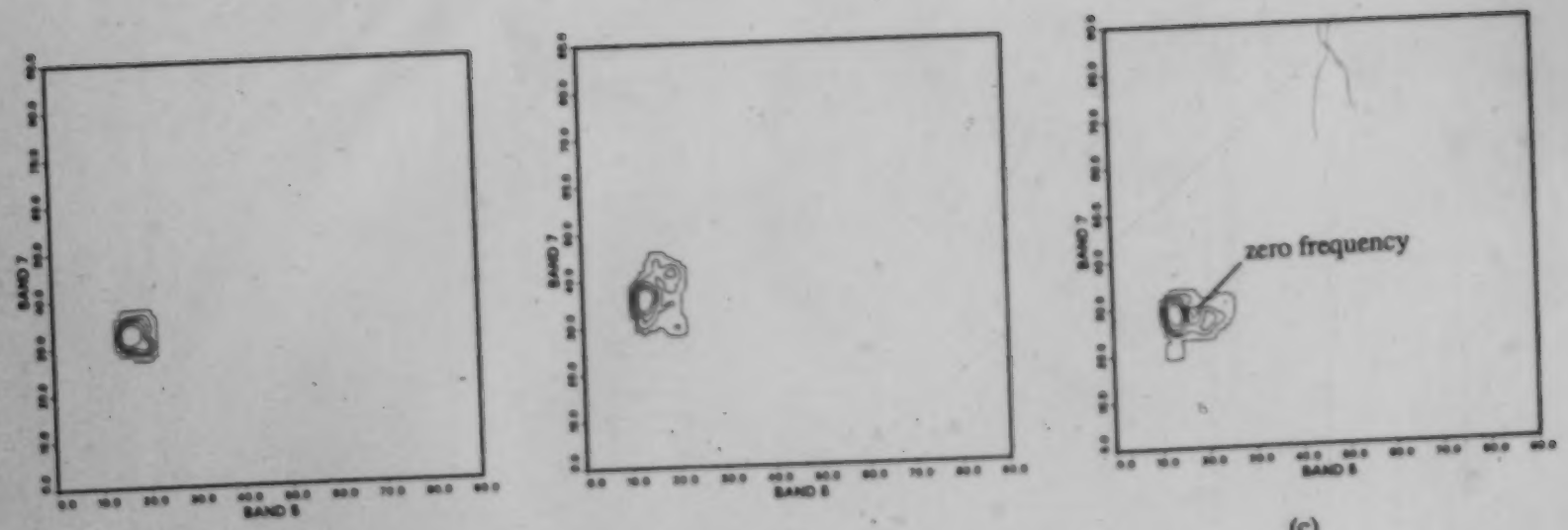

FIGURE 3.2 Original and cleaned frequency feature spaces for forest. (a) date 1 original, (b) date 2 original, (c) date 3 original, (d) date 1 clean, (e) date 2 clean, (f) date 3 clean.

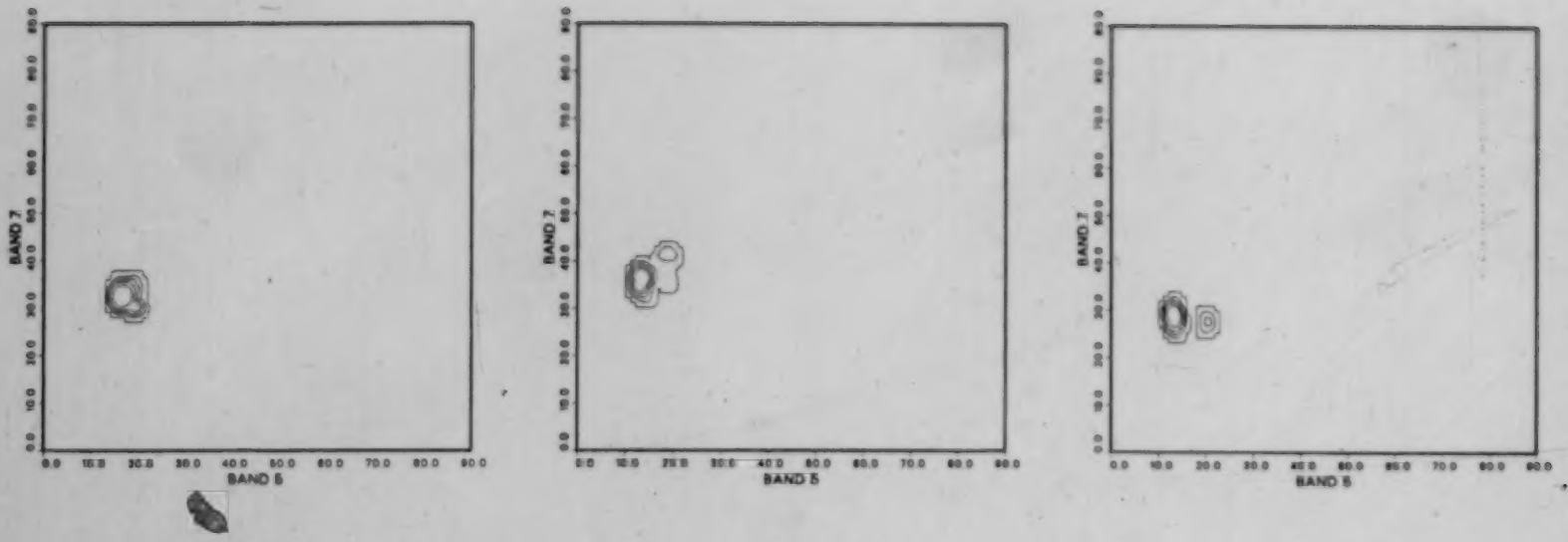

(d) (e) (f)

FIGURE 3.2 continued.

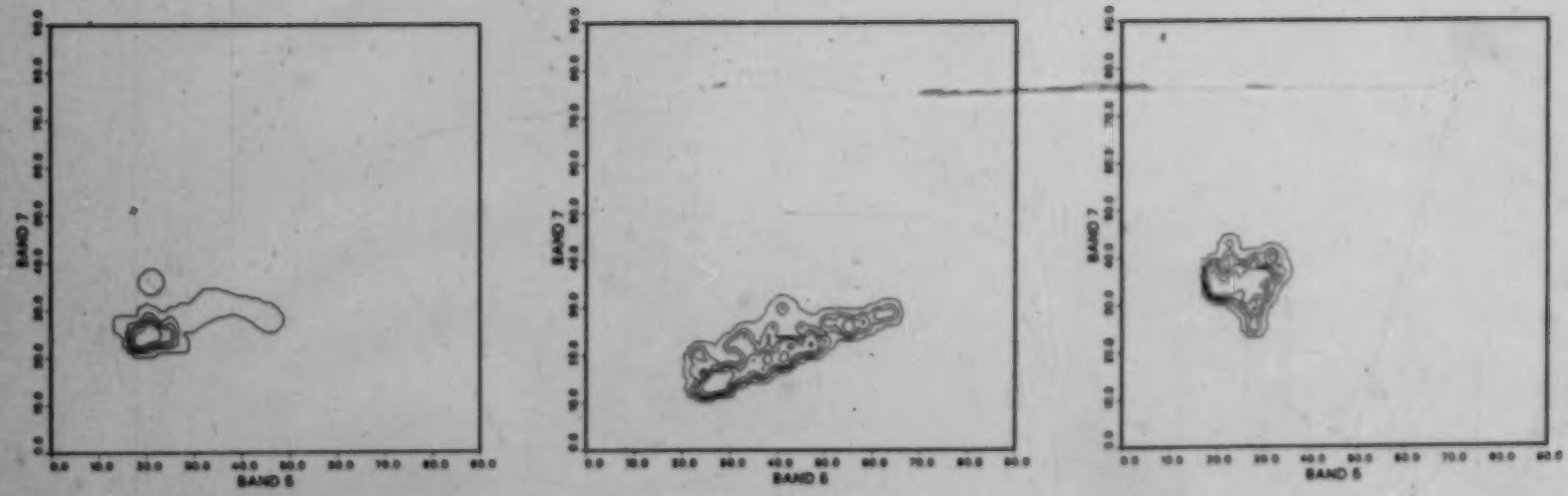

FIGURE 3.3 Original and cleaned frequency feature spaces for winter wheat and soybeans. (a) date 1 original, (b) date 2 original, (c) date 3 original, (d) date 1 clean, (e) date 2 clean, (f) date 3 clean.

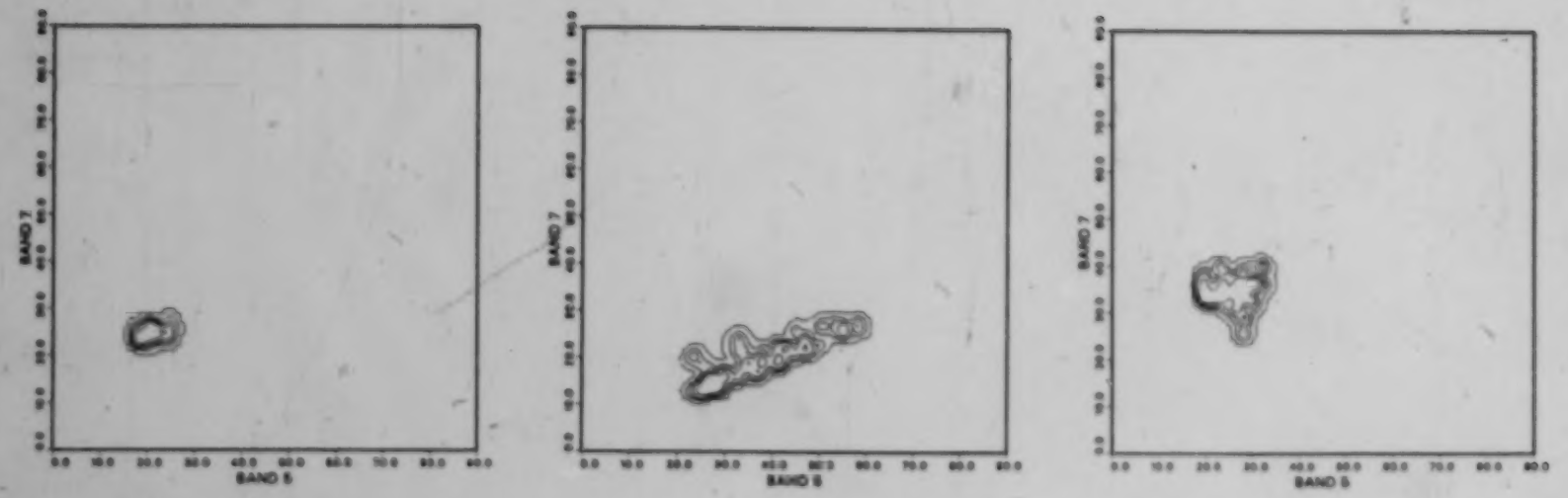

(d) (e) (f)

FIGURE 3.3 continued.

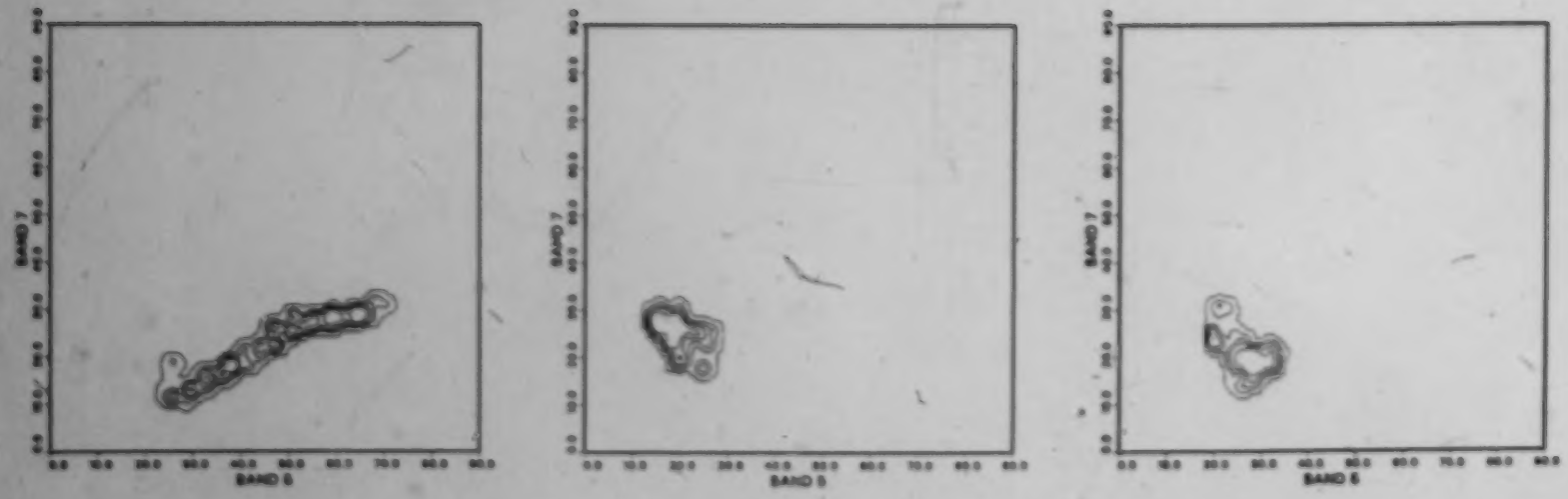

(a) (b) (c)

FIGURE 3.4 Original and cleaned frequency feature spaces for corn. (a) date 1 original, (b) date 2 original, (c) date 3 original, (d) date 1 clean, (e) date 2 clean, (f) date 3 clean.

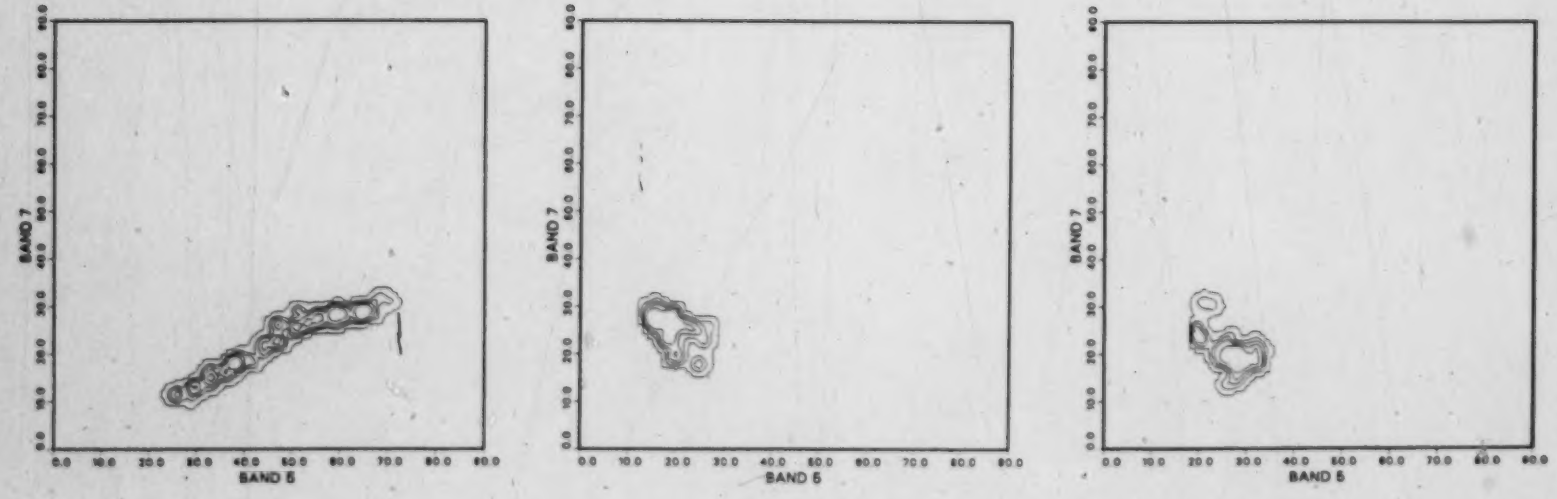

(d) (e) (f)

FIGURE 3.4 continued.

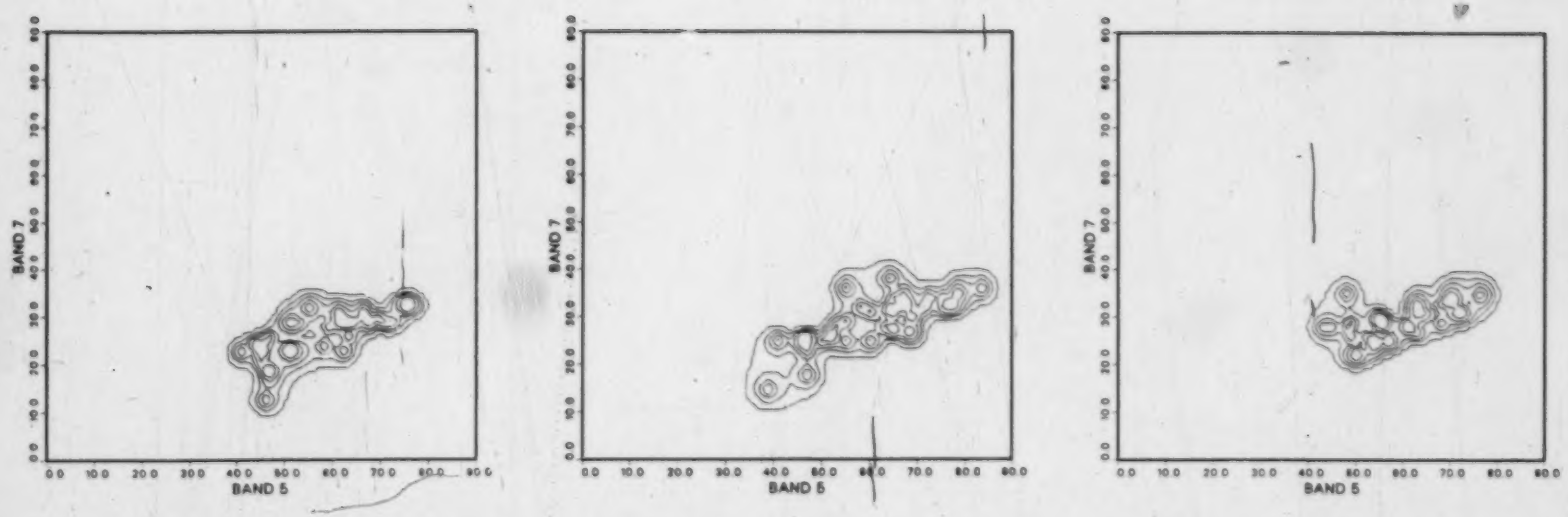

FIGURE 3.5 Original and cleaned frequency feature spaces for bare soil. (a) date 1 original, (b) date 2 original, (c) date 3 original, (d) date 1 clean, (e) date 2 clean, (f) date 3 clean.

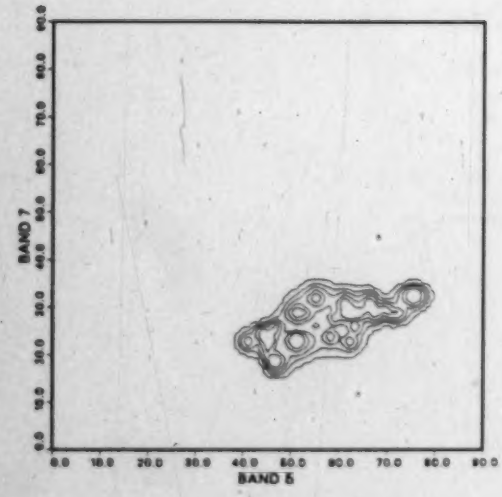

(d)

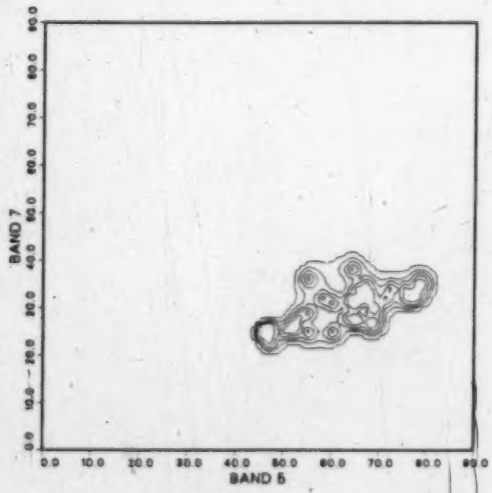

(e)

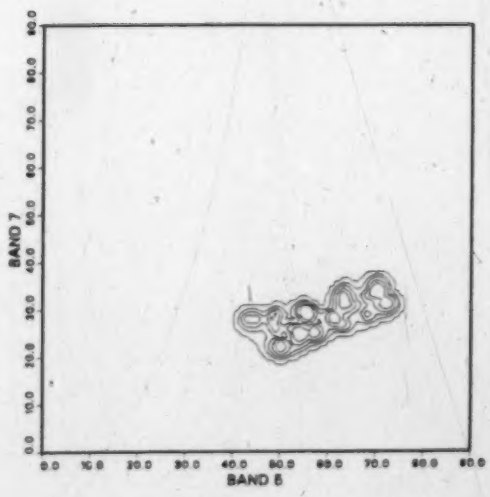

(f)

FIGURE 3.5 continued.

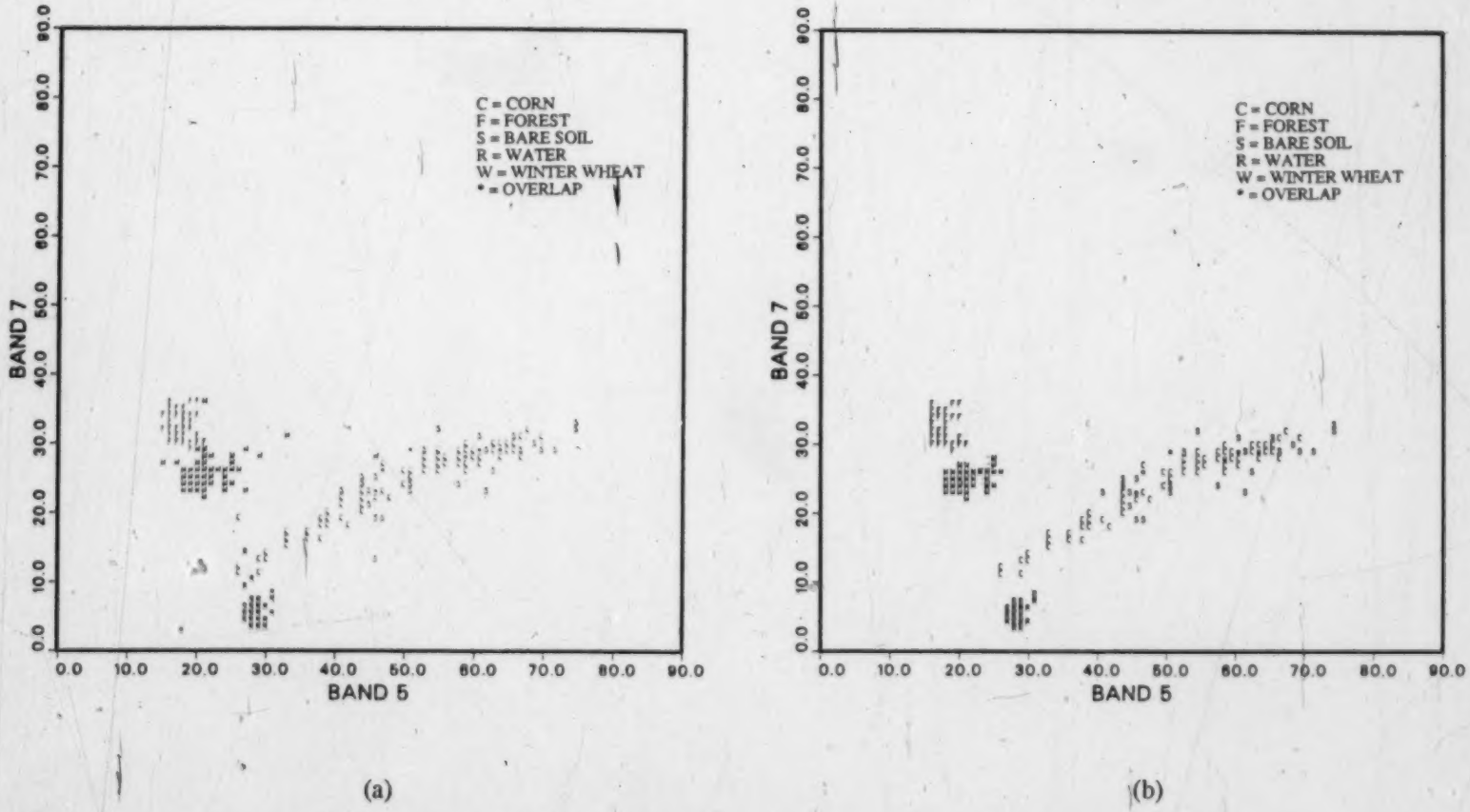

FIGURE 3.6 Original and cleaned feature spaces for date 1. (a) date 1 original, (b) date 1 clean.

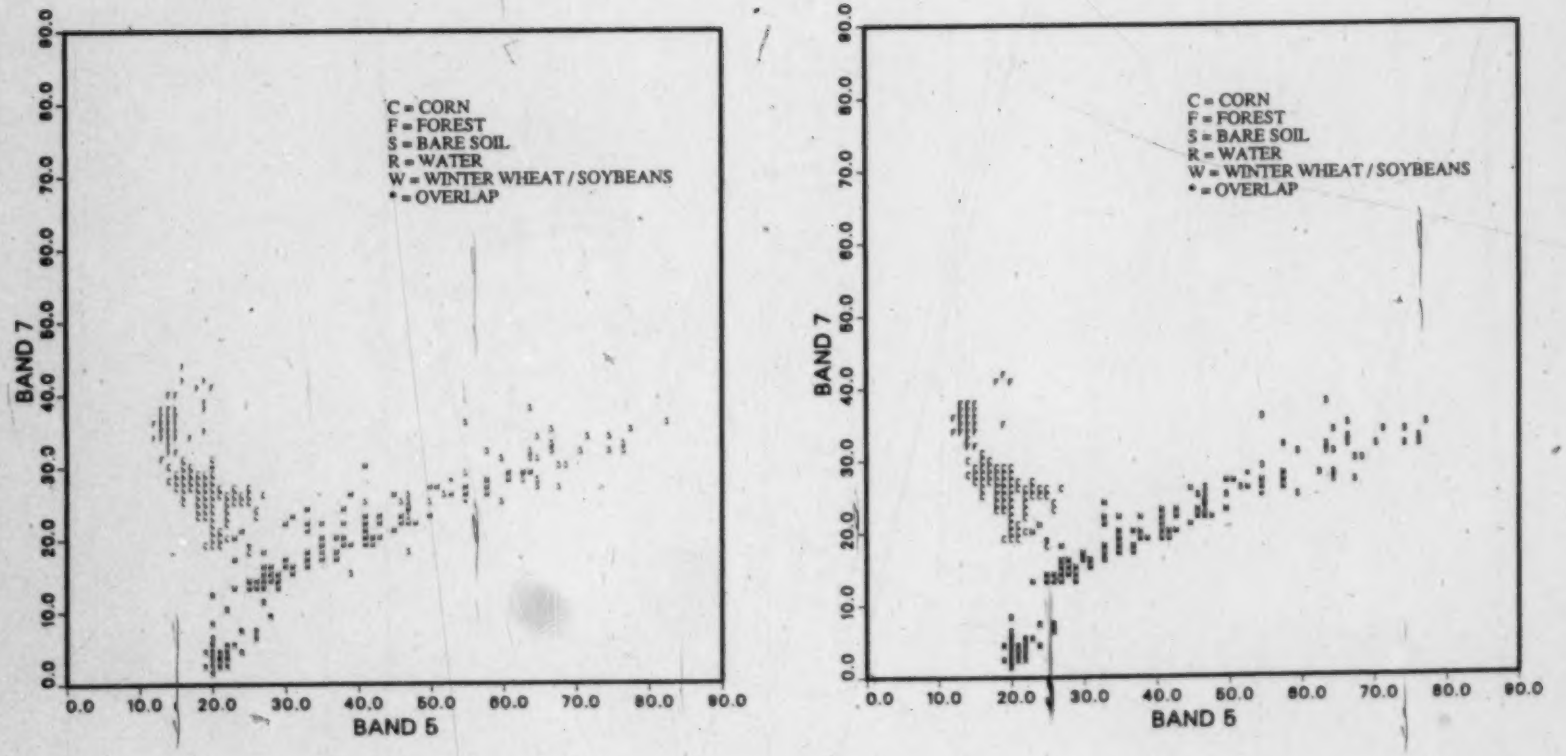

(a) (b)

FIGURE 3.7 Original and cleaned feature spaces for date 2. (a) date 2 original, (b) date 2 clean.

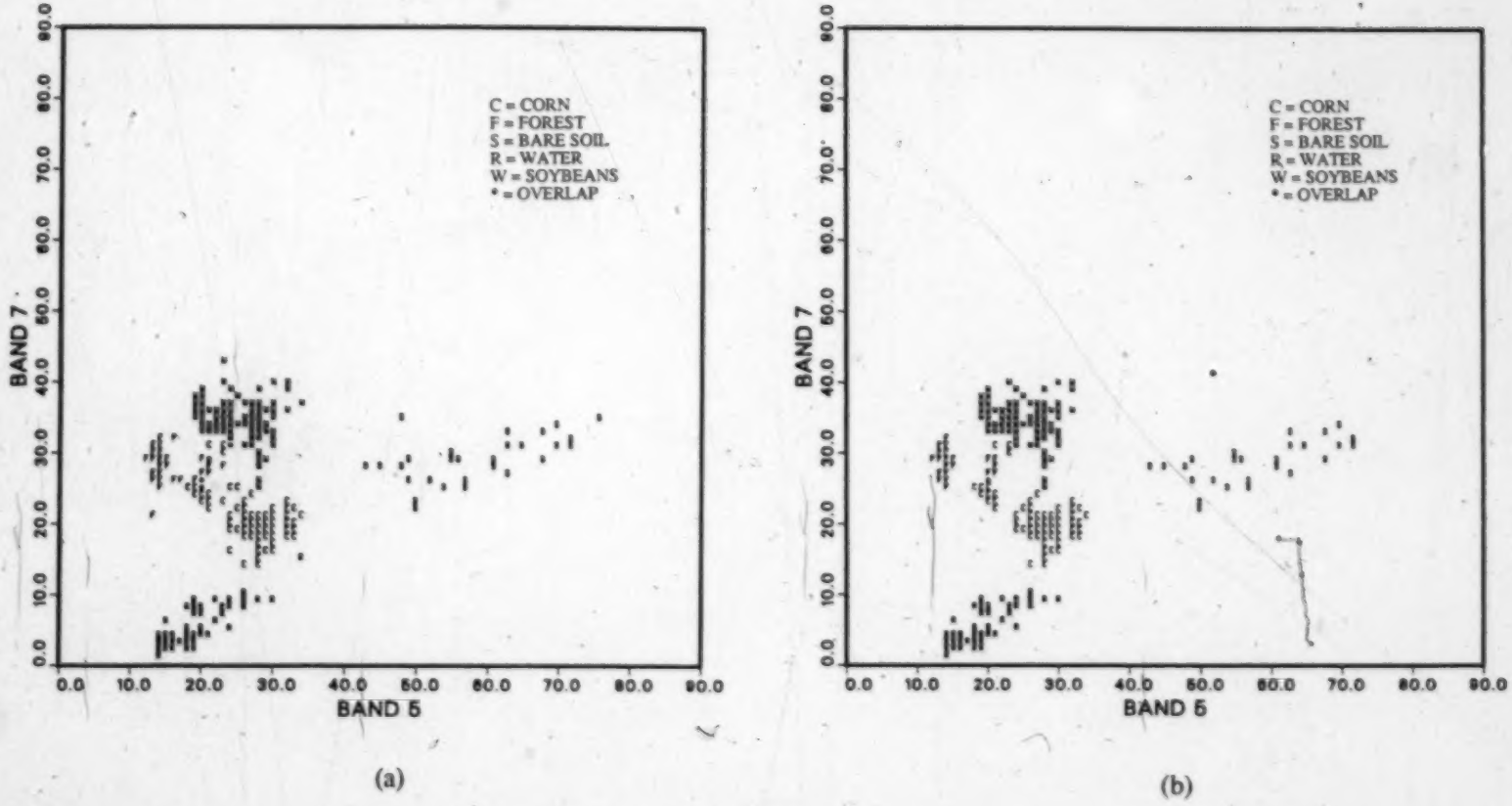

FIGURE 3.8 Original and cleaned feature spaces for date 3. (a) date 3 original, (b) date 3 clean.

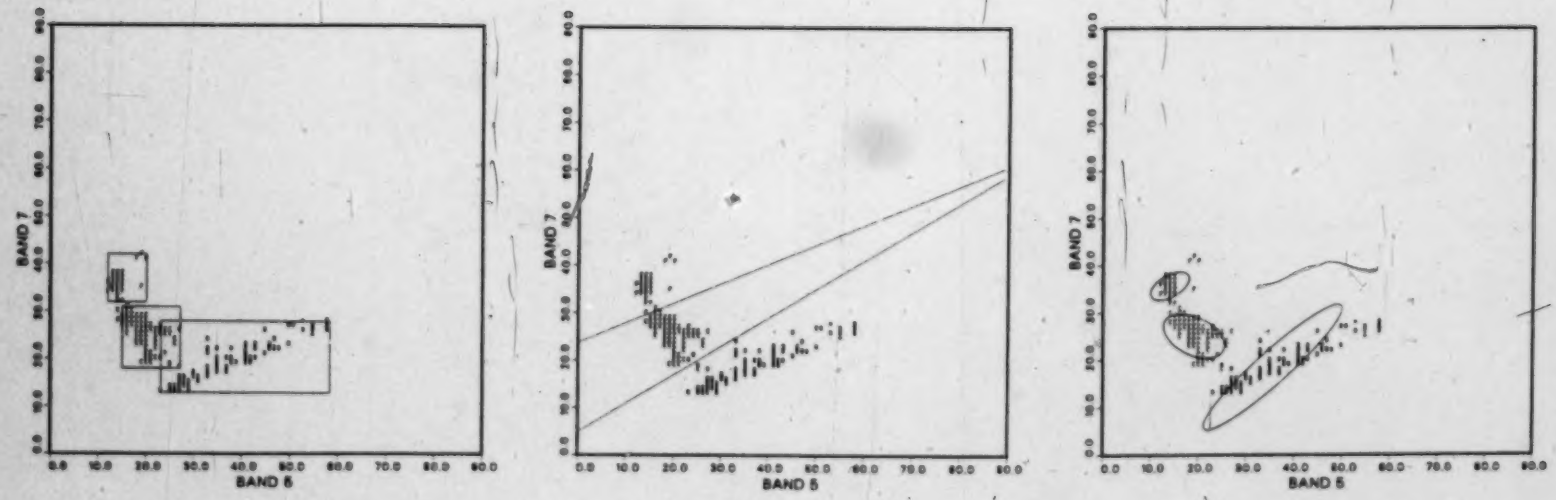

FIGURE 4.1 Decision spaces for the parametric classifiers. (a) parallelepiped, (b) linear classification function, (c) maximum likelihood.

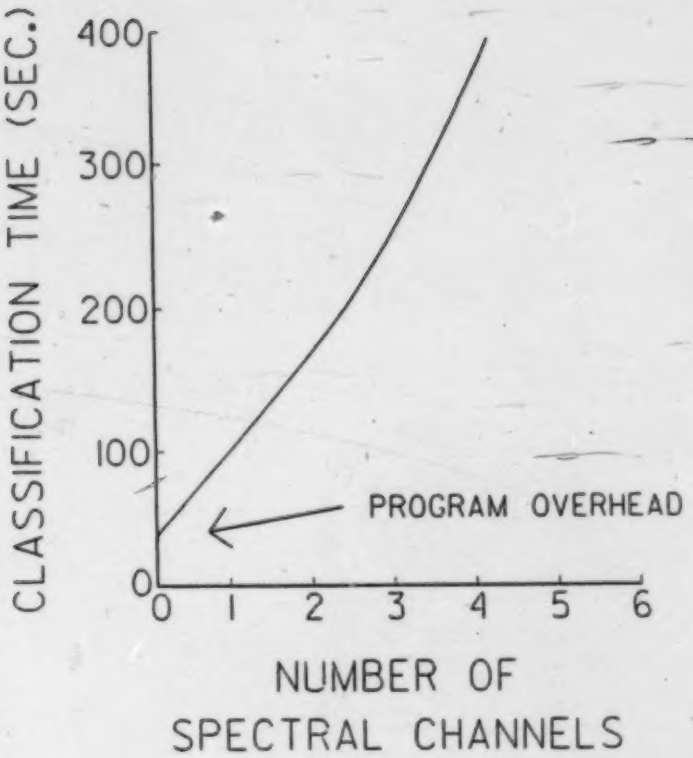

FIGURE 4.2 Increase in computing time versus the number of input channels. (Adapted from Lee and Richards 1984)

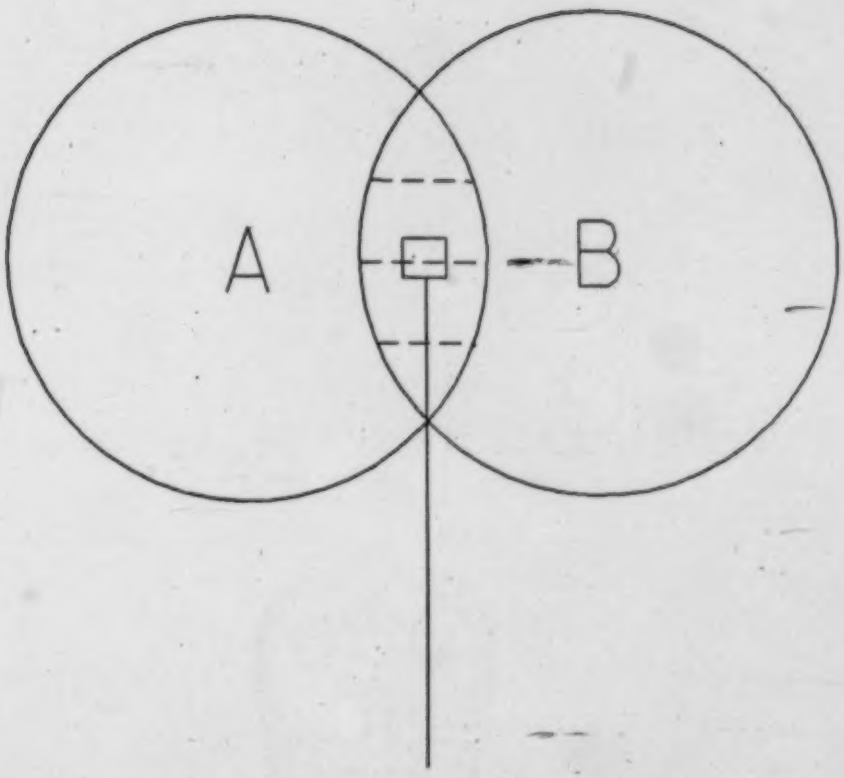

FIGURE 4.3 The method of defining overlap area for the Frequency Feature Space Template classifier.

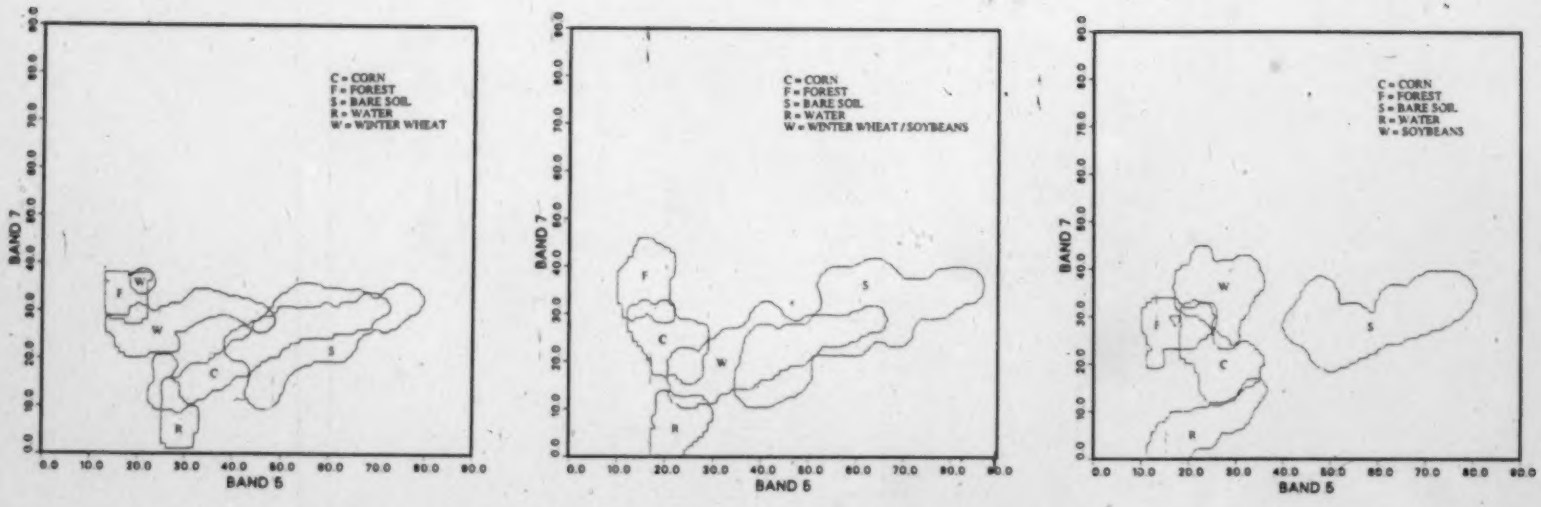
C = CORN
F = FOREST
S = BARE SOIL
R = WATER
W = WINTER WHEAT
W = WINTER WHEAT / SOYBEANS
W = SOYBEANS
BAND 7
BAND 5
0.0 10.0 20.0 30.0 40.0 50.0 60.0 70.0 80.0 90.0

(a) (b) (c)

FIGURE 4.4 Original and cleaned Frequency Feature Space Template classifier decision spaces. (a) Date 1 original, (b) Date 2 original, (c) Date 3 original, (d) Date 1 cleaned, (e) Date 2 cleaned, (f) Date 3 cleaned.

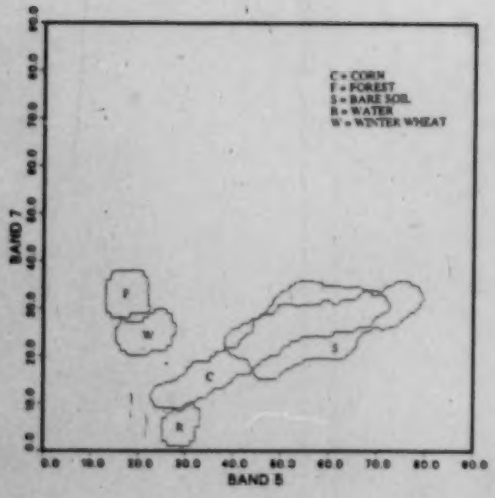

(d)

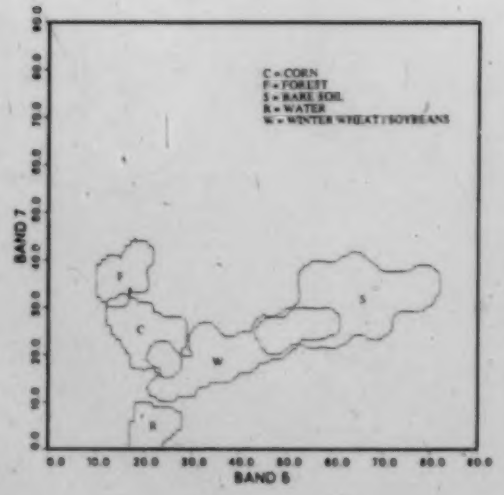

(e)

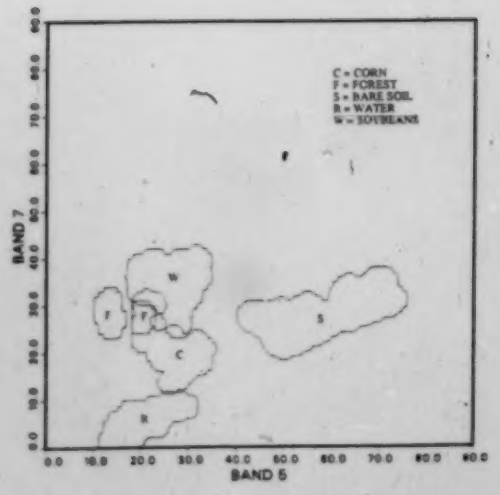

(f)

FIGURE 4.4 continued.

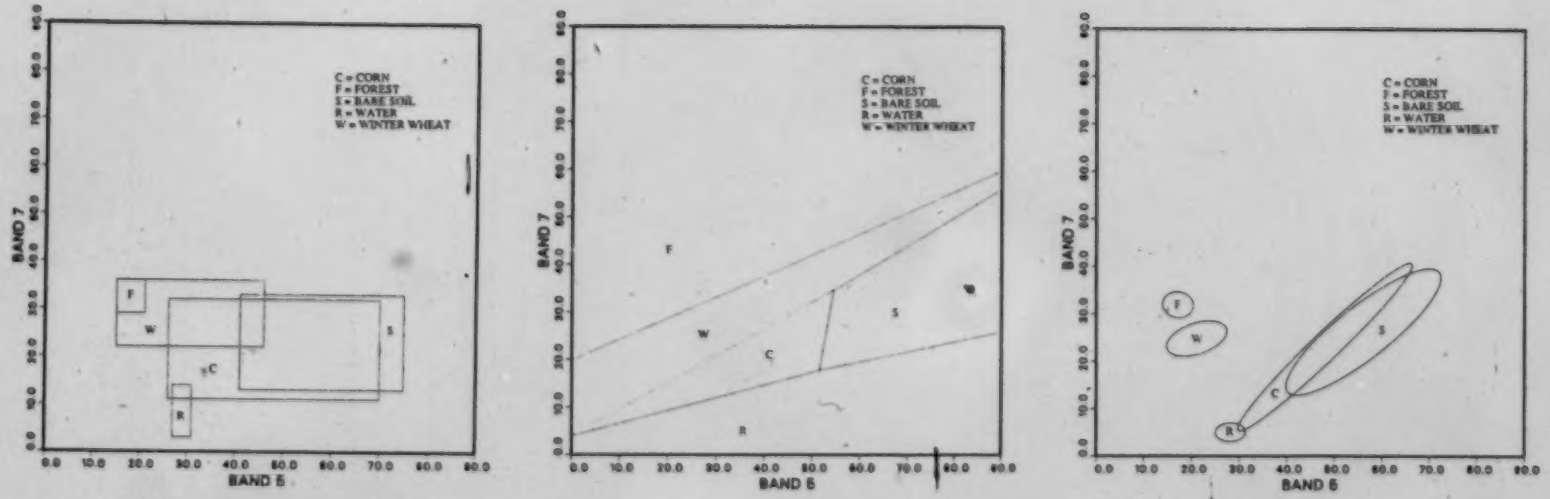

FIGURE 4.5 Original Date 1 decision spaces for the parametric classifiers. (a) parallelepiped, (b) linear classification function, (c) maximum likelihood.

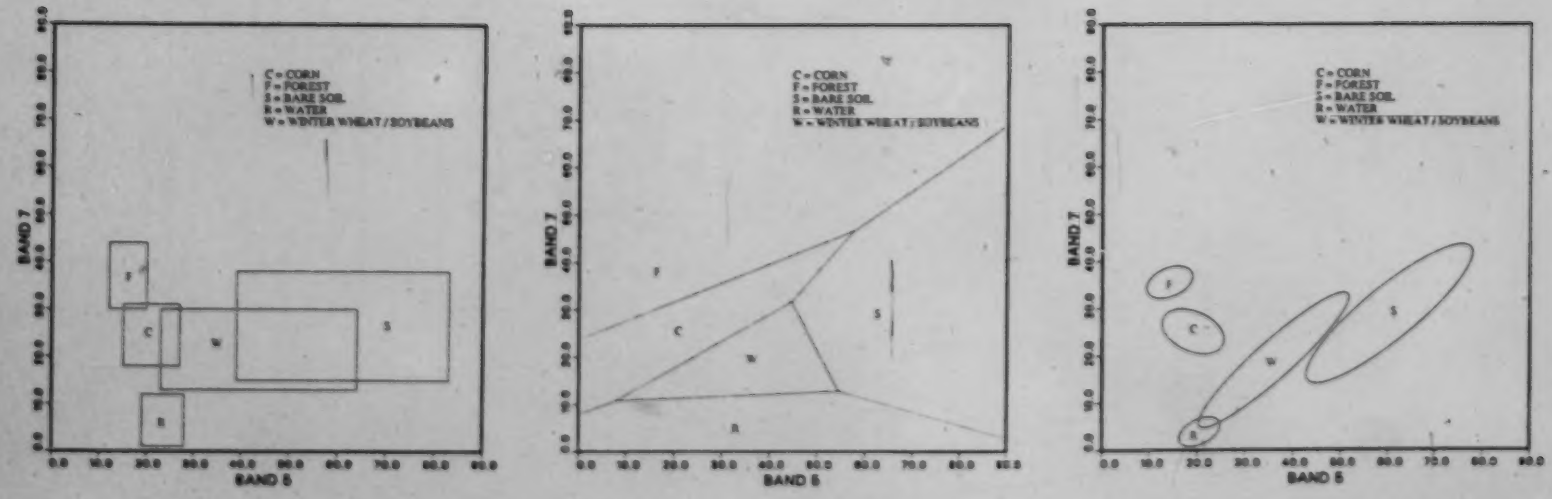

FIGURE 4.6 Original Date 2 decision spaces for the parametric classifiers. (a) parallelepiped, (b) linear classification function, (c) maximum likelihood.

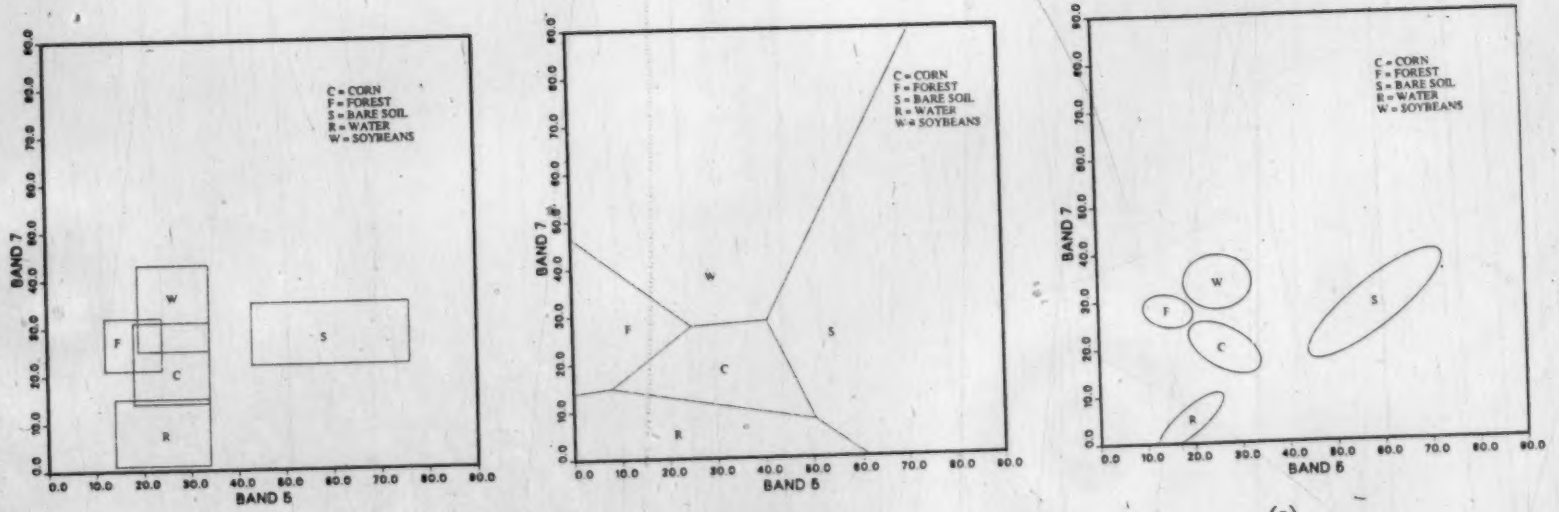

FIGURE 4.7 Original Date 3 decision spaces for the parametric classifiers. (a) parallelepiped, (b) linear classification function, (c) maximum likelihood.

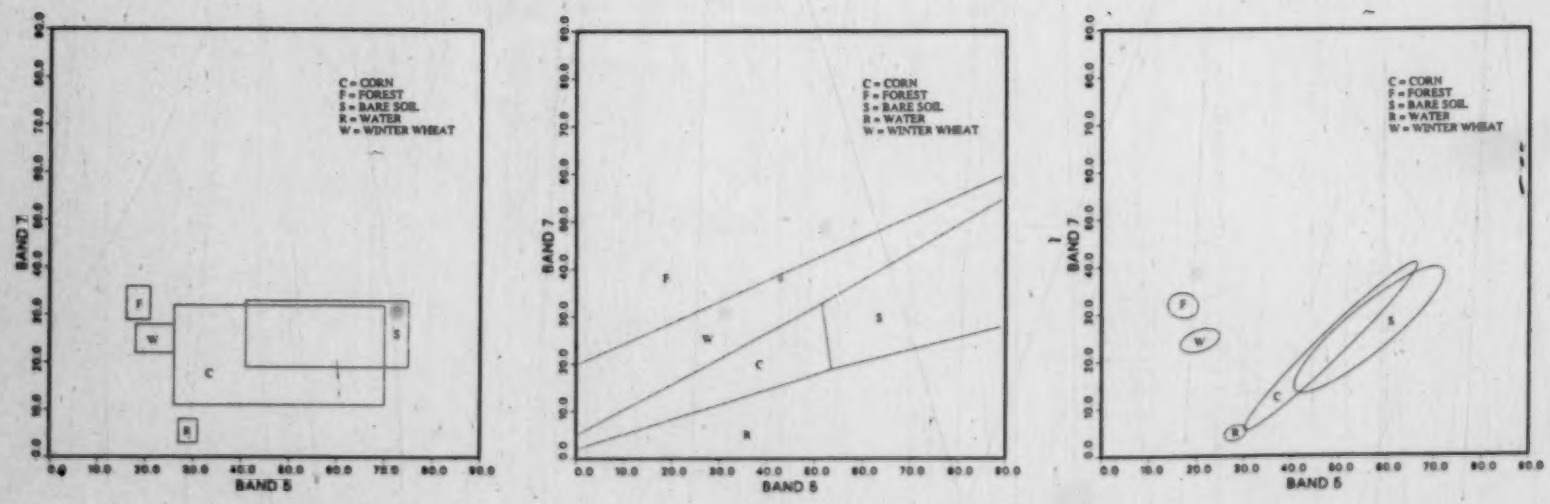

FIGURE 4.8 Cleaned Date 1 decision spaces for the parametric classifiers. (a) parallelepiped, (b) linear classification function, (c) maximum likelihood.

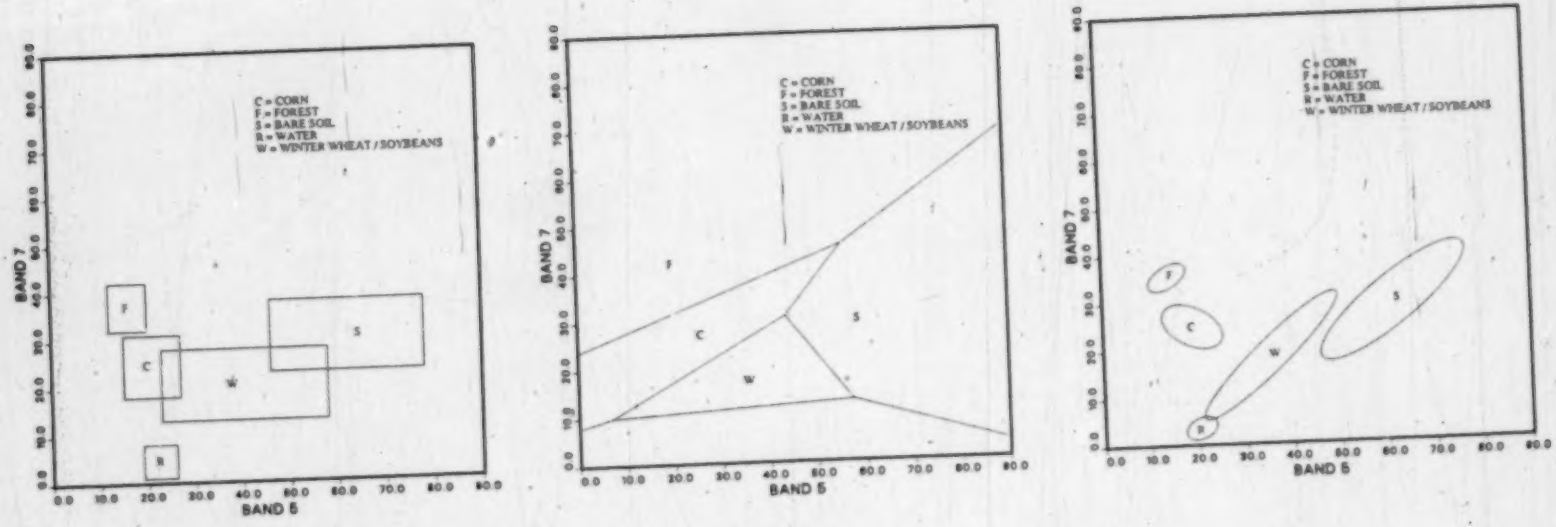

(a) (b) (c)

FIGURE 4.9 Cleaned Date 2 decision spaces for the parametric classifiers. (a) parallelepiped, (b) linear classification function, (c) maximum likelihood.

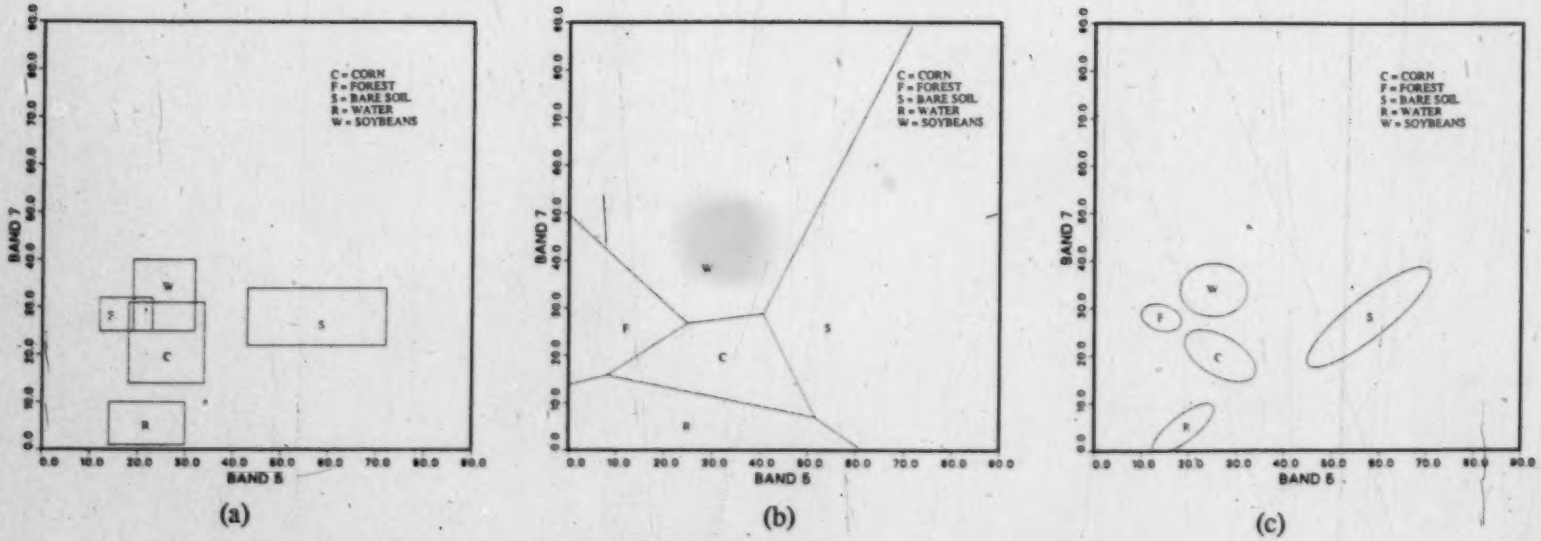

FIGURE 4.10 Cleaned Date 3 decision spaces for the parametric classifiers. (a) parallelepiped, (b) linear classification function, (c) maximum likelihood.

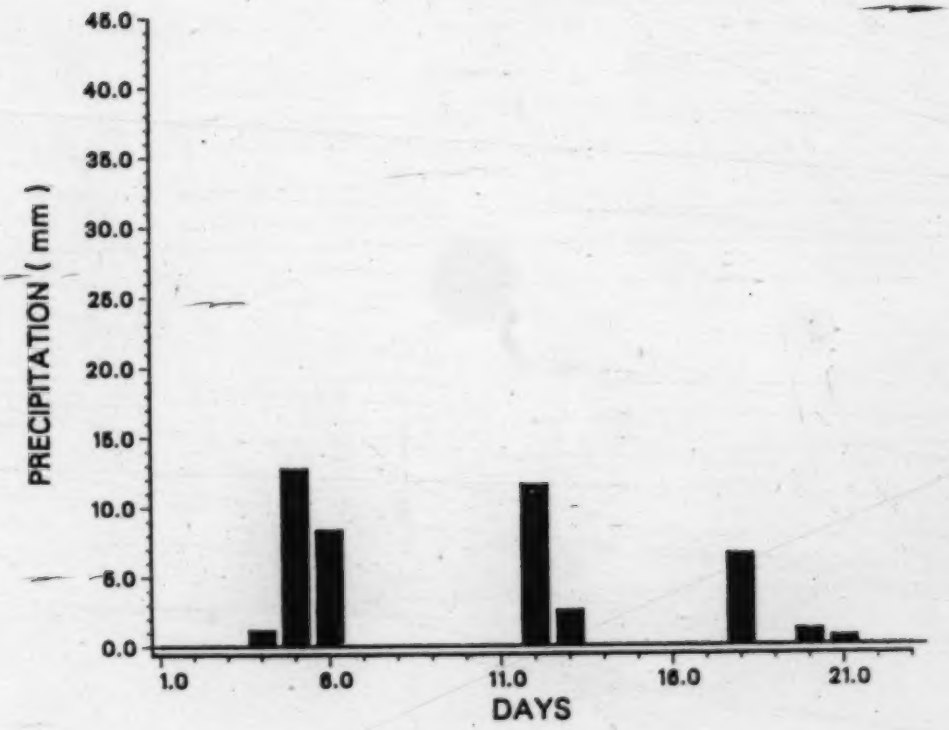

FIGURE 5.1 Precipitation in July, 1984.

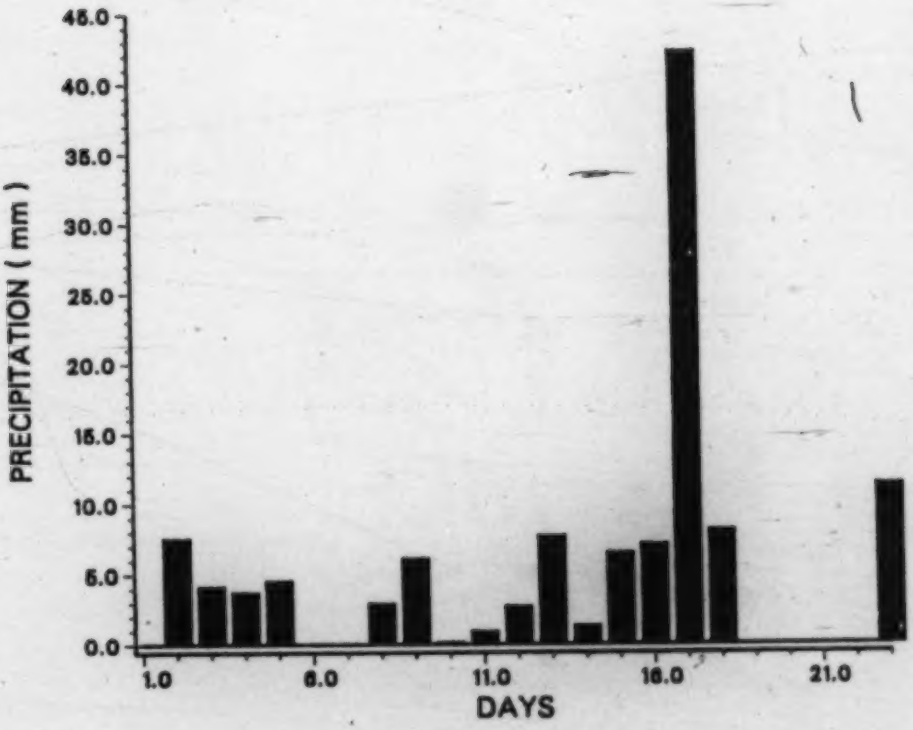

FIGURE 5.2 Precipitation in July, 1986.

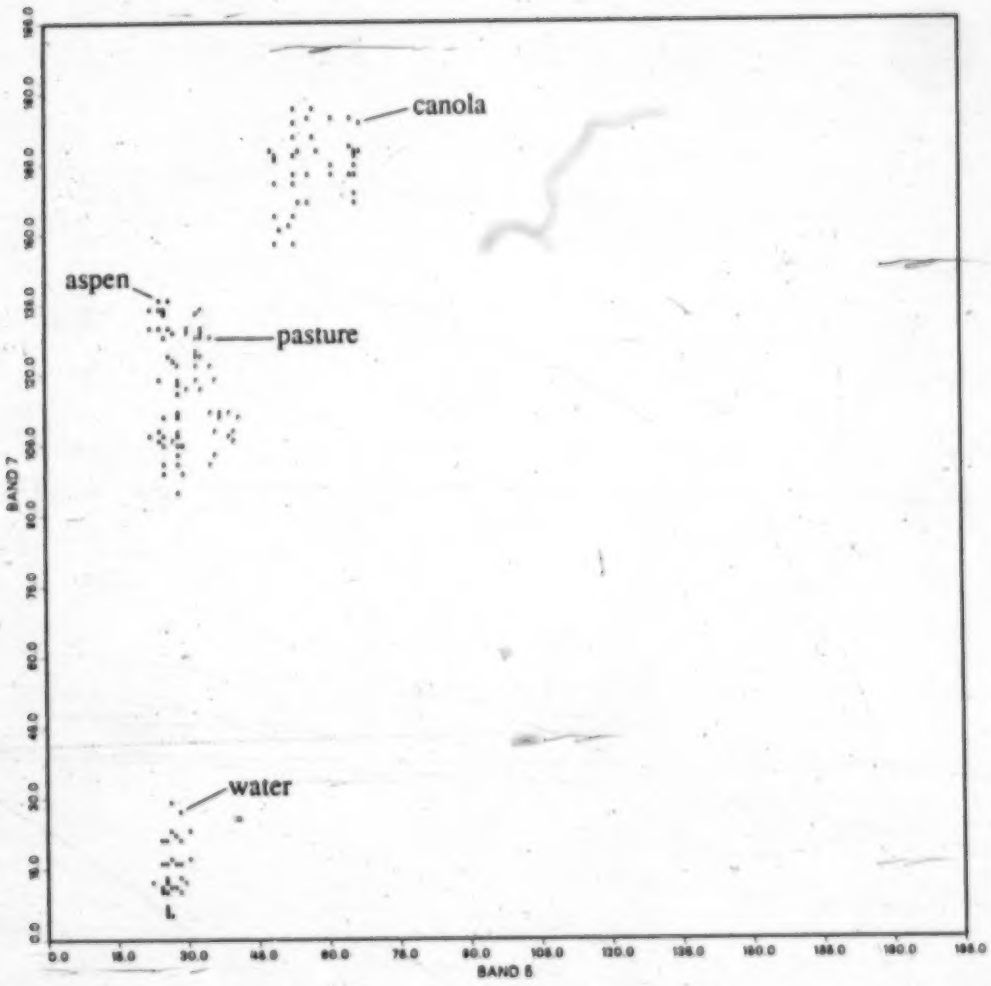

FIGURE 5.3 Cleaned Multispectral Scanner feature space plot.

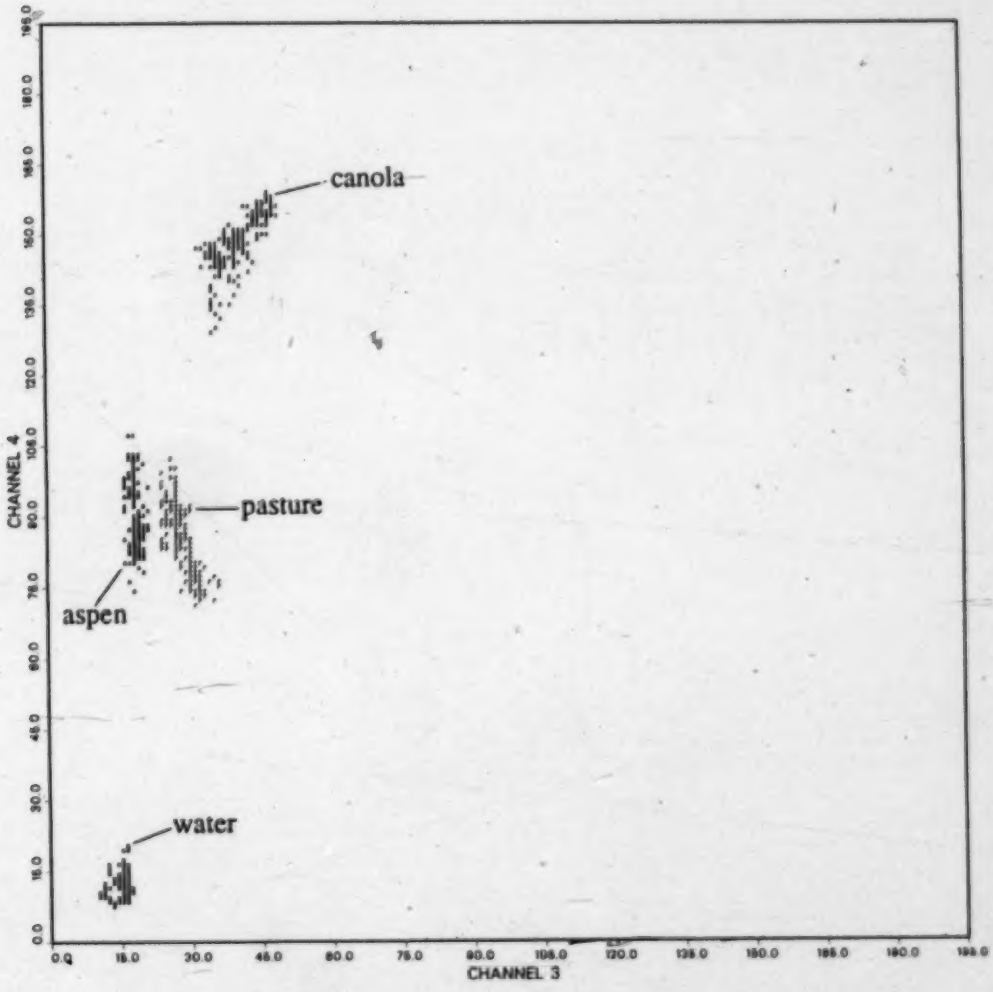

FIGURE 5.4 Cleaned Thematic Mapper feature space plot.

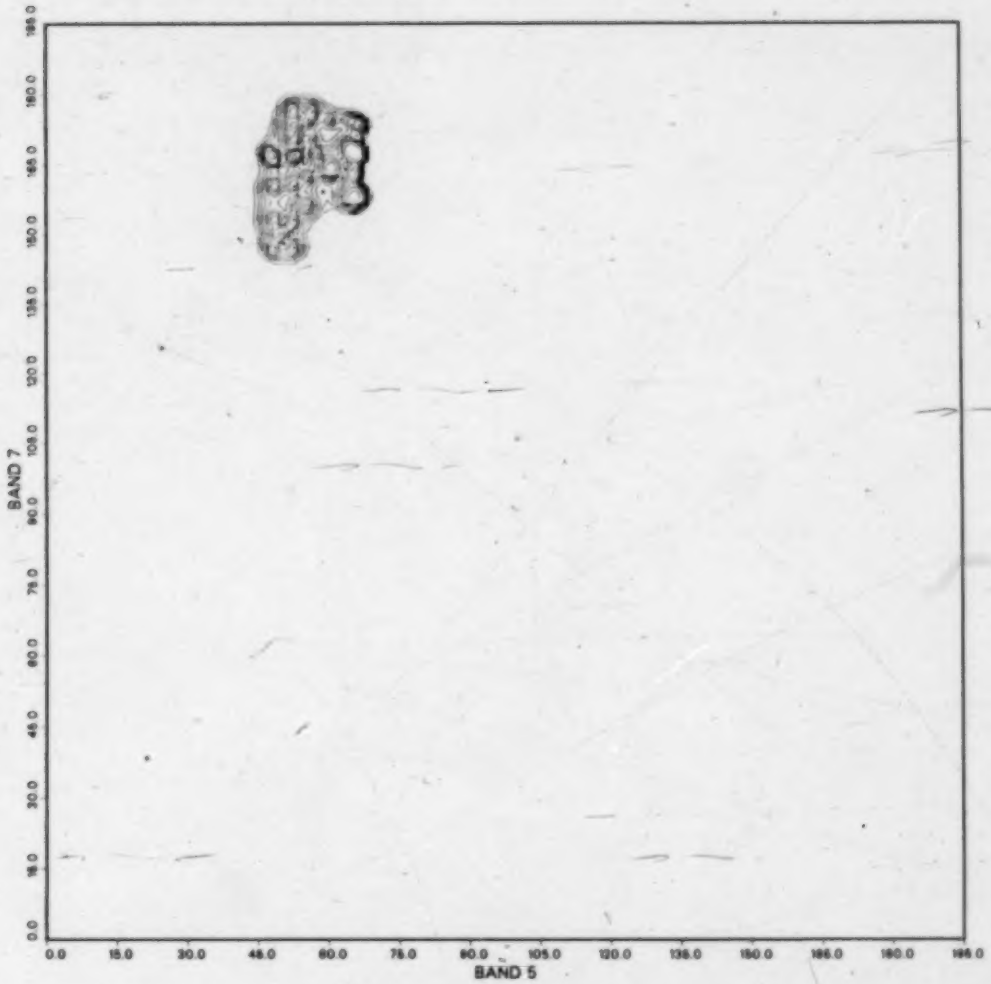

(a) canola

FIGURE 5.5 Cleaned Multispectral Scanner frequency feature space plots. (a) canola, (b) water, (c) aspen, (d) pasture. (Percent volume contours from 100% to 10% with a 10% contour interval.)

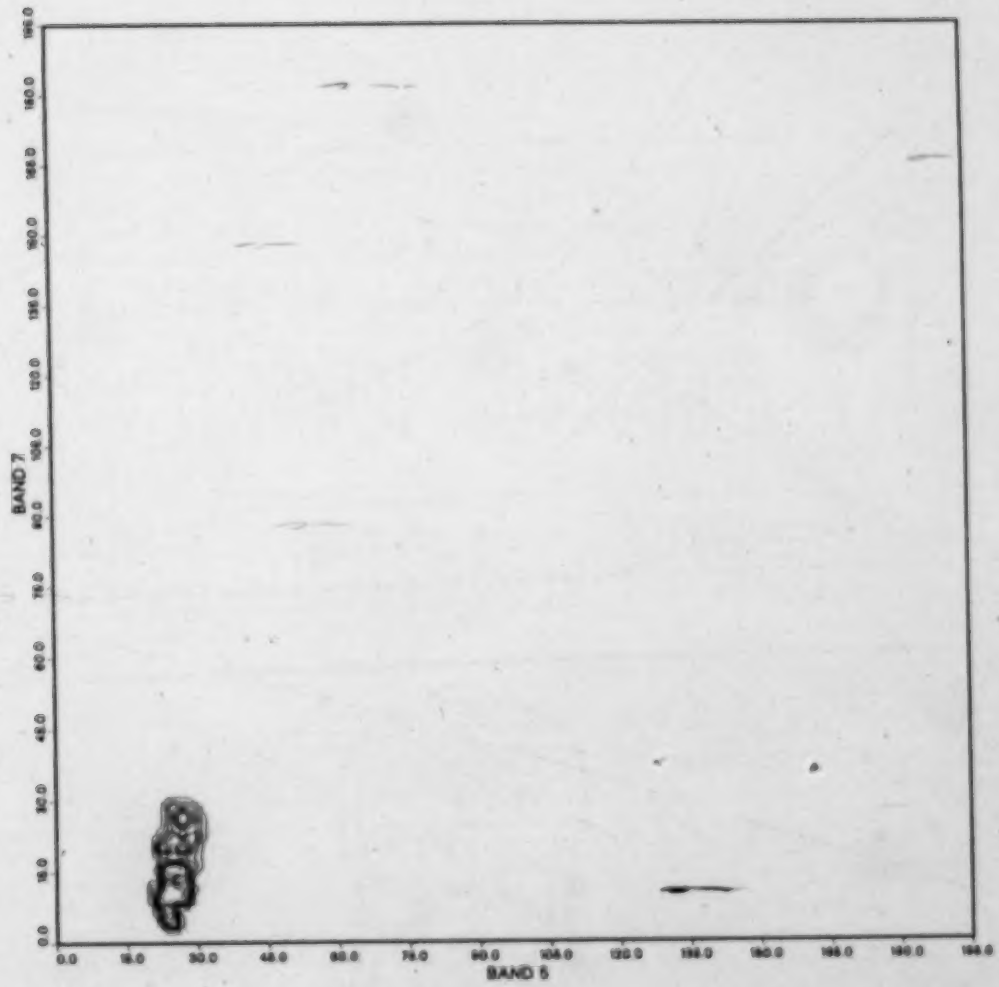

(b) water

FIGURE 5.5 continued.

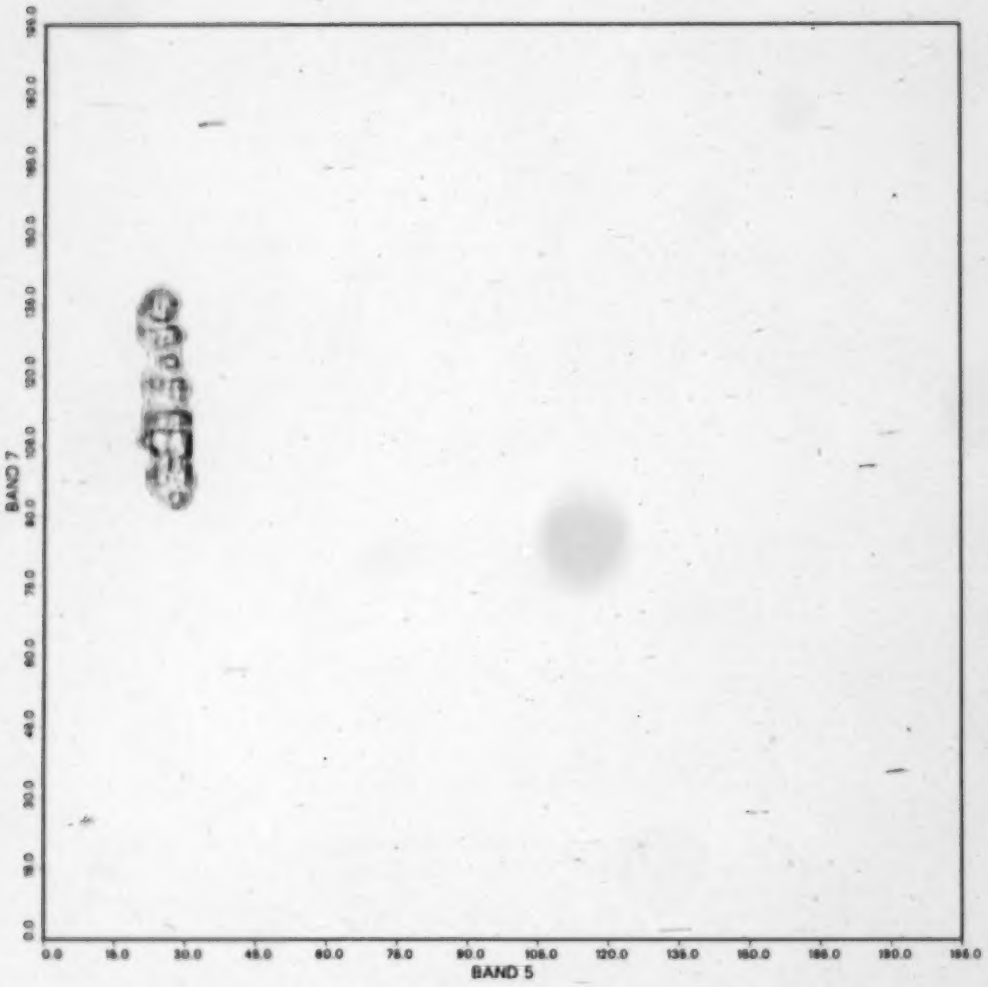

(c) aspen

FIGURE 5.5 continued.

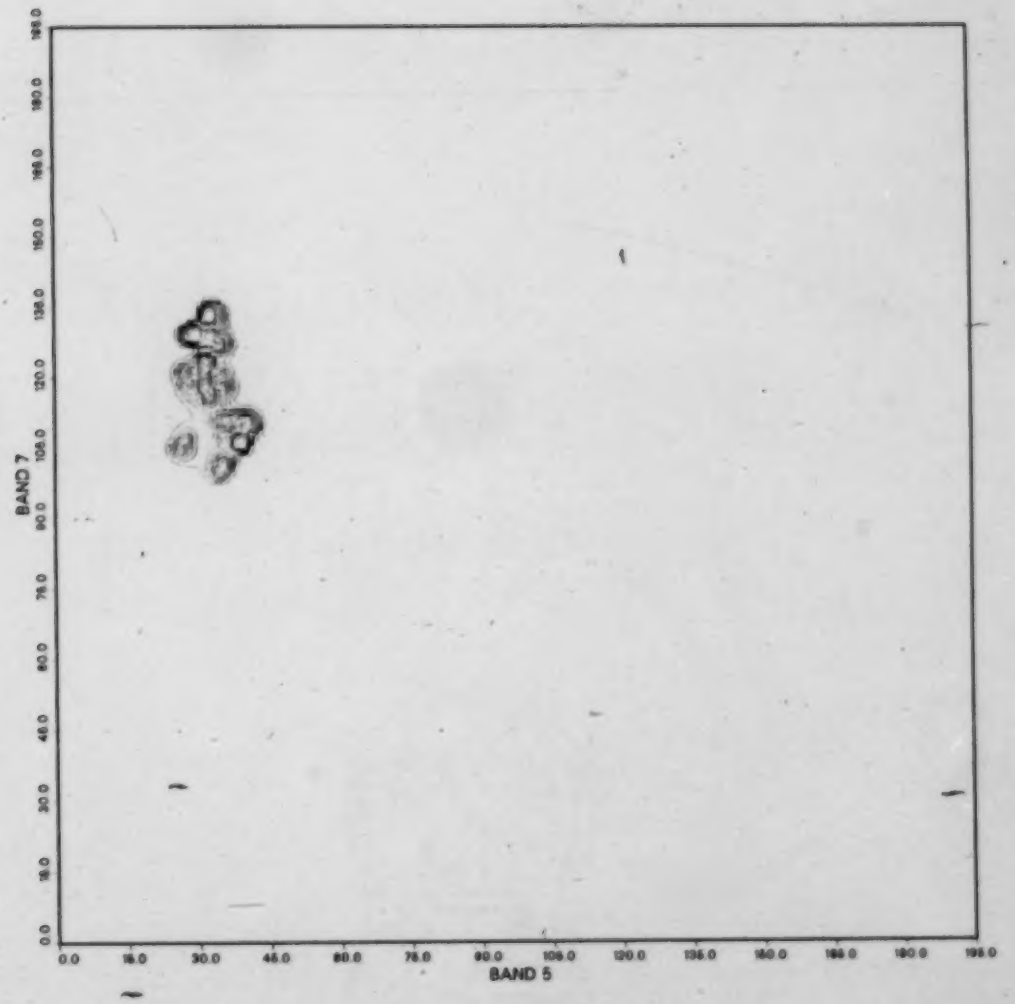

(d) pasture

FIGURE 5.5 continued.

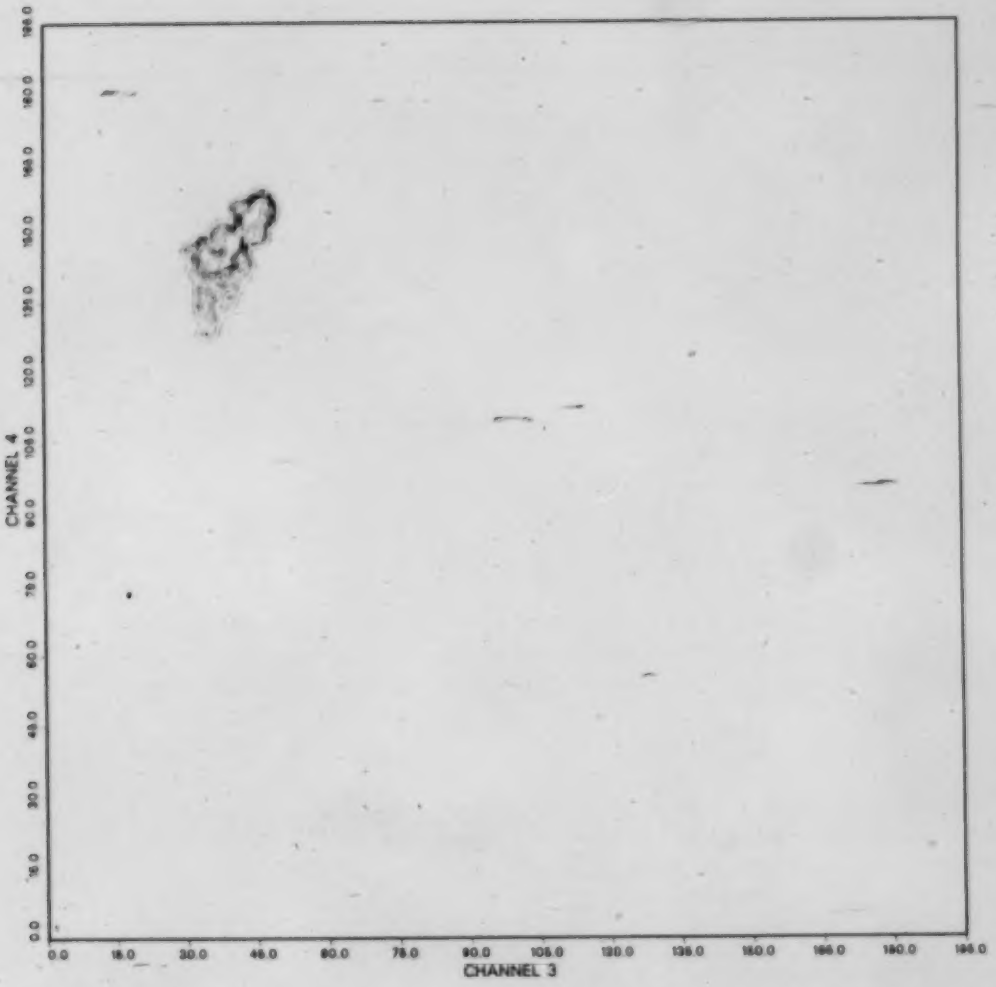

(a) canola

FIGURE 5.6 Cleaned Thematic Mapper frequency feature space plots. (a) canola, (b) water, (c) aspen, (d) pasture. (Percent volume contours from 100% to 10% with a 10% contour interval.)

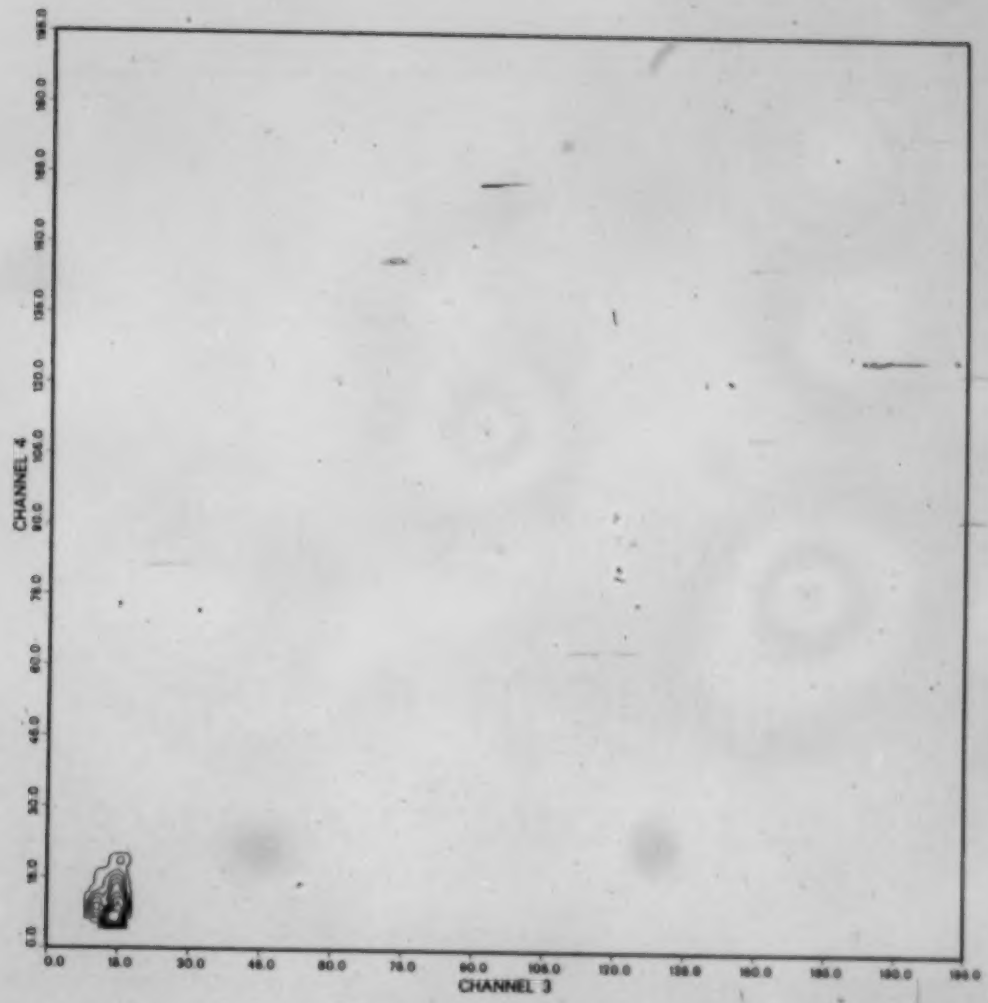

(b) water

FIGURE 5.6 continued.

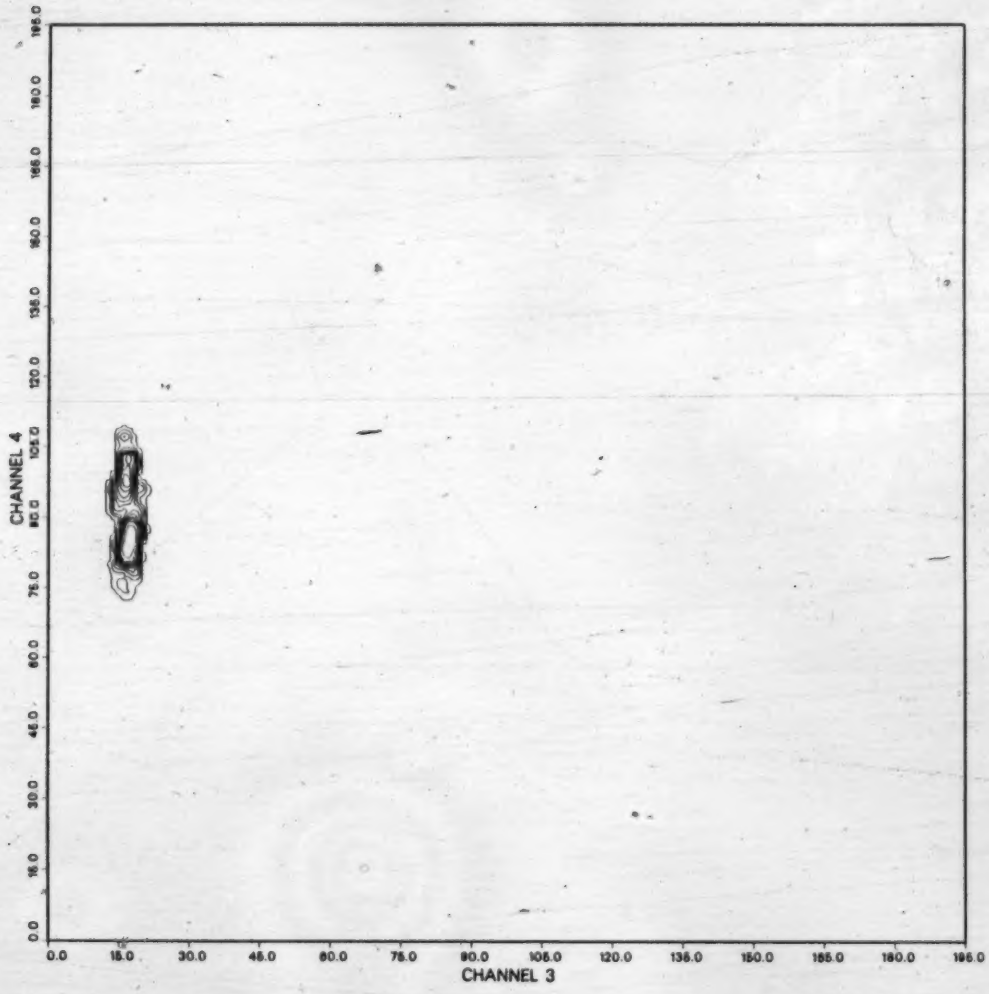

(c) aspen

FIGURE 5.6 continued.

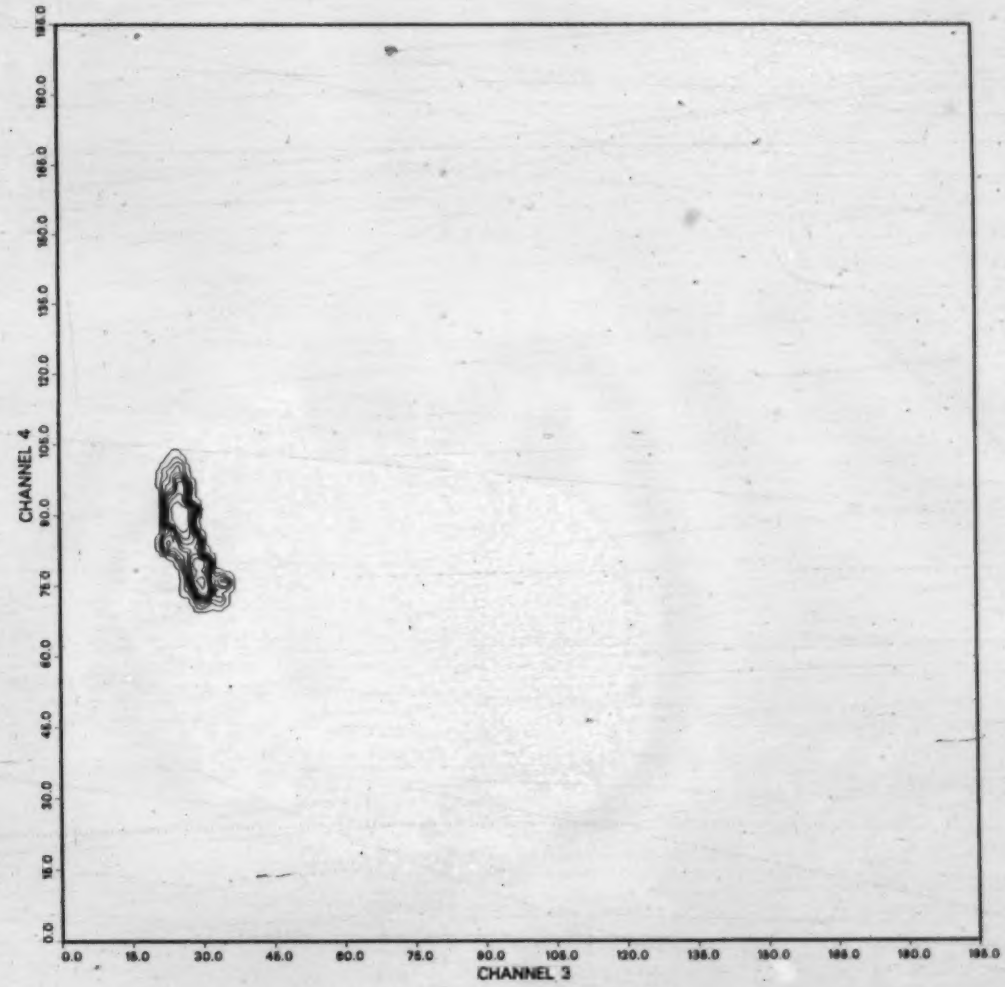

(d) pasture

FIGURE 5.6 continued.

THE QUALITY OF THIS MICROFICHE IS HEAVILY DEPENDENT UPON THE QUALITY OF THE THESIS SUBMITTED FOR MICROFILMING.

UNFORTUNATELY THE COLOURED ILLUSTRATIONS OF THIS THESIS CAN ONLY YIELD DIFFERENT TONES OF GREY.

LA QUALITE DE CETTE MICROFICHE DEPEND GRANDEMENT DE LA QUALITE DE LA THESE SOUMISE AU MICROFILMAGE.

MALHEUREUSEMENT, LES DIFFERENTES ILLUSTRATIONS EN COULEURS DE CETTE THESE NE PEUVENT DONNER QUE DES TEINTES DE GRIS.

PLATE 5.1 Multispectral Scanner image of the Alexander Indian Reservation. (Spectral bands 7, 5, and 4 used to generate image.)

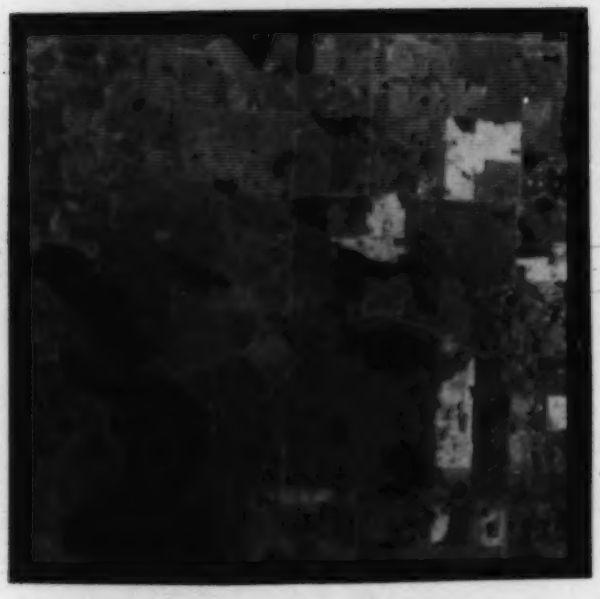

PLATE 5.2 Thematic Mapper image of the Alexander Indian Reservation.
(Spectral channels 4, 3, and 2 used to generate image.)

(a)

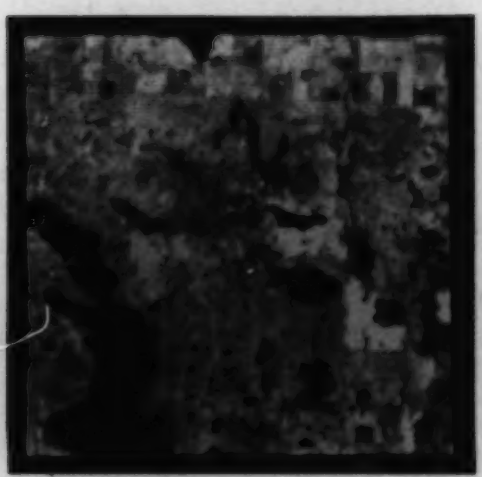

(b)

PLATE 5.3 Multispectral Scanner red and infrared radiation channel images.
(a) red channel, (b) infrared channel

(a)

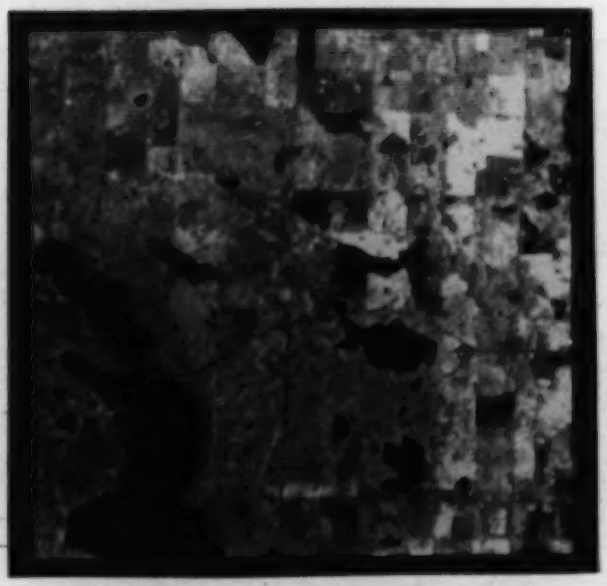

(b)

PLATE 5.4 Thematic Mapper red and infrared radiation channel images.
(a) red channel, (b) infrared channel.

PLATE 5.5 Multispectral Scanner training field locations.

PLATE 5.6 Thematic Mapper training field locations.

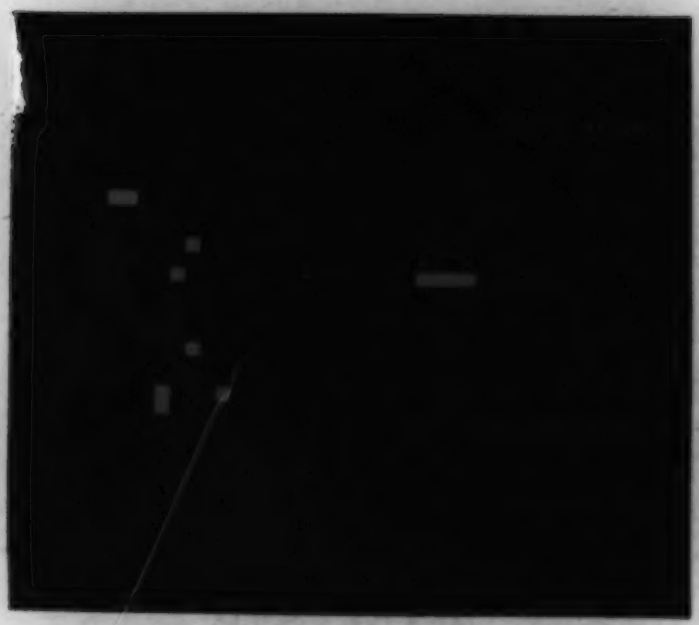

PLATE 5.7 Differenced grid for pasture. (Values are unscaled.)

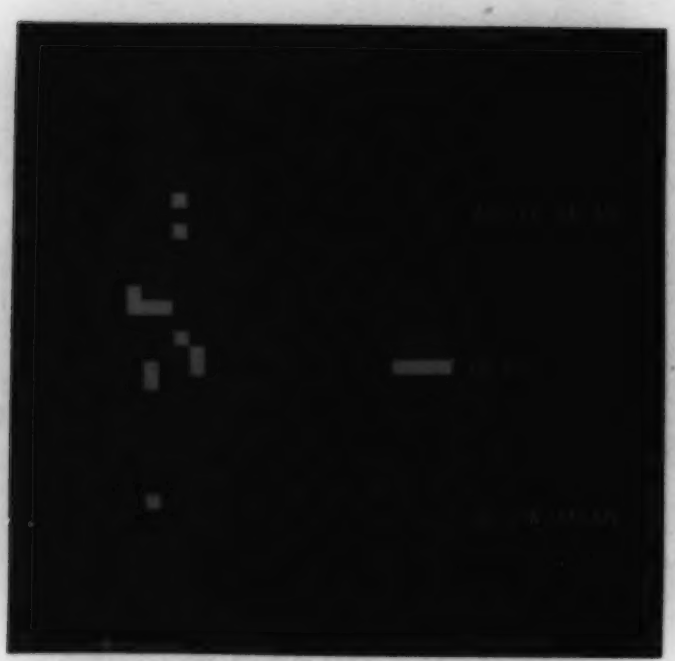

PLATE 5.8 Differenced grid for aspen. (Values are unscaled.)

PLATE 5.9 Differenced grid for water. (Values are unscaled.)

BIBLIOGRAPHY

Alberta Environment, 1986, Remote Sensing Newsletter, no. 18, Edmonton, Alberta, pp. 11,12.

Secretary from the Alexander Indian Reservation, 1986, personal communication.

American Society of Photogrammetry, 1983, Manual of Remote Sensing, Second Edition, Volume II, The Sheridan Press, U. S. A. p. 1914.

Atmospheric Environment Service, 1984, Monthly Meteorological Summary, Environment Canada, July 1984, Edmonton Municipal Airport, Alberta, p. 1.

Atmospheric Environment Service, 1986, Monthly Meteorological Summary, Environment Canada, July 1986, Edmonton Municipal Airport, Alberta, p. 1.

Barrett, E. C., Curtis, L. F., 1982, Introduction to Environmental Remote Sensing, Second Edition, Chapman and Hall, New York, U.S.A., p. 259.

Batchelor, B. G., 1974, Practical Approach to Pattern Classification, Plenum Publishing Company Ltd., New York, U.S.A., p. 17.

Brooner, W. G., Simonett, D. S., 1971, "Crop Discrimination with Color Infrared Photography: A Study in Douglas County, Kansas", Remote Sensing of Environment, 2, pp. 21 - 35.

Crane R. B., Malila, W. A., Richardson, W., 1972, "Suitability of the Normal Density Assumption for Processing Multispectral Scanner Data", IEEE Transactions on Geoscience Electronics, vol.10, pp. 158 - 165.

Crist, E. P., Cicone, R. C., 1984, "Comparisons of the Dimensionality and Features of Simulated Landsat-4 MSS and TM Data", Remote Sensing of Environment, vol. 14, pp. 235 - 246.

Davis, J. C., 1973, Statistics and Data Analysis in Geology, John Wiley & Sons, Inc., Toronto, pp. 442 - 444.

Ebdon, D., 1985, Statistics in Geography, Second Edition, Billing and Sons Ltd., Worcester, Great Britain, pp. 53 - 55, 65 - 71.

Eyton, J. R., 1983, "A Hybrid Image Classification Instructional Package", Photogrammetric Engineering and Remote Sensing, vol. 49, no. 8, pp. 1175 - 1181.

Eyton, J. R., 1984, "Complementary-Color, Two-Variable Maps", Annals of the Association of American Geographers, vol. 74, no. 3, pp. 477 - 490.

Eyton, J. R., 1987, personal communication.

Eyton, J. R., Li, R., and Ulaby, F. T., 1979, "Combined Radar and Landsat Multitemporal Crop Classification", Remote Sensing Laboratory, RSL Technical Report 360-10, the University of Kansas Centre for Research, Inc., NASA contract NAS 9-15421, 55p.

Hall, R. J., Crown, P. H., and Titus, S. J., 1984, "Change Detection Methodology for

Aspen Defoliation with Landsat MSS Digital Data", Canadian Journal of Remote Sensing, vol. 10, no. 2, pp. 135-142.

Hardy, R. L., 1971, "Multiquadric Equations of Topography and other Irregular Surfaces", Journal of Geophysical Research, vol. 76, no. 8, pp. 1905-1914.

Harnett, D. L., 1982, Statistical Methods, Third Edition, Addison - Wesley Publishing Company, Don Mills, Ontario, pp. 708 - 713, A-58.

Holmes, R. A., 1984, "Advanced Sensor Systems: Thematic Mapper and Beyond", Remote Sensing of Environment, 15, pp.213-221.

Jones, P., 1985, "Remote Sensing: Hopes for an Expanding Marketplace", Space World, vol. 5, no. 11, pp. 9-13.

Kirby, M., Steiner, D., 1978, "The Appropriateness of the Affine Transformation in the Solution of the Geometric Base Problem in Landsat Data", Canadian Journal of Remote Sensing, vol. 4, no. 1, pp. 37 - 48.

Klecka, W. R., "Discriminant Analysis", Sage University Paper series on Quantitative Applications in the Social Sciences, 07-019, Beverly Hills and London: Sage Pubns., pp. 42 - 44.

Lee, T., Richards, J. A., 1984, "Piecewise Linear Classification Using Seniority Logic Committee Methods, with Application to Remote Sensing", Pattern Recognition, vol. 17, no. 4, p. 463.

Lillesand, T. M., Kiefer, R. W., 1979, Remote Sensing and Image Interpretation, John Wiley & Sons, Toronto, pp. 30, 396, 465, 466.

Maynard, P. F., Strahler, A. H., 1981, " The Logit Classifier: A General Maximum Likelihood Discriminant For Remote Sensing Applications", Proceedings of the Fifteenth International Symposium on Remote Sensing of Environment, Ann Arbor, Michigan, pp. 213 - 222.

Richard, R. R., Merkel, R. F., Meeks, G. R., 1978,"NS001MS - Landsat-D Thematic Mapper Band Aircraft Scanner", Proceedings of the Twelfth International Symposium on Remote Sensing of Environment, Ann Arbor, Michigan, pp. 719 - 727.

SAS Institute Inc., 1985, SAS User's Guide: Statistics, Version 5 Edition, Cary, North Carolina, USA, pp. 317 - 333, 377 - 401.

Scholz, D., Fuhs, N., Hixson, M., 1979, "An Evaluation of Several Different Classification Schemes: Their Parameters and Performance", Proceedings of the Thirteenth International Symposium on Remote Sensing of Environment, Ann Arbor, Michigan, pp. 1143 - 1149.

Schowengerdt, R. A., 1983, Techniques for Image Processing and Classification in Remote Sensing, Academic Press, Toronto, pp. 58, 136.

Seevers, P. M., Peterson, R. M., 1978, "Application of Remote Sensing in Agricultural Analysis", Introduction to Remote Sensing of the Environment, Richardson Jr., B. F. editor, Kendall/Hunt Publishing Company, Iowa, U.S.A., p. 268.

Shlien, S., 1979, "Geometric Correction, Registration, and Resampling of Landsat Imagery", Canadian Journal of Remote Sensing, vol. 5, no. 1, pp.74 - 88.

Short, N. M., 1982, The Landsat Tutorial Workbook: Basics of Satellite Remote Sensing, NASA Reference Publication 1078, pp. 410-412, 428.

Sollers, S. C., Petersen, G. W., Henninger, D. L., Borden, F. Y., 1974, "The Use of Remote Sensing and Natural Indicators to Delineate Floodplains - Preliminary Findings", Proceedings of the Ninth International Symposium on Remote Sensing of Environment, Ann Arbor, Michigan, pp. 667 - 682.

SPOT IMAGE, 1984, Programme D'Evaluation Preliminaire SPOT: PEPS, Centre nationale D'etudes spatiales, France, p.3/1.

Sutherland, I, 1986, personal communication.

Swain, P. H., 1978, Remote Sensing: The Quantitative Approach, McGraw Hill, U.S.A., Swain, P. H., and Davis, S. M. editors, p.151.

Taranik, J. V., 1978, "Principles of Computer Processing of Landsat Data for Geologic Applications", United States Department of the Interior Geologic Survey, Open-File Report 78-117, Sioux Falls, South Dakota, pp. 17-19.

Toll, D. L., 1985, "Effect of Landsat Thematic Mapper Sensor Parameters on Land Cover Classification", Remote Sensing of Environment, pp. 129-140.

Ulaby, F. T., Eyton, J. R., Li, R. Y., Burns, G. F., 1979, "Annual Repeatability of Multidate Radar Crop Classifications", Remote Sensing Laboratory, RSL Technical Report. 360-1, the University of Kansas Centre for Research, Inc., NASA contract NAS 9-15421, 25p.

Unwin, D. J., 1975, An Introduction to Trend Surface Analysis, Concepts and Techniques in Modern Geography No. 5, United Kingdom, 40pp.

Verdin, J., 1983, "Corrected vs. Uncorrected Landsat 4 MSS Data", Landsat Data Users Notes, Issue No. 27, Sioux Falls, South Dakota, U.S.A., pp.4 - 8.

Wasrud, J., Lulla, K., 1985, "Evaluation of Classification Algorithms", Proceedings of the Nineteenth International Symposium on Remote Sensing of Environment, Ann Arbor, Michigan, pp. 433 - 441.

Appendix 1: Computer Programs Used in Thesis

The total length of the programs used are very long therefore only the names of the programs and the functions of the programs are listed. Programs suffixed with a '*' were programmed in whole or in part by J. Ronald Eyton. Programs suffixed with a '**' were programmed in whole or in part by Olaf Niemann.

POLY.L* - to generate a polynomial trend surface grid
GENCONT.L - to contour a polynomial trend surface grid
SMQE.L* - to generate a multiquadric surface
PERCONT.L - to contour a multiquadric surface
ZSMOOTH.L* - to smooth the spectral triplets
GENFREQ.L - to create spectral triplets from spectral pairs
TRAIN.L - to read in spectral values from training fields
KS.L - Kolmogorov-Smirnov test for bivariate normality
CHI.L* - to output chi-square deciles
PERCENT.L - to change frequency surface grid to a percent surface grid
VOLTEN.L - to determine 10% percent surface volume contours
CCT.L **- to unpack Dipix TO format MSS scene onto Michigan Terminal System
CCT2.L** - to unpack Dipix TO format TM scene onto Michigan Terminal System
BVSTD.L* - to plot bivariate standard deviational ellipses
DISCRIM - SAS linear discriminant function
LINDISC.L* - to generate linear discriminant function grid
FASTCLUS - SAS clustering routine
PIPED - to plot parallelepiped decision spaces
TWOFOUR.L** - to change I*2 grid to I*4 grid
GRDCRE.FOR** - to create an Intergraph grid file from an unformatted grid file
WINDOW.L - to list out percent frequency surface triplets greater than zero
RESCALE.L - to change percent frequency surface triplets into pairs for Kolmogorov-Smirnov test
SYMB.L - to plot feature space pixel locations
DESCRIBE - MIDAS program to output descriptive statistics
HIST.L* - program used to create histogram and descriptive statistics for data.